Seeding of Titanium Surfaces and Nitinol Stents with Blood-Derived Endothelial Cells

by

Alexandra Elizabeth Jantzen

Department of Biomedical Engineering
Duke University

Date:_____

Approved:

_____
George A. Truskey, Supervisor

_____
Hardean Achneck

_____
David Katz

_____
Bruce Klitzman

_____
William Reichert

Dissertation submitted in partial fulfillment of
the requirements for the degree of Doctor
of Philosophy in the Department of
Biomedical Engineering in the Graduate School
of Duke University

2014

ABSTRACT

Seeding of Titanium Surfaces and Nitinol Stents with Blood-Derived Endothelial Cells

by

Alexandra Elizabeth Jantzen

Department of Biomedical Engineering
Duke University

Date:_____
Approved:

_____
George A. Truskey, Supervisor

_____
Hardean Achneck

_____
David Katz

_____
Bruce Klitzman

_____
William Reichert

An abstract of a dissertation submitted in partial
fulfillment of the requirements for the degree
of Doctor of Philosophy in the Department of
Biomedical Engineering in the Graduate School of
Duke University

2014

Abstract

Covering the metal surface of blood-contacting cardiovascular implants (stents, ventricular assist devices) with functional endothelium may reduce the incidence of clotting and restenosis complications and also reduce the need for risky anticoagulation therapy following implantation of such devices. We developed a novel cell therapy for seeding autologous endothelium onto blood-contacting vascular stents at the point of care to reduce thrombosis and stent restenosis. The proposed research tested the following hypotheses: (1) autologous endothelial cells (ECs) can spread on titanium (Ti) tubes and reduce thrombosis on the Ti surface *in vivo*; (2) shear stresses on the surfaces of an implanted carotid artery stent will be conducive to EC retention and function under arterial flow; and (3) nitinol stents seeded with ECs at the point of care will remain adherent and functional after stent deployment and arterial fluid shear stress conditions *in vitro* and *in vivo*. Based on the experiments reported herein, the primary conclusions of the dissertation are as follows: (1) autologous ECs significantly reduce thrombosis on Ti surfaces implanted into the bloodstream *in vivo*; (2) shear stresses on stent surfaces under carotid artery flow conditions are sufficiently low to be compatible with EC retention and function; (3) ECs seeded onto nitinol stents by infusion at the point of care are retained and spread to form a functional layer following deployment and arterial flow conditions both *in vitro* and *in vivo*.

Dedication

I would like to dedicate this dissertation to my immediate family: Ann, Charles, Meredith, Cole, and Sammy.

Contents

List of Tables

List of Figures

Acknowledgements

I would like to thank my dissertation adviser, Dr. George Truskey, for his guidance and encouragement throughout my graduate career. Without this, I may not have completed this work and would certainly not have enjoyed such a rich experience. I would also like to thank Dr. Hardean Achneck for the opportunity to collaborate with his lab on this project which fit my interests and career path so well. I thank all my committee members for their support and helpful input. I am grateful to Dr. Fu-Hsiung"Jimmy" Lin for his help and expertise, lent on so many occasions. Vrad Levering and Tracy Cheung, my two long-suffering officemates over these years, are gratefully acknowledged for their patient listening, good advice, and sociable company. I would like to thank my labmates: Cindy Cheng for frequent help and making the lab a great place to work, and Brittany Davis for contributing so much to our positive atmosphere. I thank all of the graduate students who have become my good friends during our time together at Duke for making this a good place to be.

1. Background, significance, specific aims, and hypotheses

1.1 Background and significance

1.1.1 Clinical need for and use of nitinol stents

Atherothrombotic diseases are projected to be the leading cause of death worldwide in 2020[1]. Two specific subcategories of atherosclerotic disease, peripheral vascular disease and coronary artery disease, are commonly treated by stents.

1.1.1.1 Peripheral artery disease

Peripheral arterial disease (PAD) affects approximately 8.5 million people in the United States[2], including 12-20% of individuals over the age of 60[3]. The most severe & deadly form of the disease, critical limb ischemia, affects an estimated 2.8 to 3.5 million PAD patients nationally[4].

Angioplasty and stenting of the small vessels in the leg, particularly below the knee, is a frequently used technique for limb salvage. By one estimate, 300,000 stents are placed each year in peripheral arteries in the United States[5]. However, stents in vessels less than 5 mm in diameter suffer from high rates of restenosis resulting from intimal hyperplasia and thrombosis[6]. Drug-eluting stents are coated with anti-proliferative compounds such as sirolimus and paclitaxel and aim to reduce intimal hyperplasia. Such compounds nonspecifically reduce proliferation of both smooth muscle and endothelium. Drug-eluting stents represent a potential solution to restenosis, but are

still associated with serious complications and late thrombosis in a number of patients[7]. Longer-term delivery of paclitaxel to stainless steel stents has been achieved in animal studies by magnetic targeting[8,9], but is not applicable to self-expanding nitinol stents used in peripheral vasculature because they are significantly less ferromagnetic[10].

1.1.1.2 Coronary artery disease

Coronary artery disease has a large impact in our society; it was the cause of 1 out of 6 deaths in the United States in 2010[2]. An estimated 15.4 million Americans over age 20 have coronary disease[2], which is approximately double the number of people affected by peripheral arterial disease. The primary endpoint in peripheral arterial disease is often amputation, indirectly associated with mortality rates. In contrast, coronary artery disease is associated more directly with myocardial infarction and mortality. The estimated annual incidence of myocardial infarction in the United States is 620,000 new attacks and 295,000 recurrent attacks[2]. The lifetime risk of developing coronary heart disease after 40 years of age is 49% for men and 32% for women[11], according to one population study.

Angioplasty and stenting of coronary vessels and coronary grafts is a frequently used treatment for coronary artery disease. Approximately 650,000 cases of coronary stenting were performed in 2009 in the U.S., of which 75% were drug-eluting stents and 25% were bare metal stents[12]. In comparison to the traditional surgical approach of coronary artery bypass grafting (CABG), stenting has been associated with significantly

lower rates of stroke[13] but higher rates of restenosis requiring repeat revascularization. Another prospective study concluded that stenting had equivalent outcomes at 1-2 years to CABG[14], with the benefit that it is a less invasive procedure and therefore may be suitable for some patients who are not candidates for surgery.

As with peripheral vascular disease, drug-eluting stents in coronary applications are associated with late-stage thrombosis. This thrombosis is thought to be caused by either the polymer drug carrier or by incomplete formation of a protective endothelial layer[3,15]. Long-term patency rates are also negatively impacted by the small diameter of coronary vessels and stented bypass grafts[16].

1.1.1.3 Nitinol stents for vascular disease

Two kinds of stents are used in the treatment of atherosclerosis: (1) balloon-expanded stents, and (2) self-expanding stents. Balloon-expanded stents are mounted onto balloons and forcefully expanded by inflation of the balloon; these stents are often made of stainless steel or cobalt chrome alloys. Self-expanding stents, on the other hand, are delivered compressed inside a delivery sheath and expand to the final diameter when the sheath is retracted. These have the advantage of greater flexibility. Self-expanding stents typically require the use of nitinol.

Nitinol, a nickel-titanium alloy developed in the 1960's[17], is used extensively in medical devices, especially implants. The flexibility of nitinol is 10-20 times greater than stainless steel[18], meaning that nitinol stents conform very well to tortuous vessels.

Nitinol can be strained 20 times more than stainless steel without being plastically deformed[19]. Nitinol stents are typically cut from a single piece of tubing, then incrementally expanded and "set" to a desired final diameter through heat treatment. With a transition temperature for full expansion just below body temperature, nitinol stents will partly expand if unsheathed at room temperature, but will not reach their fully expanded set diameter unless warmed to body temperature. This property is termed "shape memory."

The shape memory of nitinol means that these self-expanding stents can rebound in response to external pressures with continued radial force[18], unlike stainless steel stents, which would be crushed. These important properties have led to the nearly exclusive use of nitinol self-expanding stents over balloon-expandable stents in superficial peripheral sites such as carotid and femoral arteries[20]. Superficial sites are not only subject to external compression, but vessels in the lower extremities are also subject to many forces from ambulation, subjecting stents to bending, torsion, and axial fatigue[21]. The superelastic properties of nitinol make nitinol stents well-suited to withstand these forces.

More recently, a nitinol coronary stent has been introduced clinically with the aim of improving stent-vessel apposition and reducing distal embolization in comparison to balloon-expandable coronary stents[22,23]. The therapy proposed herein for

study therefore has a wide potential application in both peripheral and coronary artery diseases.

1.1.1.4 The outer surface of nitinol consists primarily of TiO_2

When nitinol began to be used for medical implants, concerns about nickel on the surface and leaching from the implant had to be addressed. Nitinol readily forms a TiO_2 layer on its outer surface, but residual nickel content is somewhat dependent on polishing and heat treatment techniques[24]. The process of electropolishing, standard for marketed self-expanding stents, significantly decreases the Ni on the outer surface[25]. These facts support the idea that uncoated nitinol stents can support the growth of endothelial cells as we have seen previously with titanium[26,27], and that those studies can be related to the proposed work, although surface characterization is necessary to show similarity.

1.1.2 Effectiveness of nitinol stents and drug-eluting stents in peripheral arterial disease and coronary arterial disease

In peripheral arterial disease, restenosis occurs in 40-60% of femoral artery segments treated by balloon angioplasty alone after one year[28-30]. These rates are worse for extended disease segments; restenosis at one year is in excess of 70% for lesions over 100mm[31]. Bare metal stents have lower rates of restenosis than angioplasty in the superficial femoral artery, ranging from 24% to 8% at six months in one set of studies[7,32]. With drug-eluting stents for the superficial femoral artery, some clinical studies showed

reduced 12-month restenosis rates compared to bare metal stents (11% vs. 27%)[33], while another study showed no significant difference between drug-eluting and bare metal stents (22% vs. 21% at 24 months, respectively)[7]. Importantly, all studies found that restenosis occurred in a portion of the population after 6-12 months, supporting the claim that there is an unmet need and room for improving the outcomes of existing stent therapies.

In coronary artery disease, restenosis is also an important concern; data show that in-stent restenosis has a negative impact on long-term patient survival[34]. Balloon angioplasty in coronary lesions is associated with a restenosis rate of over 40%[35]. In comparison, the addition of stents improved outcomes; however, the restenosis rates in coronary lesions treated with bare metal stents range from 20% to 40%[36].

1.1.2.1 Drug-eluting stents

Drug-eluting stents (DES) have been in clinical use for coronary arteries longer than in peripheral applications, and reported rates of restenosis and late-stage thrombosis vary widely according to the stent platform, active drug, and polymer drug carrier. Reported restenosis rates at 12 months are reduced over bare metal stents, at approximately 6%[37,38]. However, the delayed healing associated with drug-eluting stents is suspected of causing late-stage thrombosis in conjunction with patients' scheduled decrease in anticoagulant and antiplatelet therapy and final release of the

drug coating[39,40]. Late-stage thrombosis is typically described as occurring 6-12 months or more after stent placement.

A variety of drugs are approved for use in DES. The drugs used in contemporary DES can be divided into two categories: 1) Rapamycins, including sirolimus, zotarolimus, everolimus, and biolimus A9; and 2) Taxanes, including paclitaxel. Drugs in both categories have their primary function as antiproliferative drugs. Paclitaxel is used in other applications as a chemotherapeutic agent for cancer, because of its antiproliferative properties[41]. Rapamycin-type drugs have been used in other applications as an immunosuppressant to prevent rejection in organ transplantation[42], and are also associated with cancer inhibition[43].

Most current DES platforms consist of three components: the physical stent scaffold, drug to inhibit neointimal hyperplasia, and a polymer to deliver the drug with a controlled release. Polymers employed in drug-eluting stents have included biostable polymers, bioabsorbable polymers, and natural biopolymers[44]. Some polymers used in first-generation DES were associated with significant inflammation[45-47]. In second-generation DES, results have shown some improvement in restenosis rates over first-generation devices in some cases[48], but higher incidence of restenosis in others[49], and no cases of very late stent thrombosis over 4 years in one stent platform[50]. Polymer degradation speed varies and is related to many factors including monomer hydrophilicity, polymer size, crystallinity, pH, and reactivity of hydrolytic groups[51].

While most DES make use of a polymer carrier, there are FDA-approved DES platforms which do not use a polymer carrier[52].

Endothelial dysfunction has been reported following drug-eluting stent implantation. A review of the literature revealed abnormal vasoconstriction in distal vessel segments after implantation of sirolimus-eluting stents and paclitaxel-eluting stents, but not in zotarolimus-eluting stents or biolimus-eluting stents, compared with bare metal stents[53]. The vasoconstriction events were observed following a variety of different provocation tests, but it is unclear how this may be associated with a clinical outcome such as stent thrombosis or restenosis.

1.1.2.2 Bioabsorbable stents

An experimental alternative to permanent metal stent implants, bioabsorbable stents are made of materials like magnesium and poly-L-lactic acid[54,55]. Bioabsorbable stents fully resorb into the bloodstream after a period of time ranging from months to years. The intent is that no lasting implant remains after this time. Despite the appeal of a non-permanent implantable device, bioabsorbable stents have the disadvantage of lower radial strength compared to metal stents; methods used to increase the strength reduce the potential for bioabsorption. It is not clear whether the vessel will remain patent following the absorption of the stent; results with a magnesium stent were disappointing and showed a 45% rate of restenosis at 4 months, close to the restenosis rates of angioplasty[54].

A more recent trial of a poly-L-lactic acid stent, coated with poly-D,L–lactic acid to facilitate release of the antiproliferative drug everolimus showed more positive results, with restenosis rates and late lumen loss at 6-24 months similar to the current generation of drug-eluting stents[55]. This was attributed to rapid changes in stent integrity during absorption, highlighting the importance of the degradation profile. Only about 30% of the stent mass is absorbed after 12 months, and it is not clear whether patency outcomes will remain positive following full absorption. A second generation version of this bioabsorbable stent device was investigated clinically, but reported slightly higher rates of late lumen loss and neointimal growth compared to the first generation device, and no improvement over metallic everolimus-eluting stents evaluated at the same time points[56]. Another polymeric bioabsorbable stent composed of poly(lactic-co-glycolic) acid and elastomer showed mild and stable levels of intimal hyperplasia in a pre-clinical ovine model[57].

Although bioabsorbable stents aim to reduce late and very late complications, isolated cases of late stent thrombosis (2 years post-stenting) have still been reported with bioresorbable stents[58]. Increasingly, bioabsorbable stent platforms are also incorporating antiproliferative drugs; because these drugs inhibit endothelial growth, it will be critical that the drug release timescale is carefully adjusted to be compatible with the stent absorption timescale, so that endothelium covers the stent structure before bulk

erosion could occur; without this endothelial coverage, embolization of the degrading stent pieces is a possibility.

1.1.3 Endothelialization of stents and titanium vascular implants

Since the first clinical use of metal stents in the late 1980's[59], patency rates have improved over those of balloon angioplasty alone, but restenosis remains a problem. Specific failure modes have been identified in the broad categories of thrombosis and intimal hyperplasia. Intimal hyperplasia is characterized by over-proliferation of smooth muscle cells (SMC) in the media layer. Commonly, intimal hyperplasia is co-localized with disruptions of the internal elastic lamina layer of the media[60]. This physical injury to the vessel is an opportunity for locally delivered cells with reparative capability to improve hyperplasia outcomes. Specifically, locally delivered endothelial cells could potentially release paracrine factors (e.g. nitric oxide), which inhibit SMC proliferation and subsequent intimal hyperplasia[61].

Given the importance of the endothelial layer and its anti-thrombogenic properties, researchers have attempted to cover metal stents with endothelial cells as early as 1988[62]. These studies have added to understanding of various cell sources and attachment methods, but none have provided a method which has led to general/widespread clinical use.

1.1.3.1 Pre-implantation seeding of stents

Direct seeding of metal stents with ECs prior to implantation has been attempted using a variety of methods. Limitations of these studies include use of immortalized or xenogeneic cell sources[63,64], pre-coating of the stent with protein or polymer[62,65-68], and prohibitively long culture of the stent and cells together[64-67].

ECs do not adhere and grow on stents manufactured from stainless steel and other metals as they do on titanium; consequently, some researchers have utilized pre-coating techniques with protein or polymer to promote adhesion of cells to these metals. Previously investigated coatings include heparinized lactone polymer[65], photocured gelatin[66], fibrin gel[67], self-assembled guanine-cytosine nanotubes[69], poly-L-lysine[70], and fibronectin[62,68,70,71]. These coatings add complexity and potential complications; fibronectin coating, for example, promotes platelet adhesion and could lead to thrombus formation on any areas of the stent with incomplete EC coverage[62,68].

Stent seeding methods used previously have largely consisted of culturing cells together with stents, with periodic rotation of the stent around its long axis to achieve even coverage. The seeding processes described are extended, ranging from 1 hour at the shortest[64] to several hours[62,65,66,71] and up to 24 hrs[67]. Following initial seeding of cells to the stents, further culture was carried out in all of these studies to allow the endothelial monolayer to achieve confluence. Prolonged culture time of the stent and cells together ranged from 2-3 days[65,67,71] to 7 days[66], or even 2 weeks[64]. Such extended

culture of cells with the device not only adds to the lead time required for the stenting procedure, but also presents issues and risks for maintaining sterility when translated to widespread clinical practice and regulatory approval. This is of particular concern when considering that all methods presented here seeded stents in an expanded configuration. For simulated delivery, stents had to be subsequently clamped onto a balloon delivery catheter (in the case of balloon-expandable stents), or compressed into a restraining delivery sheath (in the case of self-expanding stents). These extra manipulations are obviated by the proposed work.

In the case of balloon expandable stents, the abrasion between balloon and stent during expansion was found to cause loss of most cells on the lumenal surface following balloon expansion[64,71], while other studies did not address the impact of stent deployment on ECs[65]. Although some studies showed almost no lumenal cell retention after balloon expansion, others assessed coverage at 10 to 70%[71].

As an alternative to incubating the stent with cells for multiple days, Kutryk et al. proposed infusing ECs through a simple angiographic catheter to the site of stenting following deployment[63], but did not present specifics on number of cells required or extent of coverage of the stent by ECs. Another study delivered cells to a stent following deployment, but required 5-10 min cessation of flow *in vivo*. This cessation of flow is impractical in a clinical setting, especially in coronary vessels[72]. That study, which employed magnetic labeling of cultured EPCs to target magnetically charged stents,

found good seeding efficiency and coverage of cells 24 hours after the catheter-based infusion of cells[72]; however, stainless steel stents were plated with nickel to achieve the necessary magnetic charge, and this is not a practical solution for long-term biocompatibility, or for self-expanding applications. Nitinol stents did not retain sufficient charge to attract cells.

1.1.3.2 "Capture stents"

As an alternative to direct seeding, several strategies have been investigated to recruit circulating endothelial progenitor cells (EPCs) from the bloodstream. Antibodies to CD34 have been attached to stents to capture circulating EPCs. In porcine coronary arteries, these stents improved early endothelialization (2 and 5 days), but did not reduce neointimal hyperplasia at 28 or 90 days[73]. Clinical studies show that these "capture stents" are inferior to current DES[74], because the anti-CD34 antibodies were non-specific to ECs but also bound other cells, including hematopoietic stem cells and smooth muscle progenitor cells; this may result in increased neointimal proliferation[73,75]. At two year follow-up in clinical trials, a CD34-capture coronary stent showed no significant difference in target vessel failure compared to a paclitaxel-eluting coronary stent[76]. In clinical trials, a stent combining CD34 capture antibodies with sirolimus antiproliferative coating was also not significantly different from a paclitaxel-eluting stent, with no difference in target lesion revascularization after12 months[77].

Stents pre-coated with anti-VE-Cadherin (CD144) antibody were successful in capturing EPCs in healthy rabbits[78]; however, CD144 is also present on a portion of the more abundant early-outgrowth EPCs[79]. Surface-bound vascular endothelial growth factor (VEGF) exposed to the mononuclear fraction of blood *in vitro* caused an increase in VEGF-positive cells adhered to the surface over time, but was not completely specific for endothelial-like cells[80]. Covering stents with cyclic Arg-Gly-Asp peptides (cRGD) reduced neointimal area and percent area stenosis at 12 weeks in a porcine model[81], but RGD binding sites are found on many other cells and plasma proteins[82], and are not specific to ECs. Cobalt-chrome stents covered with Arg-Glu-Asp-Val (REDV) peptide in a rabbit iliac artery model showed a variety of cell types on the surface in addition to endothelium after one week, and showed no difference in endothelial coverage or degree of intimal hyperplasia compared to bare stents after four weeks[83].

A collagen matrix containing oligosaccharide sialyl Lewis X, which binds L-selectin, increased the number of mobilized EPCs when injected into a rat hindlimb ischemia model[84], although specificity of capture from the bloodstream has not been presented. Another capture strategy utilizing aptamers is under investigation but has not been tried *in vivo* and has not been shown to be fully specific to EPCs[85]. Because patients with diabetes or cardiovascular disease have greatly reduced number of circulating EPCs[86], capture stents may not be as effective as direct cell delivery, which adds the assistance of expansion in culture.

1.1.3.3 Potential advantages of catheter-based cell seeding proposal

The proposed work avoids the problems of the previously described studies for seeding stents and capturing ECs from the blood stream. This is accomplished by isolation, expansion, and seeding of ECs before implantation and deployment. Further, the proposed work will eliminate the need to culture the stent and cells together for multiple days and manipulate the stent back into/onto a delivery catheter; instead, cells will be infused at the point of care. Finally, the use of nitinol stents with their characteristic titanium oxide coating will obviate the need for additional and potentially thrombogenic coatings on the stent.

1.1.4 Blood-derived endothelial cells – an autologous cell source

Blood derived endothelial "progenitor" cells, first described by Asahara et al[87], are isolated from peripheral blood using methods described by Ingram et al.[88]. Specifically, the "late outgrowth" EPCs (also called endothelial colony forming cells or endothelial outgrowth cells) function similarly to human aortic ECs, releasing vasodilators such nitric oxide (NO)[89,90] and preventing platelet adhesion[26]. We have previously characterized blood-derived ECs for markers and gene expression[90]. Late outgrowth EPCs are superior to the more abundant early outgrowth EPCs for the proposed therapeutic use, because of their higher proliferative capacity and ability to aid vascular repair[79]. Further, EPCs are noted for their natural ability to repair damaged vasculature[91]. Arterial injury in stenting is correlated with extent of neointimal

restenosis[92], leading to the idea that direct delivery of ECs to a site of stenting could accelerate repair and reduce restenosis caused by neointimal hyperplasia. ECs seeded onto a stent have been shown to migrate into the surrounding tissue[66], further supporting this idea.

The use of blood-derived endothelial cells grown out from endothelial "progenitor" cells for clinical vascular repair is appealing for multiple reasons. Non-autologous cells present obvious problems requiring matching and immunosuppression; other proposed solutions, such as transgenic porcine cells expressing human surface markers[63], have not been investigated clinically. Sources of autologous ECs other than blood, such as digestion of saphenous or jugular veins[93], or adipose tissue microvasculature[94], require invasive surgical procedures. The reprogramming of adipose-derived stem cells to express EC markers has been demonstrated[95], but the invasive harvest procedure remains prohibitive[96]. In contrast, blood-derived endothelial cells can be obtained through a routine blood draw. Specifically, late outgrowth EPCs share many characteristics of adult endothelial cells[79]. It has been shown that EPCs can be isolated from coronary artery disease patients, and that these cells also express EC markers, proliferation potential, and produce nitric oxide[97].

The number of EPCs circulating in peripheral blood has been shown to be significantly increased following the administration of the mobilizing agent AMD3100, typically used to mobilize hematopoietic stem cells in cancer patients[98]. We have also

shown the yield of EPCs can be increased ~4.5-fold with AMD3100 in our pig model. The availability and efficacy of this agent further supports the feasibility of ECs derived from circulating EPCs as a cell source.

1.1.5 Modeling of shear stress on stents or ECs

Computational modeling of stents has been used to examine deployment forces within the stent material[99], elution profiles of drug coated stents[100], and fluid shear stresses on vessel endothelium within a fully deployed stent[101-104]. Finite element analysis (FEA) of a stent has been used to examine stresses and strains within the bulk in a stent during deployment, identifying locations and magnitudes of stress and plastic deformation during balloon expansion[99]. FEA has also been used to examine the forces within an incrementally expanded nitinol stent before it is heat treated to its set expanded diameter[105]. Additionally, FEA can predict the overall stent foreshortening following deployment, as well as elastic recoil in balloon expanded stents[99]. Through comparison with experimental results, the predictive power of the computational analysis can be assessed[106]. Commonly, FEA is used to predict fatigue behavior of stents[107], thus informing stent design and supporting applications for regulatory approval before lengthy accelerated fatigue tests have been completed. Nitinol stents intended for use in the superficial femoral or femoro-popliteal arteries are subjected to not only pulsatile fatigue, but also torsional and axial fatigue forces[21,108]. Rebelo et al. studied various computational methods for modeling pulsatile loading and patient

position on principal strains in a femoral artery stent[101]. Additionally, computational analysis has evaluated the release of drug into the lumen and into the arterial wall for drug-coated stents[100].

Computational modeling has also been used to examine fluid dynamics around a stent[100]. These studies seek to examine how a stent placed in an artery disturbs local flow patterns and imparts stress to the artery wall. In a three-dimensional flow model including recirculation through a drug-coated stent in a coronary artery[100], drug distribution was affected by stent geometry and flow, and transient accumulation of drug occurred in the vessel downstream of the stent. Other computational studies showed that thinner struts, more aligned with the primary flow direction, decrease the effect of low wall shear stress on the arterial wall[109,110]. Low wall shear stress correlates with hyperplasia leading to restenosis[111-113] and areas of inhibited EC migration onto stents.[114]. Stent strut spacing has also been shown to have a strong effect on wall shear stress, flow stagnation and recirculation[102,103,115].

To date, little is known about fluid shear stresses on the surface of stents implanted in an artery; this has been of little interest without specific applications like adhesions of cells to the struts. We are interested in these stresses as they affect EC retention in our stent seeding method, but also because transient gradients in shear affect EC function[116-118], important for future *in vitro* and *in vivo* studies. We are also interested in the degree of flow reversal observed on various stent surfaces, because the

degree of flow reversal is known to affect EC phenotype and activation of inflammatory markers.

1.1.6 Other applications of Ti in medical devices – VADs and their limitations

In addition to nitinol stents, titanium is used in other cardiovascular implantable devices which contact the bloodstream. Mechanical circulatory assist devices (MCADs) benefit heart failure patients as a bridge to transplant or a permanent destination therapy[119], with a potential for 250,000 patients annually[2]. Despite the benefits of MCADs, thrombosis and thromboembolic stroke cause significant morbidity and mortality for these patients. The potential for endothelializing these devices is related to the proposed work, but will be limited in current generation devices by prohibitively high shear stresses in the majority of the device housing[120]. Only the outlet tube is expected to have sufficiently low shear stress to allow endothelialization. While endothelializing this component may still have clinical utility and significance, and is under investigation in our lab as an extension of the methods of Aim 1, these MCAD applications will not be discussed in depth as part of this project.

1.2 Specific aims and hypotheses

The overarching goal of this project is to seed titanium cardiovascular implants with blood-derived endothelial cells (ECs) prior to implantation in order to reduce thrombosis and intimal hyperplasia. This is valuable for stents and other Ti

cardiovascular devices, and we will investigate both stents and rigid Ti tubes. We hypothesize that ECs seeded onto Ti blood-contacting surfaces minutes before implantation will create a confluent cell layer *in vivo*. We also hypothesize that adhesion and function of ECs in a deployed stent will be influenced by the shear stresses during deployment and time of adhesion prior to deployment. Specific Aims to address these hypotheses are:

Specific Aim 1: Optimize seeding of ECs onto Ti tube surfaces and characterize reduction of thrombus formation in swine. Solid Ti tubes will be used to characterize the *in vivo* response of blood to bare titanium implants and implants seeded with autologous peripheral blood-derived ECs. ECs -- derived from late outgrowth endothelial progenitor cells (EPCs) in pig blood -- will be seeded to the inner surface of Ti tubes by slowly rotating Ti tubes filled with a cell suspension. Cell attachment and coverage after seeding will be evaluated to determine parameters necessary for optimal seeding; the goal is that ECs cover the surface when spread, without requirement for division. Tubes will be implanted into the low shear stress environment of the vena cava and exposed to blood flow to evaluate the thrombosis response.

Specific Aim 1 Hypotheses: (1) ECs seeded onto Ti blood-contacting surfaces minutes before implantation will create a confluent cell layer *in vivo*. (2) This treatment

will prevent thrombosis when inserted into the pro-thrombotic environment of the inferior vena cava (IVC) in swine.

Specific Aim 2: Determine fluid stresses on implanted carotid artery stent and predict suitability of surfaces for EC seeding. ANSYS CFX modeling software will be used to calculate the shear stresses and oscillatory shear indices acting on adherent cells after implantation of the stent in a carotid artery, for both normal and hypertensive flow waveforms. Both wall shear stress and oscillatory shear index are expected to have a significant impact on the phenotype and behavior of cells seeded to the surface. We will compare the calculated shear stresses to our previous studies with ECs on titanium, to make predictions about the cells' ability to remain adherent on the surface.

Specific Aim 2 Hypothesis: Fluid stress conditions on the surfaces of an implanted carotid artery stent are amenable to supporting endothelial cell retention and antithrombotic function.

Specific Aim 3: Evaluate adhesion and function of seeded ECs on stents after deployment *in vitro* and *in vivo*. In this study, stents will be seeded with blood-derived ECs minutes before deployment, either into an *in vitro* flow circuit, or *in vivo* in the carotid artery of pigs. Stents will be seeded by infusion of a cell suspension into a modified stent delivery catheter, for both *in vitro* and *in vivo* portions of the study. The

in vitro flow circuit will simulate shear stresses *in vivo.* Retention and function of ECs on stent surfaces following physiological flow conditions will be evaluated after 24 hours. In the second part of the study, stents seeded with autologous porcine ECs will be deployed into porcine carotid arteries *in vivo* and evaluated after 48 hours of blood flow for cell presence and spreading as well as viability.

Specific Aim 3 Hypotheses: (1) Modification of a commercial stent delivery system with micropores enables rapid infusion of ECs and adhesion to nitinol stents; (2) ECs remain adherent and spread to form a functional layer after stent deployment and under arterial fluid shear stress conditions.

2. Use of autologous blood-derived endothelial progenitor cells at point-of-care to protect against implant thrombosis in a large animal model

The text and figures included in Chapter 2 were previously published in the November 2011 edition of Biomaterials. The full citation for the article is: Alexandra E. Jantzen, Whitney O. Lane, Shawn M. Gage, Ryan M. Jamiolkowski, Justin M. Haseltine, Lauren J. Galinat, Fu-Hsiung Lin, Jeffrey H. Lawson, George A. Truskey, Hardean E. Achneck. Use of autologous blood-derived endothelial progenitor cells at point-of-care to protect against implant thrombosis in a large animal model. Biomaterials, Volume 32, Issue 33, November 2011, Pages 8356–8363. http://dx.doi.org/10.1016/j.biomaterials.2011.07.066. Elsevier does not require permission for authors to reuse their own articles in a dissertation, but an optional license can be obtained and is included in Appendix B.

2.1 Chapter synopsis

This chapter describes the first phase of developing a point-of-care method for seeding titanium (Ti) vascular implants with autologous endothelium: a materials proof of concept that endothelial cells will spread on Ti surfaces *in vivo* and prevent thrombosis in contact with the bloodstream. Ti is commonly utilized in many cardiovascular devices, e.g. as a component of nitinol stents, intra- and extracorporeal mechanical circulatory assist devices, but is associated with the risk of thromboemboli formation. We propose to solve this problem by lining the Ti blood-contacting surfaces

with autologous peripheral blood-derived late outgrowth endothelial progenitor cells (EPCs) after having previously demonstrated that these EPCs adhere to and grow on Ti under physiological shear stresses and functionally adapt to their environment under flow conditions *ex vivo*. Autologous fluorescently-labeled porcine EPCs were seeded at the point-of-care in the operating room onto Ti tubes for 30 min and implanted into the pro-thrombotic environment of the inferior vena cava of swine (n = 8). After 3 days, Ti tubes were explanted, disassembled, and the blood-contacting surface was imaged. A blinded analysis found all 4 cell-seeded implants to be free of clot, whereas 4 controls without EPCs were either entirely occluded or partially thrombosed. Pre-labeled EPCs had spread and were present on all 4 cell-seeded implants while no endothelial cells were observed on control implants. These results suggest that late outgrowth autologous EPCs represent a promising source of lining Ti implants to reduce thrombosis *in vivo*.

2.2 Introduction

Titanium (Ti) is commonly utilized as a component in the engineering of cardiovascular devices. Examples include mechanical circulatory assist devices for the treatment of heart failure and nitinol vascular stents, which are coated with a layer of Ti on their blood-contacting surface and used in the treatment of peripheral vascular disease. Whereas mechanical circulatory assist devices are associated with the risk of distal thromboemboli causing strokes[121], nitinol stents carry a high risk of in-stent

restenosis and thrombosis. Approximately 40%-50% of bare metal nitinol stents in the femoropopliteal region are occluded within 2 years, and about 20% of patients who receive nitinol carotid artery stents will suffer from re-occluded stented neck vessels after only 2 years[122,123]. Further, nitinol stents occlude in >30% of patients with superficial femoral artery disease lesions after only 1 year[124]. Drug-eluting stents may provide for better outcomes. However, no significant difference was found in a head-to head comparison between bare metal stents and sirolimus drug-eluting stents implanted into the infrainguinal vasculature[7]. Even in the coronary vasculature, drug-eluting stents that once held the promise of mitigating in-stent restenosis have been hampered by an increasing risk of late-stent thrombosis, likely due to incomplete coverage with healthy endothelium secondary to the drugs used[125]. We propose to solve these problems by lining the titanium blood-contacting surfaces of intravascular devices with autologous peripheral blood-derived endothelial progenitor cells (EPCs) within minutes of implantation. Since these EPCs are derived from the same patient who would receive the cell-coated implant, there is no risk for rejection by the immune system. The anti-thrombotic endothelial coating would also reduce the necessity of anti-coagulative drugs for patients treated with intravascular devices, e.g. stents and circulatory assist devices, and reduce the bleeding complications associated with such medications.

We have recently demonstrated that it is feasible to grow blood-derived EPCs on Ti surfaces, that EPCs grow to a confluent monolayer on Ti under static conditions and

physiological flow after only a few minutes prior adhesion time, and that EPCs adhere extremely well to such surfaces, even under supraphysiological shear stresses[126]. We have further shown that EPCs on smooth Ti surfaces functionally adapt to their environment under flow, produce nitric oxide (dependent on the magnitude of shear stress stimulation), and dramatically reduce platelet adhesion[126]. In order to provide the initial feasibility and benefit of such EPC-lined surfaces in a large animal model, we lined Ti tubes with porcine blood-derived EPCs and implanted these tubes into the inferior vena cava (IVC) of the pigs from which the cells were derived. Uncoated 'bare' Ti tubes implanted under the exact same conditions served as controls. We chose swine for this study because the pig is one of the most accepted animal models for studying coagulation biology, inflammation, and specifically vascular prostheses[127-130]. Since our null-hypothesis is that EPC-linings will not be able to reduce the incidence of thrombosis, we implanted the Ti tubes into the pro-thrombotic environment of the inferior vena cava, as opposed to the aorta, to increase the likelihood of thrombosis.

2.3 Materials and methods

2.3.1 Titanium tube assembly

Ti tubes (commercially pure, grade 2) were purchased with dimensions 12.7mm ODand 9.4mm ID (TicoTitanium) and cut to a length of 45 mm. Tubes were sectioned into 3 equal segments longitudinally with a high speed steel saw. The inner surfaces were polished with a bench grinder and metalworking wheel (Scotch-Brite), followed by

manual polishing with emery cloth (3 M) to further even out the surface and remove any visible pits. Ti sections were then cleaned with Alconox soap solution and aqua regia (1:3 concentrated nitric acid to concentrated hydrochloric acid) as previously described for Ti surfaces[131]. Sets of three Ti sections were reassembled into tubes with Polyvinyl chloride (PVC) heat shrink tubing (Insultab, expanded ID 15.88 mm, recovered ID 7.95 mm). For the assembly of our seeding chamber, silicone tubing (16.64 mm OD, 9.52 mm ID, 3 cm length) was added to both ends of the Ti tube and a 'cut-off' syringe head with luer was added to one end (Figure 2.1). All components were gas sterilized prior to use (18 h, 55 °C).

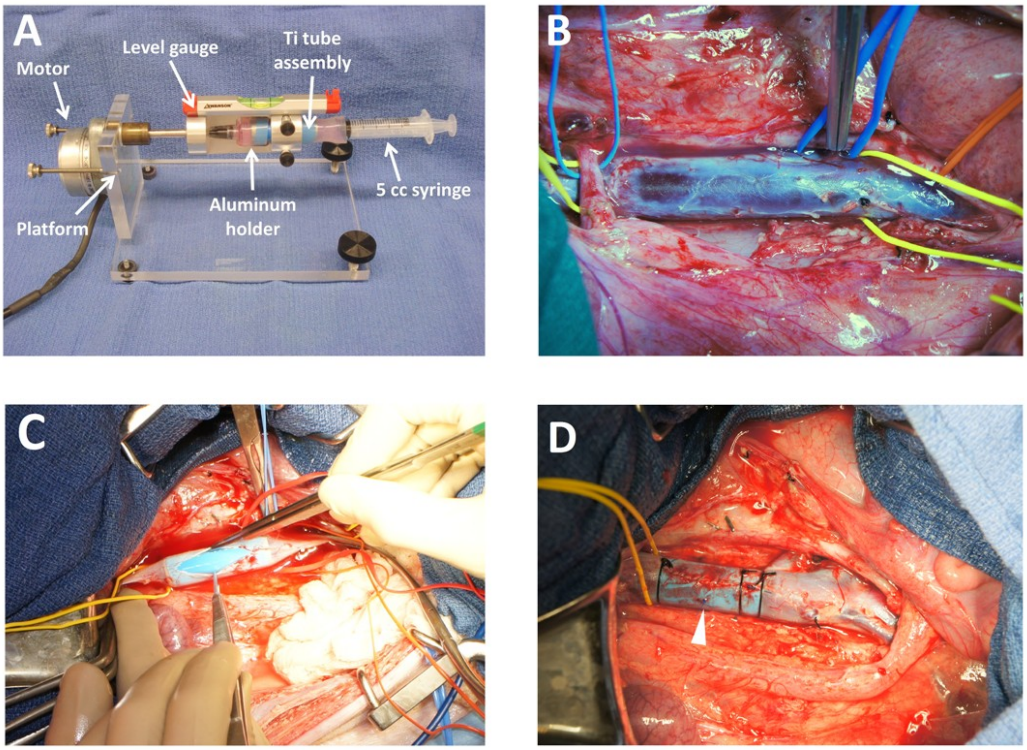

Figure 2.1: Ti tube seeding and implantation.

(A)Ti tube seeding device and Ti tube seeding chamber. The Ti tube is placed inside the aluminum holder. To assemble the seeding chamber, a 'cut-off' syringe head with luer is attached via silicone tubing to the Ti tube (left end of Ti tube) and a 5 cc syringe is attached via silicone tubing (right end of Ti tube). The level gauge ensures equal distribution of EPCs during rotation of the seeding chamber. A sterile sheath surrounding the seeding chamber has been removed in order to facilitate viewing of the seeding chamber inside the aluminum holder. (B) Intraoperative view of skeletonized infrarenal IVC, prior to venotomy. The proximal end of the IVC is encircled with a yellow vessel loop (left). The overlying right renal artery is encircled with a blue vessel loop (left). A blue vessel loop encircles the left 7th lumbar vein. The distal IVC is encircled with a yellow vessel loop at its bifurcation into the common iliac veins (right) and the right external iliac artery is encircled with an orange vessel loop as it crosses the right common iliac vein (far right). (C) Ti tube insertion into IVC. Both ends of the IVC are clamped. The blue PVC heat shrink tubing is recognizable inside the IVC. (D) Post-insertion view of the infrarenal IVC. The yellow vessel loop encircles the proximal IVC. Note the 6-0 polypropylene 'stay suture' that was placed through the adventitia and PVC heat shrink tubing to prevent the device from migrating (white arrow).

2.3.2 X-ray photoelectron spectroscopy

The atomic composition of our Ti samples was determined using a Kratos Axis Ultra X-ray Photoelectron Spectroscope and compared to the surface of a Cordis Precise RX self-expanding Nitinol stent. Spectra were obtained at 2.0×10^{-8} Torr using a monochromated aluminum K-alpha X-ray source at a power of 15 kV and an emission current of 10 mA. Survey scans were performed over the range of 5-1200 eV with a step eV of 1, a dwell time of 200 ms, a resolution of 160 eV, and a slot aperture measuring an area of 300 μm x 700 μm. A regional scan for titanium was performed on both samples over the range of 450-470 eV with a step eV of 0.1, a dwell time of 298.5 ms, a resolution of 160 eV, and the same slot aperture. In addition, a survey scan of the stent was performed using a "small spot" field of view with a 2 mm aperture measuring a 110 μm diameter spot on the stent surface and the same scanning parameters used for the previous survey scans. The elemental peaks of the samples were ascertained from survey scans using CasaXPS software and utilizing a relative sensitivity function library specific to the Kratos Axis Ultra system.

2.3.3 Optical profilometry

Surface roughness was analyzed by optical profilometry (Zygo NewView 5000). The 3D surface profiler uses non-contacting white light interferometry to acquire high resolution z-images, from which surface roughness averages (R_a) are reported according to equation (1) [132], after subtraction of a "cylinder" shape in the system software

(MetroPro, Zygo) to account for and remove the curvature of the tube itself.

$$R_a = \frac{1}{n}\sum_{i=1}^{n} |y_i| \quad (1)$$

where y_i represents the differences between the surface profile and the surface mean line for the ith data point of n equally spaced data points along a trace. Three fields (0.72 x 0.5 mm each) were measured on each of 3 Ti tube sections, and all R_a values from a single Ti tube section were averaged to obtain n = 1 for a total sample size of n = 3.

2.3.4 EPC isolation

All experiments with swine were approved by the Duke University Institutional Animal Care and Use Committee (IACUC) and were conducted in accordance with the National Institute of Health Guidelines for the Care and Use of Laboratory Animals. Yorkshire swine (2 male, 6 female, at an initial weight of 46.6 ± 0.89 kg) underwent a blood draw 30 days prior to Ti tube implantation to allow sufficient time for EPC isolation and amplification in culture (only 4 pigs actually received cell-seeded implants, the other 4 received bare metal control implants). The pigs were sedated with Acepromazine (1.1 mg/kg) and Ketamine (22 mg/kg) intramuscular. Intubation was achieved with an endotracheal tube (30 cm length, 8 mm ID), and the pigs were anesthetized with Isofluorane by mask. The pigs' groins were cleaned and sterilized with DuraPrep, and femoral vein access was obtained with a 5 F micro-introducer kit (Galt Medical) using the Seldinger technique[133]. After discarding the first 5 mL of blood, 45 mL of blood were collected into syringes containing 10 mL anticoagulant

citrate dextrose solution (Pall Corporation). This was followed by 1:1 dilution with Hank's buffered salt solution (without $CaCl_2$, $MgCl_2$, $MgSO_4$) and layered on equal volumes of Histopaque to create well-defined layers. The mononuclear cell layer was collected as described previously[126] and plated into two 12-well plates in full EPC growth medium (MCDB-131 medium with 2 mM Lglutamine, Cellgro, 2% porcine serum, Gemini Bio-Products, and EGM-2 SingleQuots,Lonza) at 37 °C, 5% CO_2.

2.3.5 Flow cytometry

For each cell isolation, EPCs were tested with flow cytometry for presence or absence of surface markers CD31 (Platelet Endothelial Cell Adhesion Molecule 1, PECAM-1), CD14 and CD45, as described for these cells previously[126]. Further, we tested for CD 106 (Vascular Cell Adhesion Molecule 1, VCAM-1) with directly fluorescein isothiocyanate-conjugated mouse anti-porcine VCAM-1 antibody (Antigenix America, APG106F). Mouse IgG1 served as isotype control.

2.3.6 Titanium tube seeding

The custom device for seeding Ti tubes was built by mounting a synchronous timing motor (Herbach & Rademan) on a plexiglass machined stand that has adjustable legs to allow adjustment of rotating device with a water leveling gauge (Swanson). The motor was connected via a stainless steel axle to a machined aluminum holder with a mold fitting the Ti tube seeding chamber of Section 2.3.1. (Figure 2.1A). For *in vitro* seeding experiments, adherent EPCs were labeled with the fluorescent dye Cell Tracker

Orange CMRA (Invitrogen) in serum-free medium (15 min, 37 °C). For *in vivo* experiments, adherent EPCs were labeled with the long-term fluorescent dye PKH26 (Sigma-Aldrich) at a concentration of 4 μM (4 min, room temperature), and the reaction was stopped with porcine serum (Gemini Bio-Products). Following labeling, cells were dissociated with Trypsin (0.25%, Lonza, at 37 °C for 3 min) and counted, then re-suspended to a final concentration of 2.0 x 10^6 cells/mL (see Section 2.4.5. for optimization of cell suspension density) in serum-free medium EBM-2 (Lonza) with EGM-2 SingleQuots (Lonza). The EPC suspension was introduced into the Ti tube by a syringe attached with silicone tubing (Figure 2.1A), and a luer cap added to the end of the 'cut-off' syringe head after purging all air bubbles from the Ti tube. The Ti tube was placed inside a sterile sheath to maintain sterility of the system and secured into the machined aluminum holder (Figure 2.1A). Next, the seeding device with cell suspension was rotated for 30 min at 37 °C in ambient air at 10 rotations per hour, as determined empirically in preliminary studies. To evaluate adherent EPCs after the seeding period, Ti tube sections were rinsed twice in phosphate-buffered saline (with $CaCl_2$ and $MgCl_2$, PBS) after seeding and fixed in 10% formalin for 15 min, followed by 2 more rinses with PBS. Cell areas were measured in 100-120 cells per Ti tube section using Image J software immediately after 30 min seeding by rotation (designated time zero) and after a 24 h static culture time following the seeding by rotation period (designated as time 24 h). Values within each Ti tube section were averaged for a single

sample; data from four samples were obtained at time zero and data from three samples after 24 h static culture. To evaluate the surface density of adherent cells after the seeding period, the total number of cells was determined in 20 random fields per Ti tube section (Image J). Cell numbers were divided by the area of each field to obtain a density. Values from all fields within each experiment were averaged to obtain each n = 1, and a total of n = 3 Ti tubes were used at each of three different EPC suspension concentrations. The overall percent of cells adherent after seeding was calculated using the cell suspension concentration, volume and surface area for each Ti tube.

2.3.7 Shear stress approximation in porcine inferior vena cava

Vessel dimensions and flow rates were measured in an exploratory surgery in a pig (50 kg, representative of the size of pigs at device implantation) with an ultrasonic perivascular flow probe (Transonic), allowing the wall shear stress τ (dyn/cm^2) to be estimated according to[134]

$$\tau = \frac{4\mu Q}{\pi r^3} \tag{2}$$

where, μ is the blood viscosity at 37 °C (0.0465 g cm^{-1} s^{-1})[135], Q is the measured volumetric flow rate (8.33 cm^3/s), and r is the measured vessel radius (0.7 cm). Therefore

$$\tau = \frac{4\left(0.0465\frac{g}{cm \cdot s}\right) \cdot 8.33\frac{cm^3}{s}}{\pi \cdot (0.7cm)^3} = 1.44\ \frac{dyn}{cm^2} \tag{3}$$

Since this shear stress is approximately ten-fold lower than the 15 dyn/cm^2 commonly used to model arterial flow[134], the IVC provides a pro-thrombotic environment in which to challenge our EPC-seeded devices.

2.3.8 Ti tube implantation in swine

Eight Yorkshire swine (2 male, 6 female, at a weight of 52 ± 1.6 kg) underwent consecutive surgeries with either EPC-seeded or bare metal device implantations (see Jantzen et al. Supplementary Data, Swine preparation for surgery and Swine laparotomy[136]). After the IVC had been identified we used sharp and blunt dissection to free the vessel from the surrounding tissue and skeletonize it circumferentially from the level of the right renal vein proximally to its iliac bifurcation distally (Figure 2.1B). Several lumbar veins were ligated with silk sutures and divided to prevent any retrograde bleeding around the implanted Ti tube once venous circulation was restored. Before proceeding any further, the Ti tube seeding was initiated in the operating room with fluorescently-labeled EPCs with our seeding device as described in Section 2.3.6. Unseeded bare metal Ti tubes were implanted as controls.

100 USP/kg of heparin was administered intravenously 5 min prior to clamping the IVC (and completion of the seeding process). A profunda clamp was placed, first on the distal end of the IVC at the iliac bifurcation, then proximally just distal to the right renal vein using a 45° straight vascular clamp. A # 11 scalpel blade was used to create a

small venotomy in the middle of the exposed segment. This was extended with Potts scissors to fashion a longitudinal venotomy measuring 4 cm in length (Figure 2.1C).

The Ti tube was implanted (see Jantzen et al. Supplementary Data, Ti tube insertion[136]) and two 2-O silk ties were placed around the IVC containing the device (at the proximal and distal end of the Ti tube) to prevent the development of a false lumen (Figure 2.1D). Moreover, one 6-O polypropylene 'stay suture' was placed through the IVC's adventitia into and through the heat shrink PVC tubing to prevent migration of the device inside the IVC (Figure 2.1D). The abdomen was then closed and the pig recovered (see Jantzen et al. Supplementary Data, Swine abdominal closure[136]). All surgeries were accomplished without any unforeseen complications. The blood loss was minimal in all procedures. The duration of IVC clamp time was similar between the groups (Figure 2.2A). Furthermore, there was no significant difference in the total anesthesia time or the time pigs were immobilized for surgery between the cell-seeded treatment group and control group (Figure 2.2B). All eight pigs in the study mobilized and fully recovered before device explantation 3 days later.

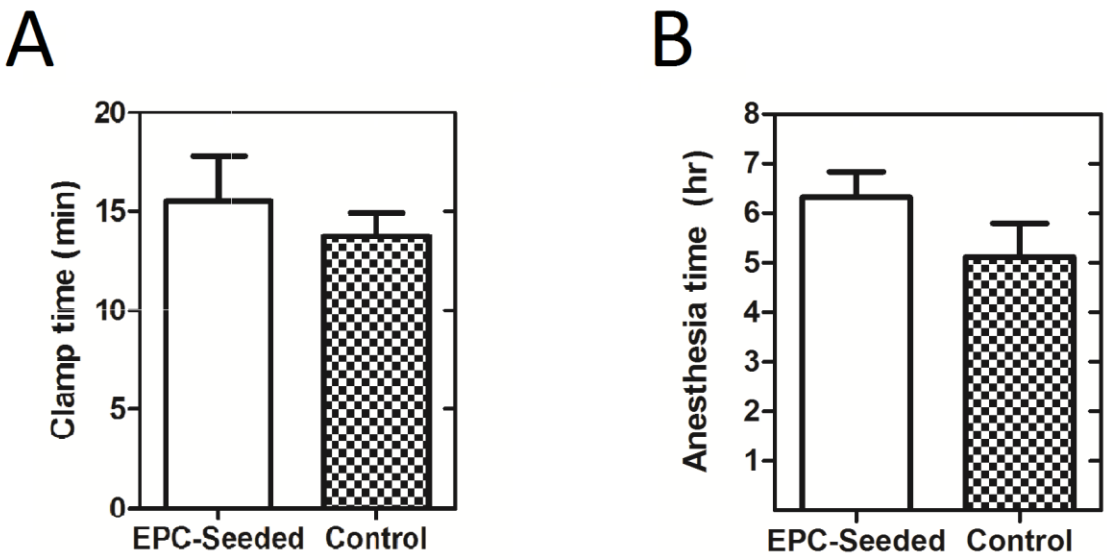

Figure 2.2: Intraoperative clamp times of IVC during insertion and total time of anesthesia during surgery (in hours).

(A) Intraoperative clamp times of IVC during device insertion. Clamp times were not significantly different between EPC-seeded and control implant groups (15.5 ± 2.3 min and 13.8 ± 1.2 min, respectively, p = 0.517, n = 4 for each group, two-tailed t-test). (B) Total time of anesthesia during surgery (in hours). Duration of anesthesia was not significantly different between EPC-seeded and control implant groups (6 h 19 min ± 31 min vs. 5 h 7 min ± 41 min, p = 0.21, n = 4 for each group, two-tailed t-test).

2.3.9 Ti tube explantation

Three days after implantation, pigs were sedated, intubated and anesthetized as described above. The laparotomy and dissection were conducted as outlined previously and the Ti tube was explanted en bloc after clamping the IVC proximal and distal and transecting the IVC proximal and distal with heavy scissors. The pig was euthanized after the device had been explanted with Euthasol euthanasia solution (390 mg/mL Pentobarbital Sodium and 50 mg/mL Phenytoin Sodium at 1 mL/10 lbs) according to our IACUC protocol. The Ti tube was immediately rinsed with PBS x 3 and its lumen photographed from both ends with a high resolution digital camera (Nex-3, Sony). The implant with clot (if present) was then submerged in 3.7% paraformaldehyde for fixation for 4 h. After fixation, the Ti tube was opened by incising the PVC heat shrink tubing with a # 15 scalpel blade and its inner surface photographed as well. None of the pigs received any form of anticoagulation other than the initial heparin bolus 5 min prior to implantation of the device (treatment and control alike).

2.3.10 Thrombosis scoring

Thrombosis outcomes of explanted Ti tubes were classified into three categories: 'Fully clotted,' 'partially clotted,' or 'no clot.' Clots in the 'fully clotted' category extended throughout the entire length and cross-section of the tube lumen, whereas 'partial clots' did not fill the tube, either in length or in cross-section. Tubes, which were clean with no significant thrombosis, were classified as 'no clot.' Outcomes were scored

by presenting the gross photographs of the device lumina and their opened sections to three separate reviewers, who were blinded as to whether the device had been seeded with EPCs or was a control implant. Where the reviewers disagreed in their classification, we biased their assessment towards the null-hypothesis, that there is no difference in outcome between cell-seeded and bare Ti tubes, e.g. if a bare metal tube were rated 'partially clotted' vs. 'fully clotted,' we would classify it as 'partially clotted.'

2.3.11 Immunohistochemistry/microscopy

In addition to the pre-implantation label PKH26 (Sigma-Aldrich), cell nuclei of fixed Ti tube segments were stained with Hoechst 34580 nucleic acid stain (Invitrogen, diluted 1:1000 in PBS x 15 min). To stain Ti tube sections for PECAM-1 (cell-cell junctions), samples were incubated with mouse anti-porcine CD31 (Antigenix America #APG311, diluted 1:100, for 1 h at 37 °C) after blocking with 10% normal goat serum (Gibco, for 30 min at RT). Samples were then rinsed x 3 with PBS and incubated with the secondary antibody goat anti-mouse AlexaFluor488 (Invitrogen #A-11001, diluted 1:500, for 45 min at 37 °C). Appropriate positive and negative control experiments were performed to rule out non-specific antibody binding to Ti surfaces. Following 3 more washes with PBS, samples were visualized with an upright Leica DMRB fluorescent microscope with a Qimaging Qicam monochrome digital camera and Image Pro Plus software (Leica). Cell surface area was determined with Image J software, after seeding x 30 min vs. subsequent *in vivo* experiments x 3 days, as described in Section 2.3.6. The

confluent density was calculated by counting the number of cells per field as described in 2.3.6. Additionally, samples were imaged with a Zeiss 780 confocal upright fixed stage microscope and 10x objective (Zeiss), and images were captured with Zeiss software.

2.3.12 Statistics

To evaluate cell spreading, a one-way ANOVA was performed comparing the area of cells at time point zero after seeding, after 1 day of static culture, and after 3 days *in vivo* (on the Ti tube implanted surface), followed by a post hoc two-tailed t-test. A one-way ANOVA was also used to test for differences in cell adhesion percentage with cell suspension density. Assuming a linear relationship between adhesion density and cell suspension[137,138], correlation of these variables was performed with a linear regression analysis, followed by an F-test to confirm that the slope was significantly different from zero. A two-tailed t-test was used to compare IVC clamp time between treatment and control groups and total time of anesthesia between both groups, respectively. To compare thrombosis between control and cell-treated implants after 3 days *in vivo*, a 2 x 3 contingency table was used with the Fisher's exact test[139]. The significance level was assumed to be 0.05 for all tests. Results were reported as mean ± standard error.

2.4 Results

2.4.1 Ti surface composition

X-ray photoelectron spectroscopy indicated that the chemical composition of the nitinol self-expanding stent (Cordis) was very similar to our manufactured Ti tube surfaces. Regional scans of Ti 2p ranges showed that both our Ti tube and nitinol stent were composed of Ti primarily as TiO_2, with Ti $2p_{3/2}$ peaks matching an expected peak at 458.8 eV[140] (Figure 2.3A,B). Of particular interest, XPS revealed the absence of nickel on the stent surface in the survey scan, confirming that polishing of the nitinol stents by the manufacturer results in a titanium oxide outer layer on the alloy surface.

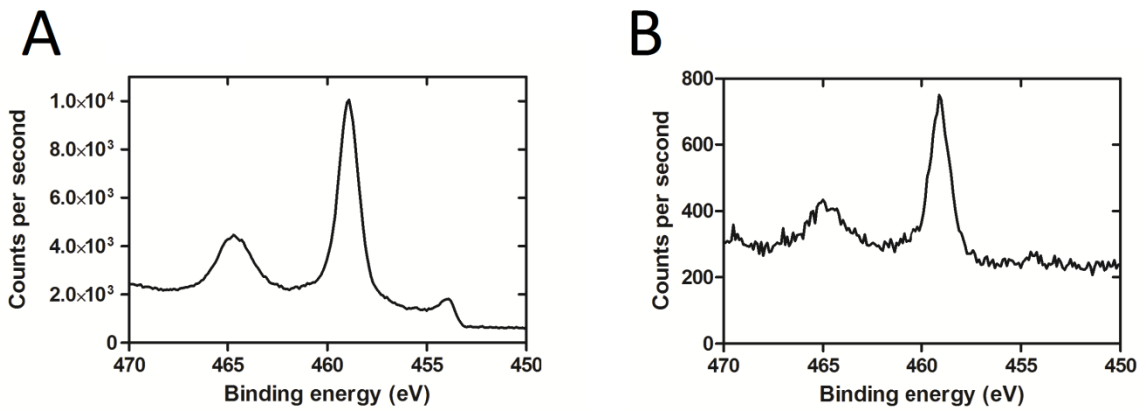

Figure 2.3: XPS spectrum of Ti tube and nitinol stent.

(A) XPS spectrum of Ti tube with binding energy peaking at 458.9 eV, corresponding to the Ti $2p_{3/2}$ electron configuration. (B) XPS spectrum of the nitinol stent with binding energy peaking at 459.1 eV, indicating comparable TiO_2 composition. Note that the nitinol stent was imaged in its expanded state with a small field of view focusing on a stent strut only, whereas the titanium tube was imaged with a larger field of view, which is reflected by the difference in signal intensity (measured in counts per second) between the Ti tube and nitinol stent.

2.4.2 Ti surface topography

The surface topography of our Ti tubes was evaluated with optical profilometry. The roughness average (Ra) for the titanium tubes was found to be in the sub-micrometer range (0.59 ± 0.02 μm, n = 3), similar to roughness values reported for nitinol alloys used in biomedical applications [141].

2.4.3 Flow cytometry results

All EPCs exhibited typical cobblestone morphology by phase contrast microscopy and tested positive for presence of PECAM-1 and negative for surface markers CD14 and CD45. Further, we confirmed absence of VCAM-1 for cells cultured *in vitro*, which, if present, would indicate an undesirable pro-inflammatory activated phenotype of our endothelial progenitor cells [142,143].

2.4.4 EPC adherence and spreading on Ti tube surface *ex vivo*

EPCs seeded onto Ti tubes with our seeding device (Figure 2.1A) and cultured under static conditions for 24 h adhered to and spread on the Ti surface and formed a confluent layer. Cell areas were significantly greater after 24 h of static culture than immediately following cell seeding (852.0 ± 23.2 mm^2 vs. 184.5 ± 6.1 mm^2, $p < 0.0001$, Figure 2.4A). We found in these seeding experiments with static culture that seeding concentrations of 1-2 x 10^6 cells/mL resulted in confluent cell coverage after 24 h.

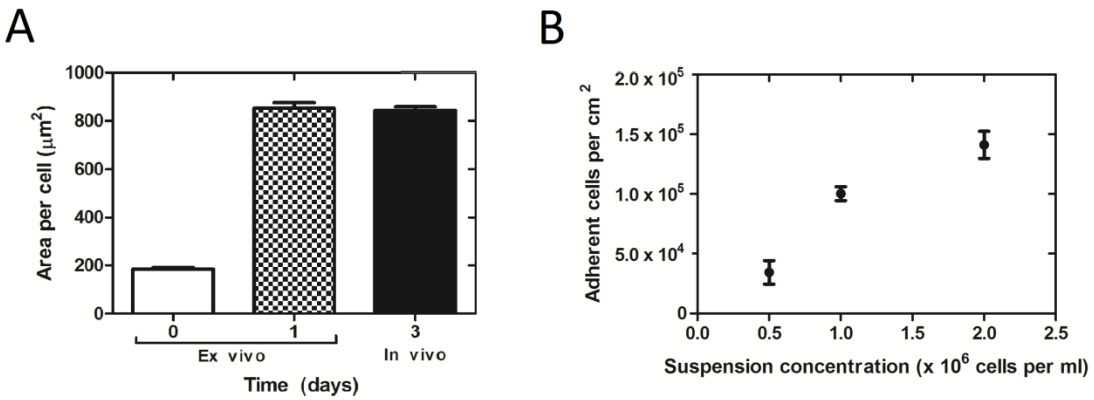

Figure 2.4: EPC Spreading on Ti tubes and EPC surface coverage with suspension density.

(A) EPC Spreading on Ti tubes at time zero after seeding, after 1 day of static culture *ex vivo*, and after three days *in vivo*. EPCs' area was significantly greater at 1 and 3 days than at time zero ($p < 0.0001$, n = 3 at 1 day, n = 4 at 0 and 3 days, 1-way ANOVA and post hoc t-test). (B) EPC surface coverage with suspension density. The number of adherent cells per area significantly increased as suspension concentration increased ($p < 0.001$, $r^2 = 0.82$, n = 3 for each concentration, linear regression analysis).

2.4.5 EPC suspension density

The number of adherent cells inside the Ti tubes immediately after the 30 min seeding process increases with the cell suspension concentration (Figure 2.4B). To compensate for any possible loss of EPCs during handling in the surgical implantation, we determined the optimal seeding density of 2×10^6 cells/mL. This resulted in a greater number of cells adhering to the surface than required for a confluent layer of EPCs inside the Ti tubes ($1.41 \pm 0.11 \times 10^5$ cells/cm^2 adherent vs.$1.04 \pm 0.03 \times 10^5$ cells/cm^2 at confluence after 24 h of static culture, n = 3 for each concentration tested). The optimal suspension density was used for all *in vivo* experiments. Only 34% ± 9% (n = 9) of the total number of cells in suspension adhered, and the percentage of adherent cells was not significantly different for different suspension densities ($p = 0.27$).

2.4.6 Thrombosis results

Thrombosis results, as scored by blinded reviewers, are as follows: In the bare metal control group, 2 of 4 implants were fully clotted (Figure 2.5A,B) and 2 of 4 implants were partially clotted (Figure 2.5C,D). All EPC-seeded Ti tubes (4 of 4) were free of clot after 3 days implantation (Figure 2.5E,F). By Fisher's exact test[139], the treatment significantly protected against thrombosis ($p < 0.03$).

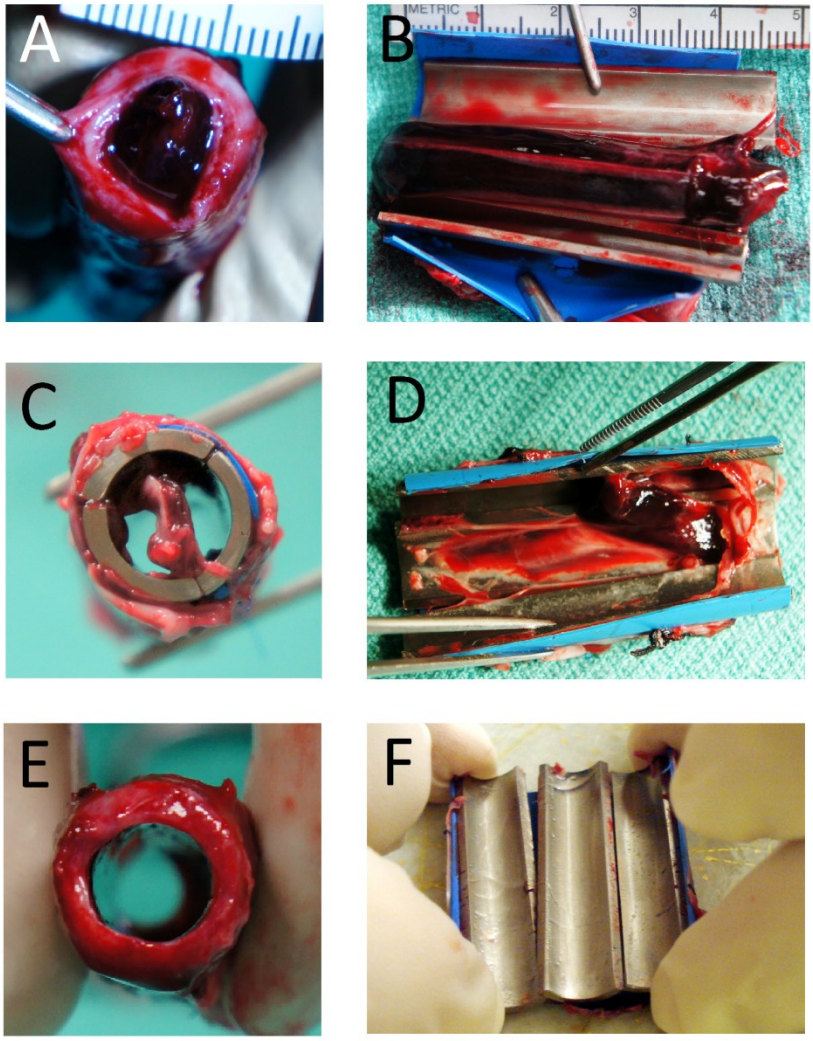

Figure 2.5: Categorization of thrombosis outcomes.

Representative pictures of Ti tubes (A,B) fully clotted, (C,D) partially clotted, and (E, F) not clotted. Tubes are shown in two orientations -a transverse view with tubes intact (left column)- and in a longitudinal view of the inner surface after tube dissection (right column).

2.4.7 EPC retention and spreading inside Ti tubes *in vivo*

The autologous fluorescent EPCs, which were seeded onto Ti tubes before surgery, were visualized on every one of the 4 cell-seeded implants after 3 days *in vivo* and found to have spread on the surface to form a confluent monolayer (Figure 2.6A,B). The area per cell was significantly greater after 3 days exposed to blood flow than immediately following cell seeding ($842.5 \pm 16.0\ \mu m^2$ vs. $184.5 \pm 6.1\ \mu m^2$, $p < 0.0001$), but not significantly different than the area of confluent cells cultured under static conditions *ex vivo* ($842.5 \pm 16.0\ \mu m^2$ vs. $852.0 \pm 23.2\ \mu m^2$, $p = 0.74$, Figure 2.4A). All endothelial cells visualized on the EPC-seeded Ti tubes contained PKH26 (red), suggesting that they were of pre-seeded EPC origin. Immunohistochemical counterstaining of the pre-labeled fluorescent EPCs on the explanted Ti device surface with anti-PECAM-1 antibodies confirmed that all endothelial-like cells on the Ti surface had maintained their endothelial-like-morphology *in vivo* (Figure 2.6A,B). Since there were no endothelial cells observed on the surface that did not exhibit the pre-implantation florescent EPC label, we conclude that no 'fall-out' endothelial cells from blood had adhered to and populated the implant surface. Anti-PECAM-1 staining of thrombus-free areas in the partially occluded Ti tubes failed to reveal any endothelial cells. However, we did find clusters of leukocytes (based on nuclear morphology) in those areas of bare metal implants (Figure 2.6C).

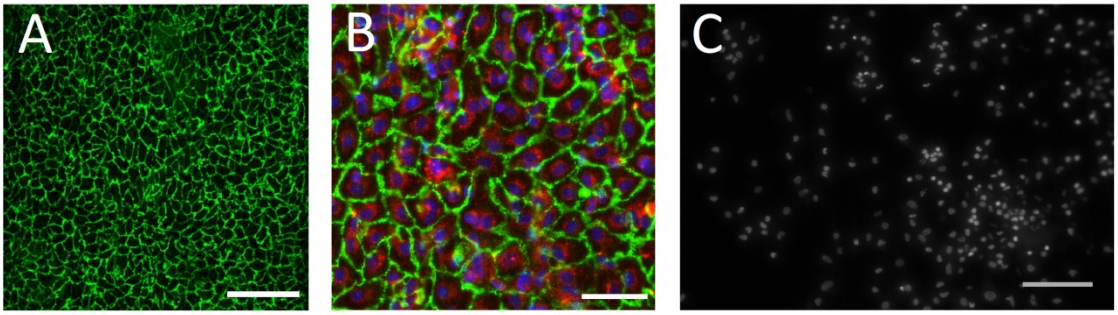

Figure 2.6: Cells on Ti surface following 3 days *in vivo* implantation.

EPCs on Ti surface were stained for PECAM-1 (green) after 3 days in porcine IVC. (A) Scale bar = 200 μm (B) EPCs additionally showing pre-implantation stain PKH26 (red) and nuclei stained with Hoechst 34580 (blue). Scale bar = 50 μm. (C) Cell nuclei on bare metal control implant surface stained with Hoechst 34580, showing presence of macrophages, T cells and granulocytes in a non-uniform distribution. Scale bar = 100 μm.

2.5 Discussion

Our results demonstrate that blood-derived EPCs can protect against thrombosis in a short-term large animal model. We chose to use pigs as the animal model for this study because their anatomy and physiology closely resembles that of humans[144]. Additionally, the vessel size of our 50 kg pigs is very similar to those of children or small adults.

Since our *ex vivo* studies had previously demonstrated that late outgrowth EPCs on Ti surfaces can withstand more than 5-10-fold higher shear stresses than they would encounter in the arterial circulation [126], we elected to evaluate the EPCs' functional benefit in the low shear stress environment of the inferior vena cava, which biases our outcomes towards thrombosis, rather than implanting them into the higher shear stress environment of the aorta. Furthermore, porcine blood is hypercoagulable as compared to human blood[127]. Still, EPC treatment was able to prevent clot formation in all 4 of 4 implants. Moreover, in our earlier studies we had shown that EPC treatment blocks platelet adhesion to the titanium surface [126]. Therefore, we believe that EPC treatment will even more so prevent thrombosis in humans, especially when utilized to line intravascular devices in the higher shear stress environment of the arterial system. In order to prevent the introduction of bias in evaluating our surgical outcomes -- device thrombosis or patency -- we had 3 different investigators, who were blinded to the treatment of Ti tubes, and had them score the degree of thrombosis in high resolution

photographs of the implants. Whereas everyone had judged the cell-treated devices to be free of clot, there was some disagreement among investigators in 2 control implants as to whether they should be classified as fully thrombosed or partially thrombosed. According to our scoring system, these were automatically biased towards the null-hypothesis of no difference between the groups and ranked as only partially thrombosed. Still, we were able to find a statistically significant difference in the outcomes of our 8 consecutive surgeries with $p < 0.03$.

It is well established that the duration of surgery and anesthesia time is associated with the risk for venous thrombosis [145-147]. Therefore, we compared the total time each pig was immobilized for the procedure (total time of anesthesia) between the groups. We did not find any significant difference - in fact, the anesthesia time was slightly longer in the EPC-treated device implantations as compared to that of bare metal devices. Furthermore, the cross clamp time is directly related to venous thromboembolism[148]. Therefore we compared the average clamp times between treatment group and control group and also failed to find a significant difference.

Since all technical aspects of the surgeries were identical and bias was avoided in the scoring of surgical outcomes, we conclude that our results are a real representation of the protective effect of autologous blood-derived EPCs in our large animal model. We believe that this conclusion is confirmed by the presence of our fluorescently pre-labeled EPCs in all 4 implants after 3 days *in vivo*. However, cells other than EPCs were

also observed on some of the Ti blood-contacting surfaces. These cells were present overlying confluent areas of EPCs (as confirmed by PKH26 and PECAM-1 stains, see Jantzen et al. Figure S2 A,B)[136]. Based on the cells' nuclear morphology, they appeared to be cells of the innate immune system. The distribution of these leukocytes was non-uniform with some fields of view revealing large aggregations while others showed very few, if any at all. We hypothesize that the presence of leukocytes relates to either the low shear environment "activating" EPCs, or to the short-term nature of the study and the fact that Ti tubes were explanted 3 days after the initial surgical insult. Testing of these hypotheses will be possible in future longer-term implantation studies.

One other limitation of our study is the observation that we did not find 100% of the Ti blood-contacting surface area covered with EPCs. We contribute this to the cells "peeling off" as a sheet during the disassembly process of the Ti tube. In fact, we did see distinctive "peel line" demarcations when examining our implants (See Jantzen et al., Figure S3[136]). Since the implants had been fixed in paraformaldehyde prior to disassembly, we hypothesize that cells are more strongly linked to each other than they are to the underlying Ti surface – and invariably separate from the undersurface when the Ti tube sections are broken apart. In future evaluations of currently ongoing long-term implantations, we may be able to prevent this problem by either utilizing an endoscope to examine the device lumen without taking it apart after explantation, or a Cellvizio LAB imaging system (Visualsonics) that allows for insertion of a small

diameter fiberoptic microprobe percutaneously into the IVC and device lumen to image the inside surface in live animals. We have already successfully conducted an exploratory trial with the minimally invasive Cellvizio system in 2 long-term implantations *in vivo* to ascertain presence of pre-labeled EPCs in patent implants (3 weeks, see Jantzen et al. Figure S4 A,B[136]).

Our X-ray photoelectron spectroscopy spectra and optical profilometry results show that our Ti tubes are similar to titanium-coated biomedical implants in atomic composition and surface roughness. Studies are currently underway to adapt our technology of point-of-care seeding to self-expanding Ti-coated nitinol stents. The same principles, however, can be used to coat many other implantable devices, e.g. the inflow cannula of ventricular assist devices in an effort to engineer an anti-thrombotic universal inflow conduit for mechanical circulatory support systems.

Since EPCs used in this proof-of-concept study are derived from peripheral blood, invasive methods of harvesting endothelial cells are avoided. Especially in sick patients who are most likely to benefit from implantation of cell-coated devices, an additional surgery to harvest cells could be avoided. Unlike other types of stem cells, e.g. induced pluripotent stem cells[149], our autologous EPCs have the important advantage of not requiring immunosuppression of the recipient patient. This not only avoids the significant side effects of immunosuppressive drugs but also their propensity to expose patients to opportunistic infections.

Finally, our technology avoids impractical *ex vivo* culture times of EPCs on the device surface. Whereas cell-seeding approaches have been hindered by the requirement to culture cells together with the device before implantation into a patient, we now have successfully demonstrated that blood-derived EPCs will spread on the three-dimensional Ti-blood-contacting surface after only a short seeding time with our rotating seeding device at the point-of-care and form a confluent cell layer *in vivo*. Longer-term implantation studies are currently underway with the goal of translating this cell-seeding technology into clinical practice.

2.6 Conclusions

We have demonstrated the feasibility to utilize autologous blood-derived endothelial progenitor cells to seed the blood-contacting surface of vascular devices at the point-of-care. Further we have provided first proof-of-concept in a large animal model that such EPC-coatings of titanium surfaces protect against device thrombosis. This technology can be used to protect Ti blood-contacting surfaces, e.g. nitinol vascular stents, mechanical circulatory assist devices, and blood-contacting extracorporeal devices against the devastating complications of device thrombosis and thromboemboli formation. Longer-term implantation studies are needed to pave the way for translating this technology into clinical practice.

2.7 Chapter acknowledgements

We thank Gemini Bio-Products for providing the porcine serum used in this study. We would also like to thank the NIH for supporting this work through Grant "Autologous EPC lining to improve biocompatibility of circulatory assist devices," RC1HL099863-01, and the National Science Foundation Graduate Research Fellowship for its financial support of Alexandra Jantzen. We are indebted to Steven Owen for machining Ti tubes and assembling the seeding device; George Quick, Mike Lowe and Ianthia Parker for handling our research animals; Kevin Collins for assisting with EPC isolation; Lukas Keil and Cherry Liu for collecting blood samples; Sa Do Kang and Visakha Suresh for analyzing images, and Drs. Marcus Darrabie, Dean Troupes, Antonio Jose Arciniegas and Jose Mantilla for assisting with explant surgeries.

3. Calculated shear stresses in implanted carotid stent surfaces are conducive to endothelial cell seeding and retention

Portions of the text and figures included in Chapter 3 have been submitted to the Journal of Biomechanics for publication. This article does not yet have a publication date; the Journal of Biomechanics does not require permission for authors to reuse their own articles, but an optional grant of license may be obtained as soon as one is available, through Rightslink®.

3.1 Chapter synopsis

Implantation of a vascular stent into a blood vessel is known to change flow patterns and the distribution of local wall shear stress (WSS). Point-of-care seeding of nitinol stents with endothelial cells can potentially reduce long-term complications such as intimal hyperplasia and thrombosis and improve vascular function. Implantation of a vascular stent into a blood vessel changes flow patterns and the distribution of local wall shear stress (WSS). We applied computational fluid dynamics methods to test the hypothesis that WSS and oscillatory shear index (OSI) on various surfaces of a commercial vascular stent are within a range that could support retention of rapidly seeded endothelial cells. We computed WSS and OSI on the stent under conditions representing hypertension and reduced vessel compliance. Time-averaged shear stresses were highest on lumenal stent surfaces in both normal and hypertensive flow conditions, and lower on lateral struts. Time-averaged shear stresses changed

minimally between normal and hypertensive models. Over the cardiac cycle, time-averaged shear stresses were <5 Pa (<50 dyn/cm^2) on all stent surfaces. Peak transient shear stresses were <27.5 Pa (<275 dyn/cm^2) on all stent surfaces, and highest on the lumenal surface. OSI was highest on stent lateral surfaces and lower on lumenal surfaces. Local flow reversal occurred at the vessel wall for a portion of the cardiac cycles. OSI was lower in the hypertensive flow model on all studied surfaces, corresponding to reduced vessel compliance and reduced fluctuation of the input waveform. The magnitude and temporal profile of shear stress and OSI on an implanted stent surface should enable endothelial cell retention and antithrombotic function, although regions that exhibit flow reversal may alter endothelial cell function.

3.2 Introduction

Vascular stents are commonly used to restore blood flow in a restricted coronary or peripheral artery lumen. Despite the general success of these stenting procedures, restenosis after thrombosis or intimal hyperplasia is a persistent problem in a substantial number of patients[7,33]. Covering the blood-contacting surfaces of stents with a layer of functional endothelium is an attractive strategy investigated by our group and others to reduce thrombogenicity of the material[63-65,67,68,74,136]. Shear stresses on the stent members under typical physiological conditions are of particular interest for potential endothelialization of the stent device; we have previously shown that endothelial cells (ECs) can be retained and maintain positive antithrombotic function on Ti surfaces

under sustained shear stresses of 100 dyn/cm^2, so time-averaged shear stresses at or below this level are preferred for surfaces to be seeded with endothelium.

Computational modeling of stents has been used to examine deployment forces within the stent material[99], elution profiles of drug coated stents[100], and fluid shear stresses on vessel endothelium within a fully deployed stent[101-104]. These studies examine how a stent placed in an artery disturbs local flow patterns and imparts stress to the artery wall. In a three-dimensional flow model including recirculation through a drug-coated stent in a coronary artery[100], drug distribution was affected by stent geometry and flow, and transient accumulation of drug occurred in the vessel downstream of the stent. While some of the previous work examines shear stress on the stented vessel wall, shear stresses on the stent itself have not previously been reported. Decreasing the thickness of struts (thickness measured in the radial rather than circumferential direction) could significantly reduce the areas of low wall shear stress downstream of each strut[150]. Other computational studies also showed that struts of reduced thickness, more aligned with the primary flow direction, decrease the effect of low wall shear stress on the arterial wall[109,110]. In contrast, reducing the width of modeled stent struts increased the vessel area exposed to low wall shear stress (defined as <0.5 Pa)[109]. In a slightly different application of stent modeling, computation has also been used to predict areas of likely EC denudation following expansion of a balloon-expandable stent[151].

Low wall shear stress, known to correlate with atherosclerosis, also frequently occurs between stent struts and correlates with hyperplasia leading to stent restenosis[111-113]. Low shear stress also corresponds to areas of inhibited EC migration onto stents[114]. Stent strut spacing has a strong effect on wall shear stress, flow stagnation and recirculation[102,103,115]. Although vascular stents alter blood flow patterns close to the stent structure, most previous work has focused on the adjacent vessel wall and not on shear stresses experienced by the stent struts themselves. Additionally, most previous work has focused on only healthy human waveforms and not models of vascular disease or hypertension, as we do here. While some studies have examined peripheral vascular stents, a majority of modeling has focused on coronary stents, subject to very different hemodynamics and shear stresses.

After only a 15-minute period of attachment approximately 90% of endothelial progenitor cells (EPCs) are retained on titanium surfaces, even at shear stresses of 30 Pa[126]. We also found that cells spread on a Ti surface remain adherent and express nitric oxide (NO) and antithrombotic genes when subjected to 10 Pa shear stress. We have used computational fluid dynamics modeling to assess shear stresses on the titanium housing of a left ventricular assist device, finding that all surfaces but the outlet tube experienced shear stresses above 10 Pa, and were likely not suitable for endothelialization[120]. Nitinol stents are covered with a layer of titanium oxide on the

outer surface, and so we are extending our work with Ti and endothelial cells to nitinol stents.

Our long-term goal is to endothelialize nitinol stents immediately prior to deployment, without extensive culturing of the stent and cells together. As such, the shear stresses experienced by cells on various parts of the stent geometry are of special interest to us as they relate to initial cell retention as well as longer-term viability of a seeded endothelial layer.

Our objectives in this study were to calculate shear stresses on the stent surface and the degree of reversing flow; these two parameters are expected to have a significant impact on the phenotype and behavior of cells seeded to the surface. Because patients receiving stents may be expected to have a degree of hypertension, atherosclerosis, and/or vessel stiffening, we modeled both a normal baseline carotid flow waveform, and a carotid flow waveform representing moderate hypertension with reduced vessel compliance, representing blood pressures in excess of 160/90 mmHg[152]. We compare the calculated shear stresses to our previous studies with ECs on titanium to predict whether the ECs are likely to remain adherent on the surface.

3.3 Materials and methods

3.3.1 Stent geometry modeling & meshing

The stent geometry used in this study was based on the peripheral nitinol stent Cordis S.M.A.R.T.® (Johnson & Johnson), with unconstrained dimensions 6 mm O.D. x

30 mm length. The solid model was discretized into a finite element mesh using ANSYS MeshingTM 14.5 software (SAS).

Dimensions and design pattern of stents 6 mm diameter x 30 mm length were acquired using an upright Leica DMRB microscope and QCapture Pro 7 software, as well as direct measurement of stent wall thickness. The stent geometry was generated using SolidWorks (Dassault Systèmes) and ANSYS DesignModeler (SAS). The stent was then implanted into vessel of approximately 5 mm diameter using Boolean subtraction. For the steady-state simulation, one half of the tube was modeled. To reduce computation time for transient simulations, a section of the stent and vessel equal to one-sixth circumference of the tube was modeled (Figure 3.1A), because the stent pattern repeats in 6 circumferential sections.

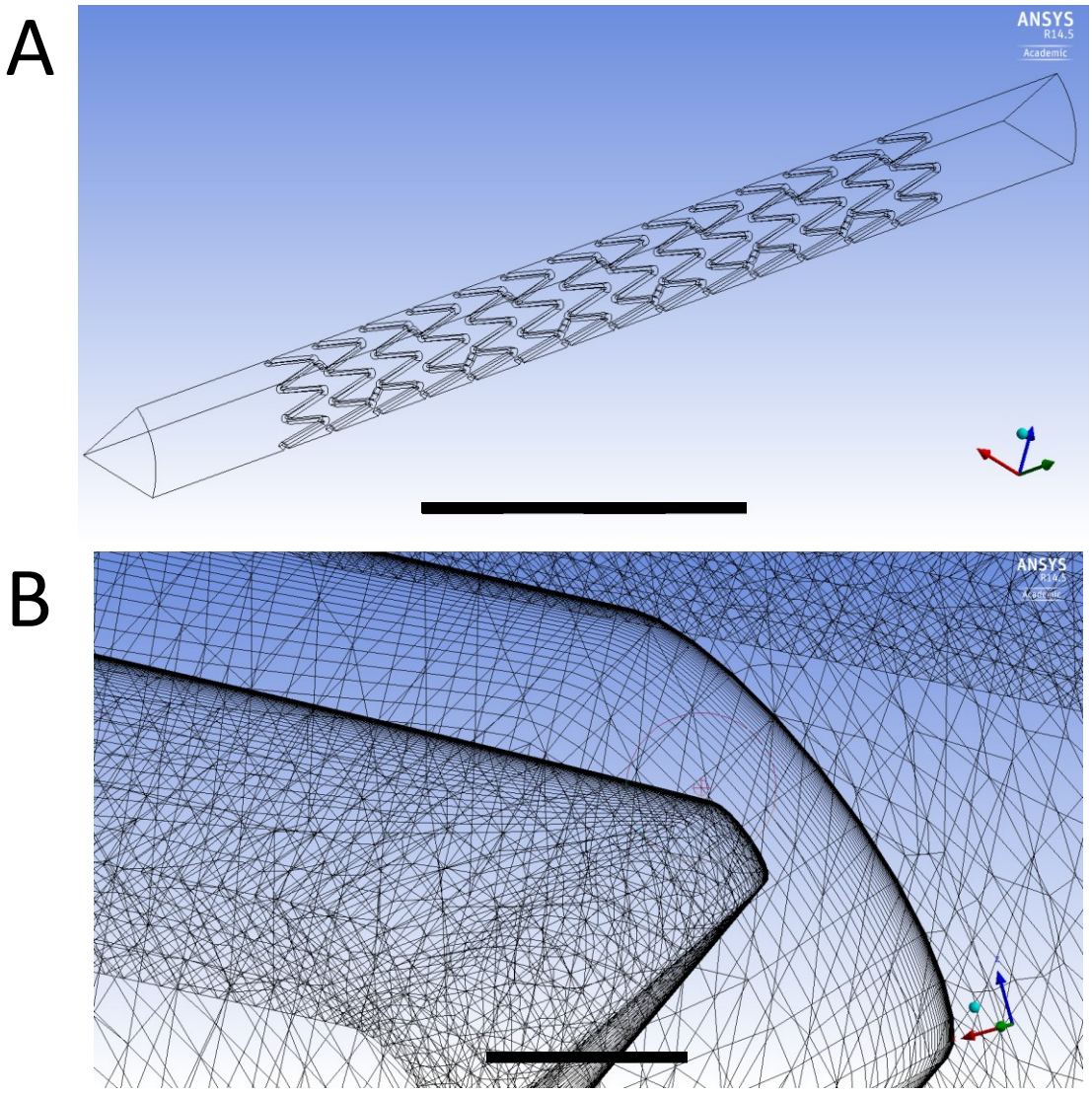

Figure 3.1: Modeled stent geometry and discretized mesh.

(A) 3-D modeled geometry of one-sixth stent circumference. Scale bar is 12 cm. (B) Close view of mesh shows high density of mesh elements near outer diameter, created by inflation of the mesh necessary for accurately resolving the boundary layer. Scale bar is 100 μm.

The solid model was discretized into a finite element mesh using ANSYS Meshing™ 14.5 software (SAS). Preliminary simulations showed that it was most important to resolve small distances near walls to capture boundary layer changes (Figure 3.1B). Elements near the wall were highly anisotropic to resolve wall shear stresses well without prohibitive computational cost. Inflation on the tube outer diameter was used to resolve the boundary layer.

3.3.1.1. Steady-State Mesh Characteristics

For the steady-state simulation, a fully-developed parabolic inlet profile was used. A combination of wedge and tetrahedral elements comprised the mesh, which had a total of 22.5 million elements and 4.2 million nodes. The mesh was refined until increasing the number of elements did not significantly change simulation outcomes.

3.3.1.2. Transient Mesh Characteristics

For transient simulations a long entrance length tube (12 cm) was added to the inlet of the stent for flow development. A combination of wedge and tetrahedral elements comprised the mesh, which had a total of 18.7 million elements and 7.2 million nodes. Orthogonal quality of the mesh was 0.87 ± 0.17 (mean ± standard deviation). The mesh was refined until increasing the number of elements did not significantly change simulation outcomes.

3.3.2 Simulation parameters

Given the arterial flow conditions, we modeled blood as a Newtonian fluid as others have done[100,104,153] with density ρ = 1060kg/m^3 and dynamic viscosity μ = 0.004Pa s^{-1}. The vessel was modeled as a rigid cylinder with stent struts contacting the inner diameter and protruding into the lumen.

We calculated two time-averaged parameters: oscillatory shear index (OSI)[154,155], and time-averaged wall shear stress (WSS_{av})[155], over the cardiac cycle simulated. These were defined as:

$$OSI = 0.5 * \left(1 - \frac{|\int_0^T \tau_y dt|}{\int_0^T |\tau_y| dt}\right) \quad (1)$$

$$WSS_{av} = \frac{1}{T}\int_0^T |\tau_w| dt \quad (2)$$

Where τ_y is the vector component of the shear stress tensor in the axial direction of flow (y), τ_w is the total WSS magnitude, t is time, and T is total simulation time (one cycle period). By this definition, the range of OSI is 0 to 0.5.

3.3.3 Input waveforms

3.3.3.1 Steady-state conditions

For the steady-state simulation, a fully developed parabolic velocity profile was imposed at the inlet. The inlet profile for tube with radius R varied with radius position r by the following equation:

$$V(r) = 2 * v_{avg} * \left(1 - \frac{r^2}{R^2}\right) \quad (3)$$

For the steady-state simulation, the average velocity v_{avg} was a constant and was set at 33.6 cm/s. This average velocity was chosen so that the total flow rate would be 7 mL/s. We had established this flow rate for the porcine carotid artery in a preliminary exploratory surgery using an ultrasonic flowmeter (Transonic).

3.3.3.2 Transient conditions

For the transient conditions, the velocity profile at the stent inlet should be the appropriate Womersley profile for unsteady flow at each time point. The complexity of the Womersley profile did not allow us to directly use this solution as an input. To achieve the Womersley profile, a "blunt" velocity profile, more flat than a parabola, was imposed at the tube inlet and allowed to develop over 12cm. This blunt velocity profile was closer to the target Womersley profile than a parabola, allowing the flow to develop more quickly. Flow was confirmed as fully developed by running a simulation with a different inlet velocity profile and verifying that the velocity profile at stent inlet did not vary significantly at any time point. The inlet profile for tube with radius R varied with radius position r by the following equation:

$$V(r) = 4/3 * v_{avg} * \left(1 - \frac{r^6}{R^6}\right) \quad (4)$$

3.3.3.3 Time-varying inlet waveforms

To model the normal human common carotid waveform, we referenced an archetypal waveform[156]. To model the carotid waveform under conditions of hypertension and reduced compliance, we used trends reported previously in the effect

of vessel compliance on carotid artery flow waveforms[157]. We fit each of these waveforms to a Fourier series representation. CFD simulations were run using ANSYS CFX 14.5 (SAS) to solve the time-dependent Navier-Stokes equations; one complete cycle was simulated.

3.3.3.4 Normal human carotid waveform

To model the normal human common carotid waveform, we referenced the archetypal waveform published by Holdsworth et al[156]. We then fit this waveform, with a stated period of 0.917 seconds (and Womersley number 3.6), to a Fourier series model with 8 pairs of sine and cosine terms. The frequency used in the Fourier series model, 6.842, was related to the period as 2π/period.

3.3.3.5 Reduced Compliance Hypertension Waveform

To model the carotid waveform under conditions of hypertension and reduced compliance, we used trends reported previously in the effect of vessel compliance on carotid artery flow waveforms[157]. Masuda et al. reported that when vessel compliance was reduced, there was a decrease in the maximal flow of the carotid velocity waveform and an increase in the second peak. We modeled the shape of the reduced (75% of normal) compliance flow waveform and matched the period to our model of the normal carotid waveform. We also adjusted the peak velocity so that the relationship between the normal and reduced compliance waveform modeled the relationship reported by Masuda[157]. Knowing that the waveform period is well within the range of

interindividual variability[156,158], and that the diameter of the vessel modeled has a strong relationship to the peak velocity, we matched these parameters to our normal model so as to isolate the specific effects of the compliance change in our simulation. This waveform was not able to be fit well with a single Fourier series. We fit this waveform to a piecewise function such that a unique Fourier series described each peak. The frequency used in the Fourier series fits here varied and was not related to the period in a straightforward way, in an effort to achieve the best fit.

3.3.3.6 Inlet Waveforms – Fourier Series Goodness of Fit

To quantitatively measure the adequacy of the Fourier reproductions, we measured the variance of the wave and compared to the variance of the Fourier series. For each captured curve having m ordinates with a mean value of y_m, we used the following equation:

$$Variance = \frac{1}{m}\sum_{i=1}^{m}(y_i - y_m)^2 \quad (5)$$

The percent of the variance represented by the Fourier series was measured by the ratio of the cumulative variance of the Fourier series (V_s) to the total variance of the raw velocity waveform (V_t). For the normotensive waveform, the percent variance captured by the addition of each pair of harmonic terms is shown in Figure 3.3.

3.3.4 Computational Simulations

CFD simulations were run using ANSYS CFX 14.5 (SAS) to solve the time-dependent Navier-Stokes equations. The total time simulated was equal to one

complete cycles of the waveform (period 0.917 s) with a timestep such that the Courant # was <20. Each timestep was iterated 8 times or until residuals for were less than 10^{-5}, whichever came first.

3.4 Results

3.4.1 Simulation convergence

For the steady-state simulation, acceptable convergence was observed. Residuals for the axial momentum terms converged to the order of 10^{-6}, and residual terms for the other two momentum directions converged to the order of 10^{-5}. For both the normotensive and hypertensive simulations, acceptable convergence was observed. Residuals for the axial momentum terms converged to the order of 10^{-7} and 10^{-6} for the normotensive and hypertensive cases, respectively, and residual terms for the other two momentum directions converged to the order of 10^{-5} for both cases.

3.4.2 Time-varying input waveforms

Reconstruction of the healthy human carotid waveform with a Fourier series consisting of the first eight harmonics showed only 0.2% variation from the template waveform (Figure 3.2A). Comparison of the Fourier series with the healthy human carotid waveform showed that 8 harmonics accounted for 99.8% of the variance (Figure 3.3). The error is therefore much less than the variability between individuals [156,159]. The piecewise Fourier series model of the carotid waveform in hypertension / reduced

compliance (Figure 3.2B) also showed 0.3% variation from the template waveform, with 7 harmonics for each piecewise section accounting for 99.7% of the variance.

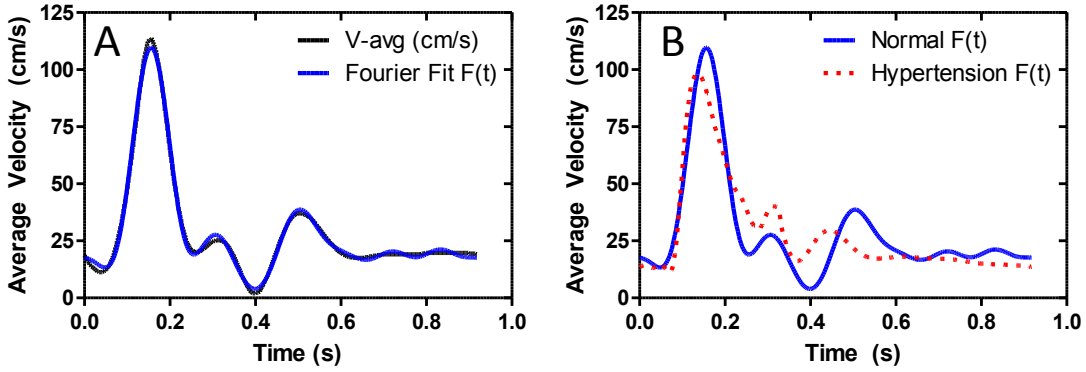

Figure 3.2: Input waveforms for normotensive and hypertensive conditions.

(A) Input waveform, Fourier Fit F(t), fit to waveform V-avg of normal carotid flow experimentally determined by Holdsworth et al. [156]. (B) Normal carotid waveform Fourier fit F(t) from (A) and reduced compliance (75% of normal) hypertension waveform Fourier fit F(t).

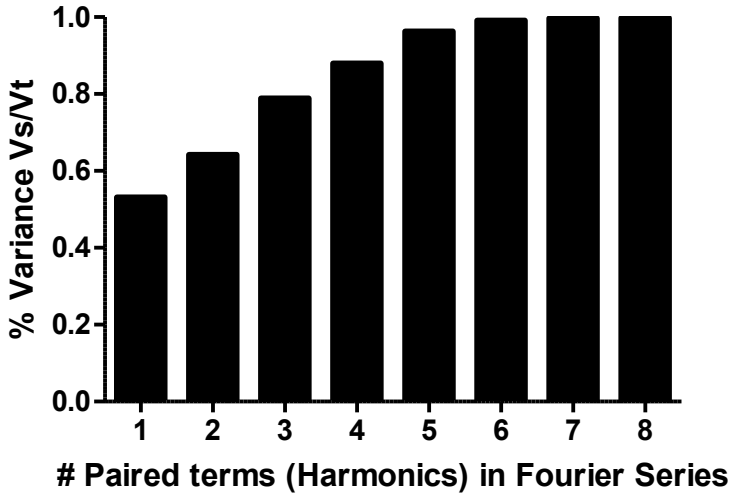

Figure 3.3: Fit of the Fourier series by number of paired terms.

Cumulative ratio of the variance of Fourier series fit (Vs) to the total variance (Vt) of the healthy archetypal human carotid waveform of Figure 1. Eight harmonics results in a Vs/Vt ratio of 99.8%.

3.4.3 Shear stresses and OSI

We examined shear stresses on the stent surface as well as the unstented vessel inlet and a representative exposed vessel wall segment in the middle of the stent. For both the normotensive and hypertensive cases, the velocity profiles at the stent inlet agreed well in shape with the Womersley solution and captured the key features of the Womersley solution. The blunted profile we used worked better for profile development than a parabolic inlet profile. By making slight changes to the inlet profile shape and confirming identical profiles at the stent inlet, we confirmed that the flow was fully developed at the stent inlet.

3.4.3.1 Steady-state simulation

Computational simulations of steady-state flow through the stent geometry revealed large variations in shear stress experienced by different stent surfaces (Figure 3.4). On lateral surfaces of the stent, a large shear stress gradient exists, and shear stresses vary by one order of magnitude along the width of the strut. Steady-state shear stresses on key surfaces are reported in Table 3.1.

For the steady-state simulation, OSI was not calculated as there was no time component. We instead calculated a degree of flow reversal caused in the steady-state condition due to flow patterns around the stent geometry. Based on a measure of the fluid volume with a negative axial velocity, 3.6% of the fluid volume flowing through the stent experienced flow reversal.

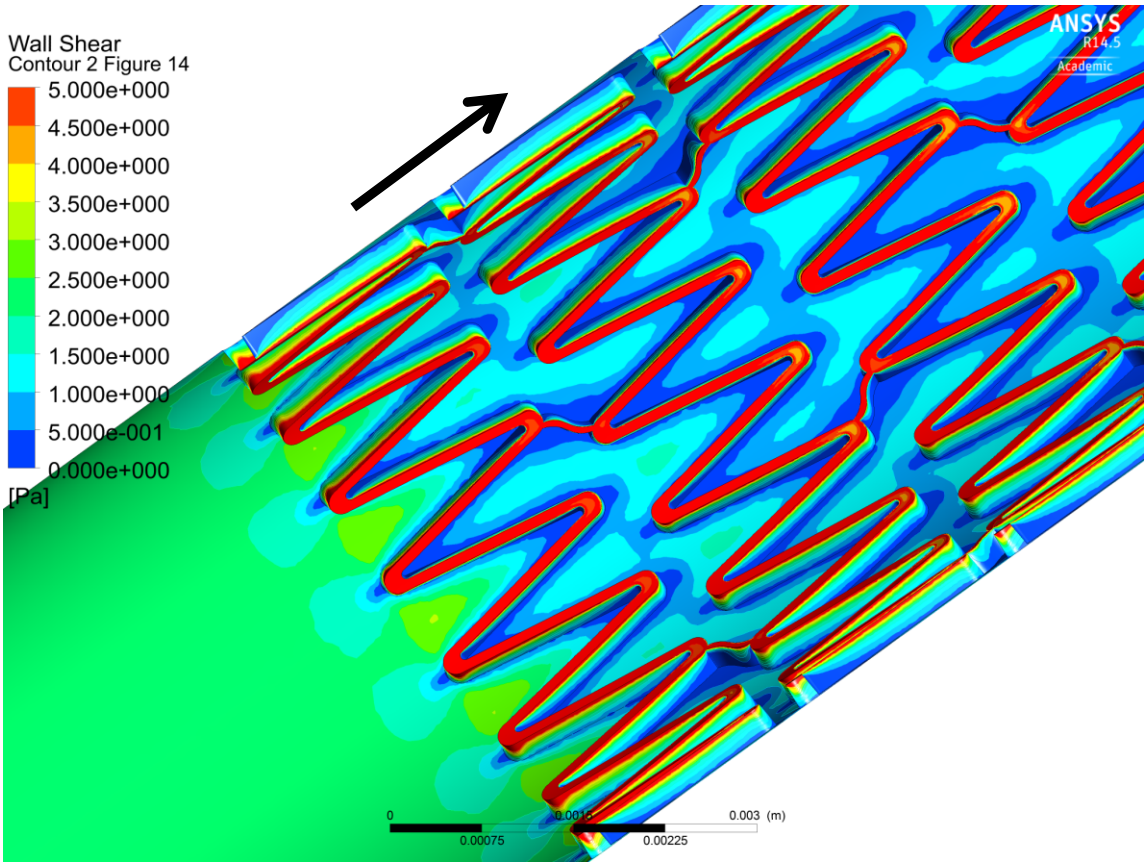

Figure 3.4: Contour plot of total wall shear stress on stent under steady-state flow condition.

Contour plot of total wall shear stress on stent under steady-state flow condition and baseline shear stress approximately 20 dyn cm^{-2}. Flow direction denoted by arrow. Note lateral surfaces of stent struts experience a high shear stress gradient and vary from approximately 5 to 50 dyn cm^{-2} along the width of the surface.

3.4.3.2 Normal human carotid waveform

Lateral and lumenal surfaces of the stent were exposed to a wide range of shear stresses and circulation patterns. Instantaneous shear stresses were calculated at points of interest in the cardiac cycle, including systolic acceleration (Sa), just before peak systole as the flow starts to level, peak systole (Sp), systolic deceleration at the local minimum following peak systole (Sd), and diastole (D) at the local maximum in diastole (Figure 3.5).

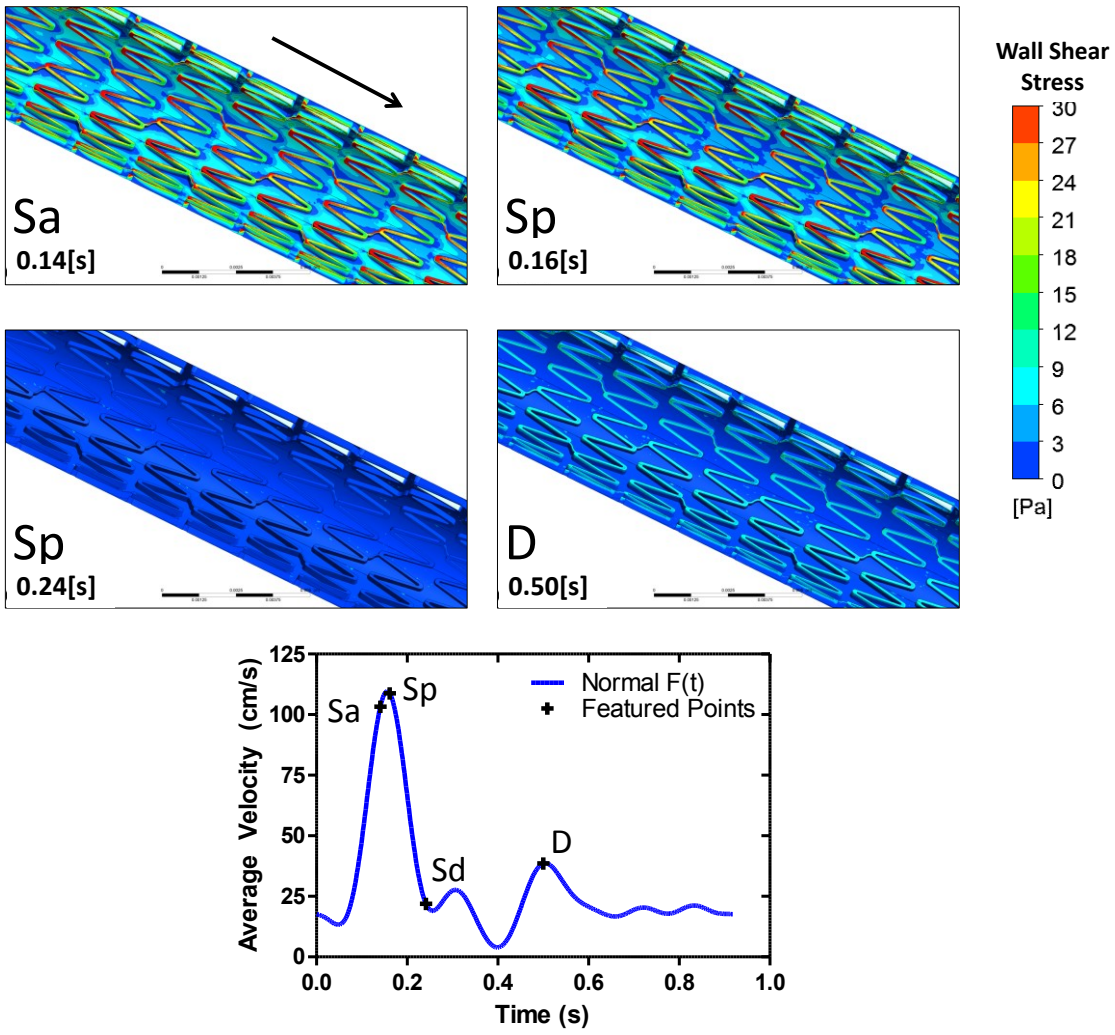

Figure 3.5: Instantaneous total wall shear stress (WSS) contours on stent and surrounding vessel during key points of normotensive waveform.

Key timepoints are systolic acceleration (Sa), peak systole (Sp), systolic deceleration (Sd), and diastole (D) in a normal human carotid artery. Flow direction is shown by the arrow and is identical in all panels. The flow waveform and the corresponding time points in the cardiac cycle are shown at bottom.

As expected by its greater protrusion into the vessel lumen, average shear stress over the entire cycle was greatest on the lumenal surface (4.92 Pa), compared to 1.81 Pa for the inlet, which represents an unstented vessel wall. In contrast, shear stresses on the lateral surfaces in the middle of the stent length were lower (between 1.1-1.2 Pa).

Examining vector components of the shear stress tensor in the axial direction of flow allows positive and negative shear stresses to be distinguished with respect to the flow direction. Shear stress contours of axial wall shear stress (WSSaxial) show areas with negative flow. At the cardiac cycle global flow maximum of peak systole, shear stresses on nearly all surfaces are positive in the axial direction (Figure 3.6A), with small areas of recirculation occurring in corner areas protected by "zig-zag" pattern of the stent. In contrast, in the cardiac cycle global flow minimum, shear stresses on nearly all surfaces are negative in the axial direction (Figure 3.6B), with only small areas of positive shear stress in locations mirroring those protected areas seen in Figure 3.6A.

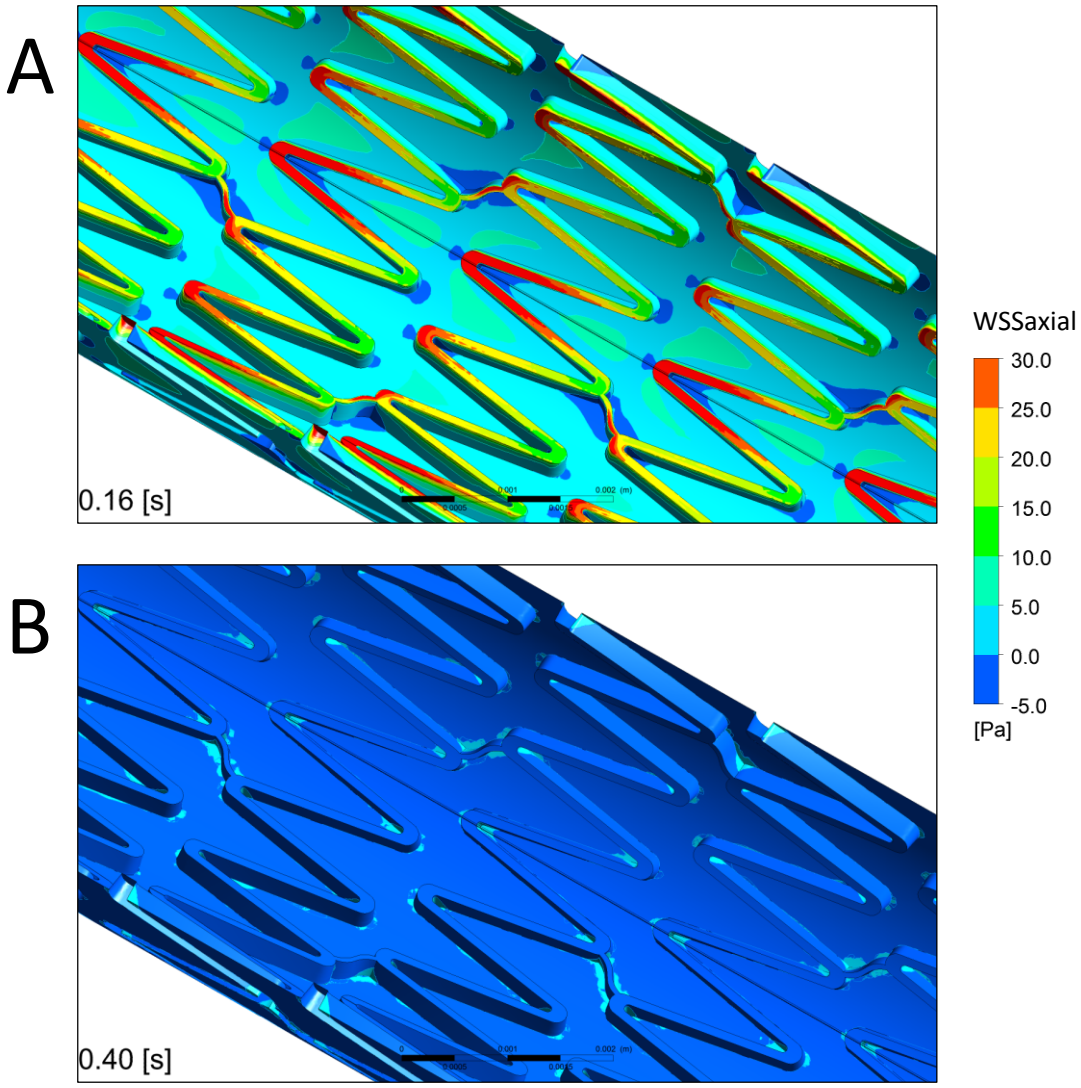

Figure 3.6: Instantaneous axial wall shear stress (WSSaxial) contours in normotensive condition.

(WSSaxial) contours on stent and surrounding vessel during (A) cardiac cycle global maximum flow (0.16 s) and (B) global minimum flow (0.40 s) in a normal human carotid artery. Positive flow direction is shown by the arrow and also marks the positive axis with respect to WSSaxial.

Average shear stresses and OSI on specific surfaces are reported in Table 3.1., and surfaces of interest are labeled on a stent diagram in Figure 3.7. All values represent an average over the surface area of interest. Close examination of shear stress contours (Figure 3.8A) reveals that shear stresses vary over many strut surfaces both axially and radially. Shear stresses vary most on strut lateral surfaces. The variation ranges from nearly 0.5 Pa at the vessel wall and near 5 Pa at the lumenal edge of the lateral struts. On these lateral struts, shear stresses reach minimum values at the vessel wall, but are also decreased at the "inside" corner of each zig-zag shape of the stent, where flow reattachment is hindered in comparison to the more open spaces between struts.

The OSI at the vessel inlet, before the flow reaches the stent, is non-negligible (0.14, Figure 3.8B). OSI on the lumenal stent surface is less at 0.11, whereas OSI on the first row of struts is higher, 0.14-0.15. Oscillations are increased on stent faces and exposed vessel walls in the middle of the stent length, with 0.17 OSI and 0.21 OSI, respectively. The high OSI on the vessel wall is expected and correlates with flow separations and low shear stresses previously reported around stents[102,104]. Non-zero values of OSI are consistent with the presence of negative axial shear stress representing flow reversal in the global flow minimum of the cardiac cycle.

Table 3.1: Time-averaged shear stress and oscillatory shear index on specific surfaces of interest.

		Steady-State Condition	*Normal Human Carotid Waveform*		*Hypertension/Reduced Compliance*	
Surface		**WSS (Pa)**	**WSSav (Pa)**	**OSI**	**WSSav (Pa)**	**OSI**
Strut A	*first row*	2.38	2.17	0.14	2.08	0.05
	mid-stent	1.47	1.19	0.17	1.17	0.09
Strut B	*first row*	1.91	1.51	0.16	1.47	0.07
	mid-stent	1.47	1.11	0.17	1.09	0.10
Inlet C		2.09	1.75	0.14	1.76	0.04
Lumenal D		5.63	4.92	0.10	4.80	0.01
Wall E		0.63	0.57	0.21	0.55	0.15

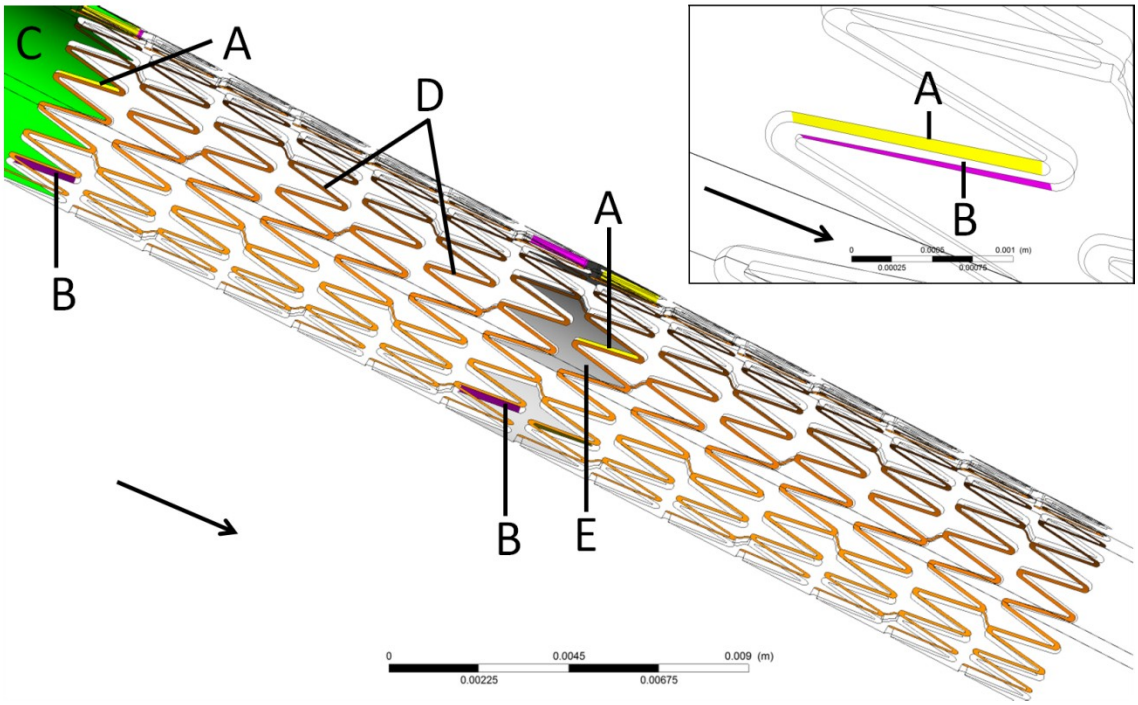

Figure 3.7: Schematic of key named surfaces referenced in Table 3.1.

(A) Upstream lateral surface, pictured in first row of struts and also mid-stent (yellow). (B) Downstream lateral surface, pictured in first row of struts and also mid-stent (magenta). (C) Inlet portion of vessel (green). (D) Lumenal surface of stent (orange); surface extends throughout length of stent. (E) Vessel wall between struts, mid-stent (gray). Note that specific stent struts A and B repeat multiple times around the circumference in the schematic, which is an instance transform to depict half the stent; one-sixth of the stent was modeled, so surfaces repeat. Inset: Close-up view of upstream and downstream lateral strut surfaces A and B. Flow direction is indicated by arrow.

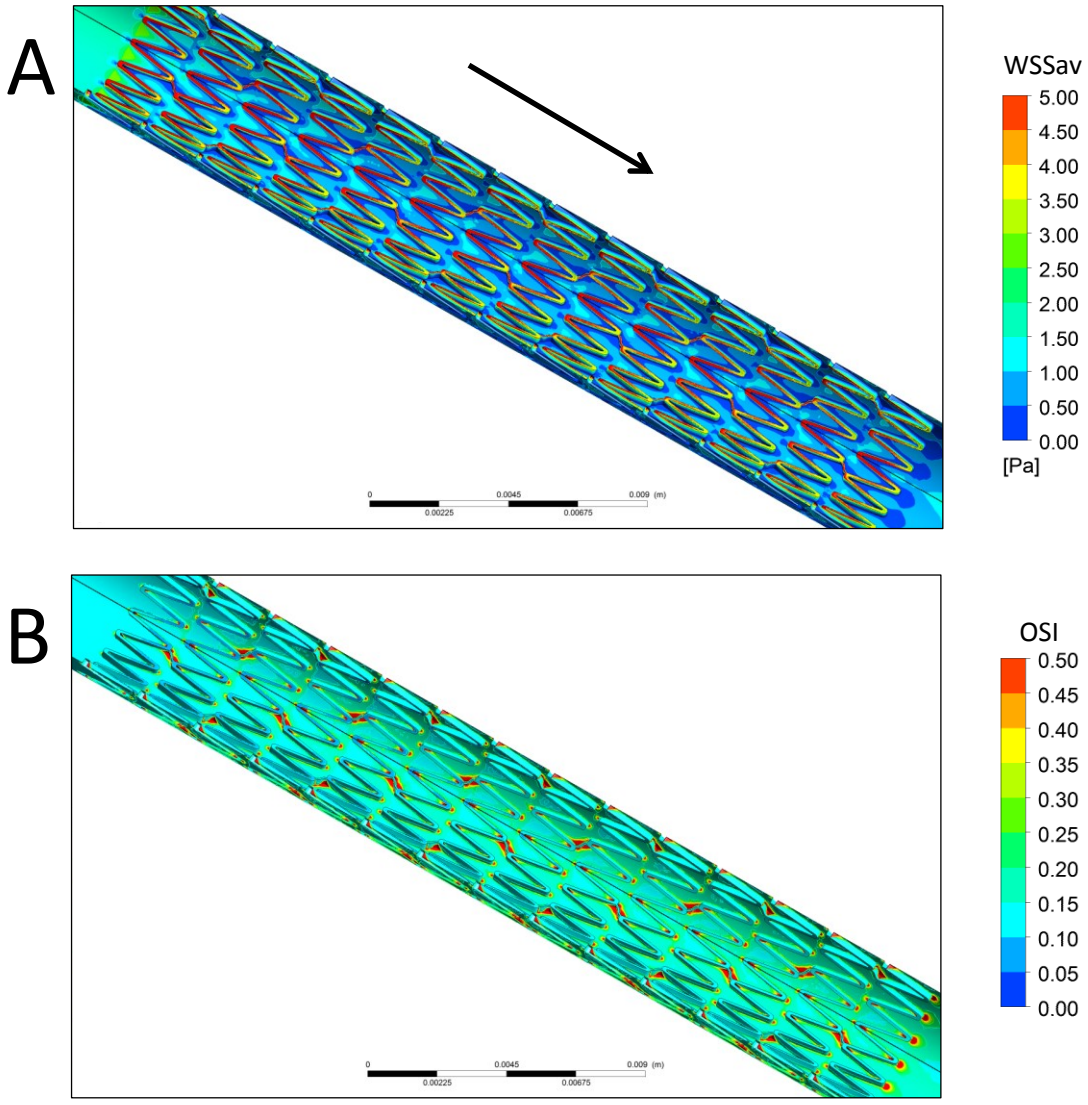

Figure 3.8: Contour plots of (A) time-averaged Wall shear stress (WSSav) and (B) oscillatory shear index (OSI) on stent surfaces in a normal human carotid artery.

Flow direction is shown by the arrow and is identical in both panels.

3.4.3.3 Reduced compliance hypertension waveform

In the simulation of reduced compliance and hypertension, many trends were similar to the normal carotid simulation. Total flow integrated over the cardiac cycle differed by only 1% from the normotensive waveform, so the differences in shear stress and OSI are attributed to the different shape of the waveform rather than an overall shift in flow. Instantaneous shear stresses were calculated at Sa, Sp, Sd, and D in the respective waveform (Figure 3.9), and time points were similar but not identical to those of the normal carotid simulation. Average shear stress remained highest on the lumenal surface, at 4.8 Pa (vs 4.92 Pa under normal conditions). Shear stresses on the lateral surfaces in the middle of the stent length remained lower than on the lumenal surface - approximately 1.1-1.2 Pa for both hypertensive and normal conditions (Figure 3.10A).

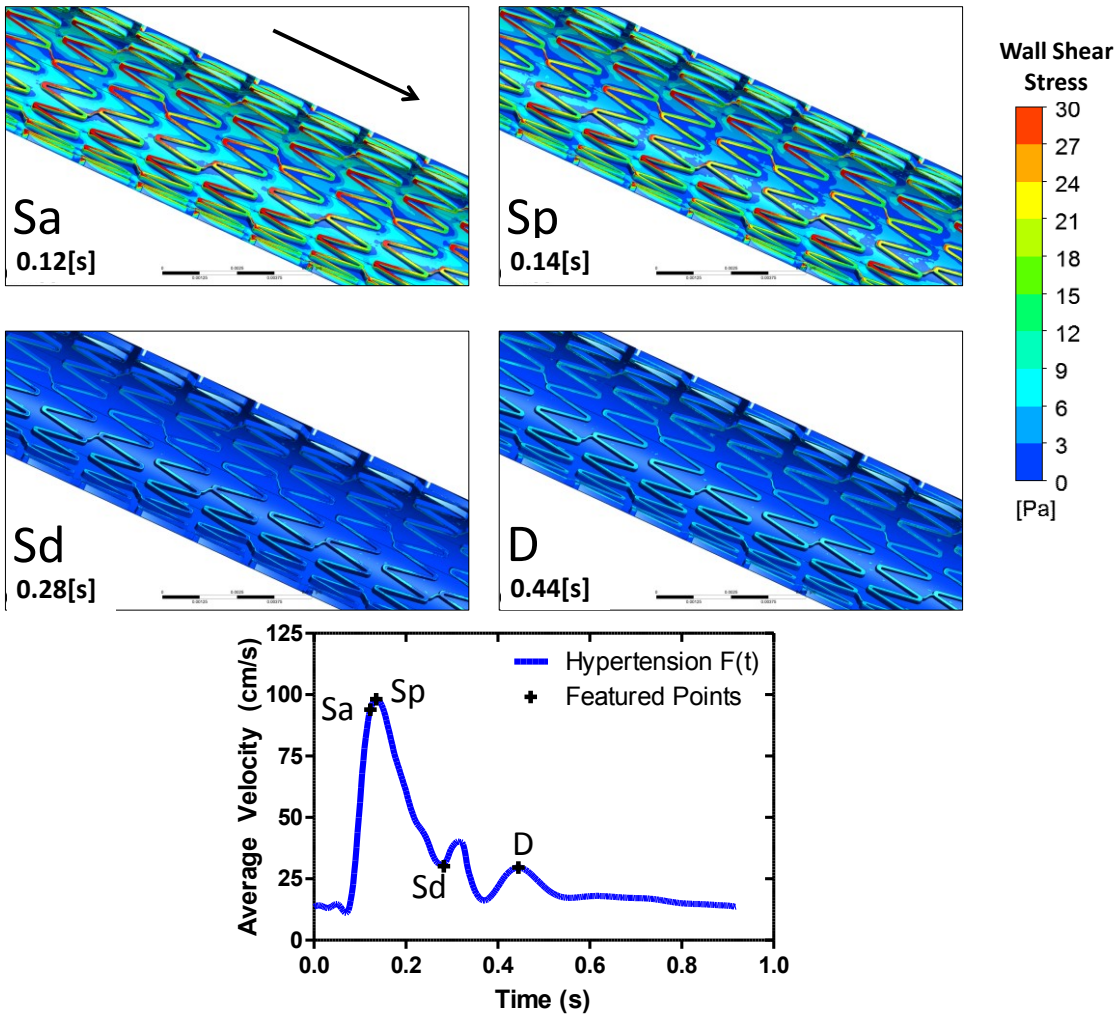

Figure 3.9: Instantaneous total wall shear stress (WSS) contours on stent and surrounding vessel during key points of hypertensive waveform.

Key timepoints are systolic acceleration (Sa), peak systole (Sp), systolic deceleration (Sd), and diastole (D) in a carotid artery with reduced compliance. Flow direction is shown by the arrow and is identical in all panels. The flow waveform and the corresponding time points in the cardiac cycle are shown at bottom.

While minimal changes to the shear stresses were seen from the normotensive to the hypertensive condition at the locations in the waveform chosen, greater changes were observed in OSI. OSI on the vessel inlet, before the flow reaches the stent, is minimal (0.04, Figure 3.10B). OSI on the lumenal stent surface is much lower (0.01) and OSI on the first row of struts (0.05-0.07) is approximately half that of the normotensive case as well. OSI is reduced from values obtained for the normotensive case, on stent faces and exposed vessel walls in the middle of the stent length, with 0.09 OSI and 0.15 OSI, respectively.

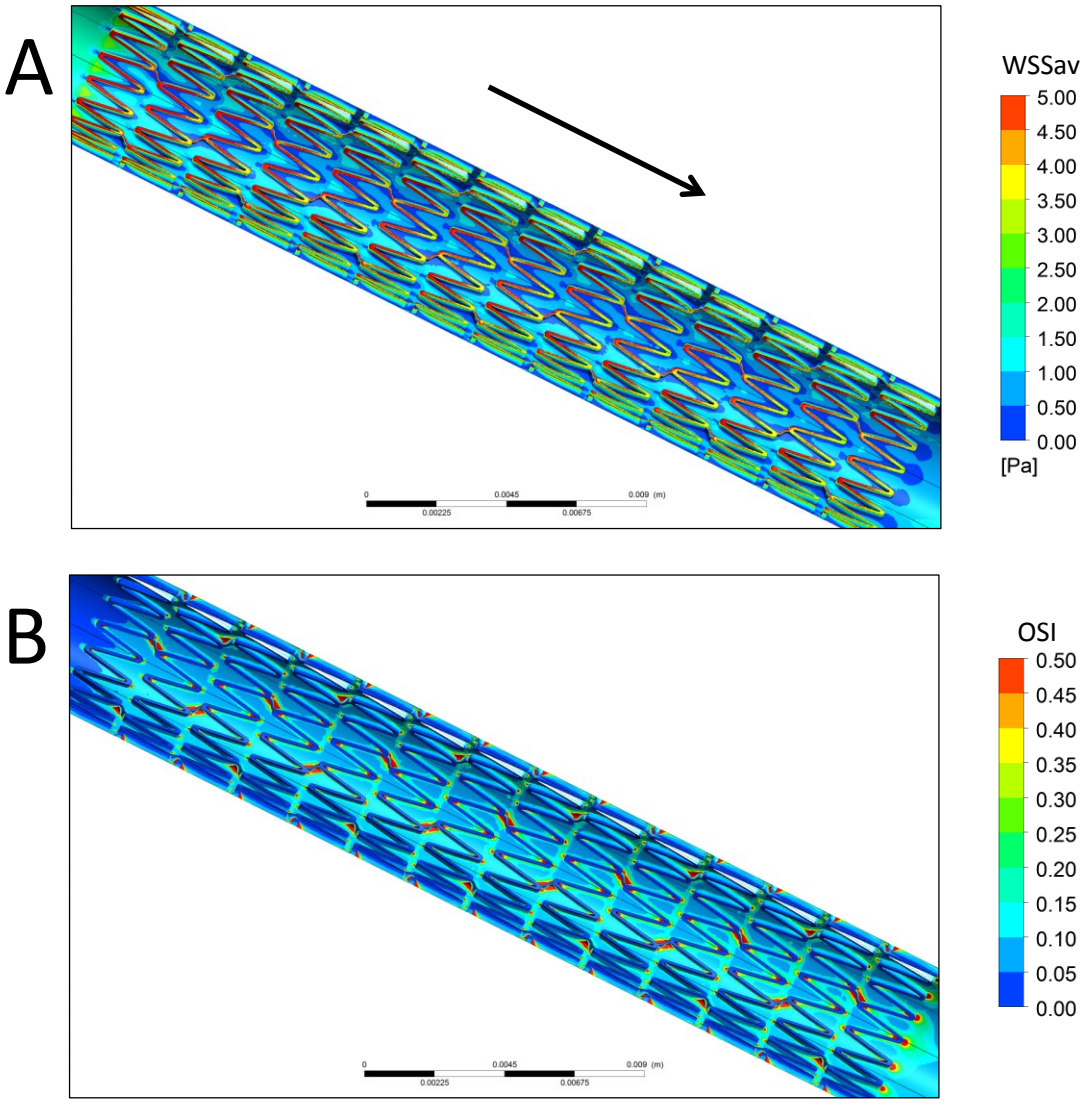

Figure 3.10: Contour plots of (A) time-averaged Wall shear stress (WSSav) and (B) oscillatory shear index (OSI) on stent surfaces in a human carotid artery with reduced compliance.

Flow direction is shown by the arrow and is identical in both panels.

3.5 Discussion

The results of this study indicate that the blood-contacting surfaces of a carotid stent are exposed to a range of shear stresses, and varying degrees of flow reversal. Average shear stresses are close to 5 Pa at the highest, on the lumenal stent surfaces and are similar in both normal and hypertensive cases. In contrast, OSI on all stent surfaces is lower by approximately half in the hypertensive case, indicating a lesser degree of flow reversal.

To date, only the shear stresses on the walls of a stented vessel have been reported[101-104,150], not shear stresses on the surface of the stent itself. While average shear stresses on the vessel walls of a stented vessel (0.5-0.6 Pa in these models) are typically lower than on an unstented vessel (1.8-1.9 Pa in these models), we find that shear stresses on the stent itself are generally higher than the 1.8 Pa shear stress calculated on the adjacent unstented vessel wall.

The carotid waveform model of hypertension studied here is for a vessel with 75% of the original vessel compliance. This is representative of moderate hypertension. In a patient population with blood pressure exceeding 160/90 mmHg, the vessel compliance in large arteries is reduced to 80% of the value found with age-matched normotensive individuals[152]. Vessel stiffness increases with age, both with and without hypertension[160-162]. When the elasticity of a vessel is reduced, the timing of the reflected

waves is changed and results in a decrease in the maximum flow velocity as well as an increase in the second peak of the flow waveform[157].

EC adhesion *in vivo* is influenced by the shear stresses on implanted stents as it relates to our goal of endothelializing peripheral stents. We have previously shown that fully spread ECs are retained on uncoated Ti surfaces under sustained shear stresses up to 10 Pa[126]. In this study, the highest time-averaged shear stress in a stented healthy carotid artery is 4.92 Pa and is on the stent's lateral surface; this is below our previously studied long-term shear stress of 10 Pa, and we anticipate that seeded ECs will be retained under these conditions. In comparison, the highest transient shear stress on the stent surface is 27.5 Pa, on the lateral surface, during the healthy cardiac cycle. In the model of moderate essential hypertension, the highest transient shear stress on the stent surface is 26.5 Pa, on the lateral surface. The highest time-averaged shear stress is 4.80 Pa, on the lateral surface. We have shown previously that even ECs which are not fully spread are approximately 90% retained under short-term shear stresses of 30 Pa after a 15-minute period of attachment[126]. Based on this result, we would expect that most ECs seeded onto a stent at the point of care to be retained when deployed into a carotid artery under these normotensive or hypertensive conditions, despite a short period of attachment in our seeding method. Further supporting this, we have observed good coverage of cells in preliminary *in vivo* experiments.

Stenting of the vessel increases OSI on vessel endothelium both within and slightly downstream of the stent; OSI in an unstented common carotid artery has previously been reported from zero to 0.10, [154,163], but was calculated at 0.14 on the unstented inlet tube under our 'normal' flow conditions. This non-negligible OSI can be explained by looking at the Womersley velocity profile. For a time period around the flow minimum, velocity near the wall is reversed despite an overall positive flow (Figure 3.11).

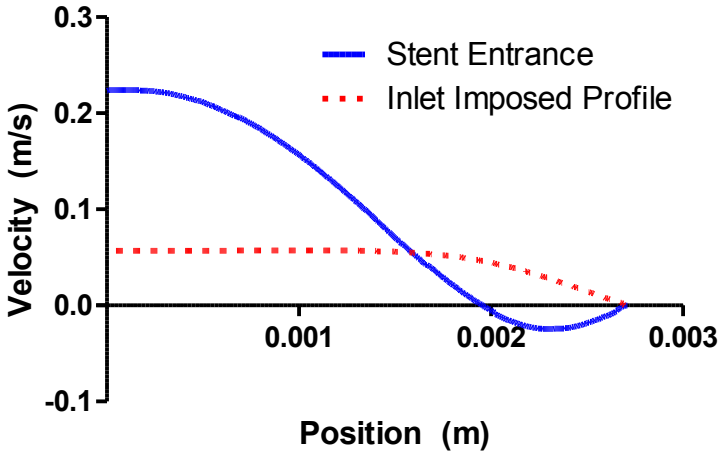

Figure 3.11: Velocity profiles at t = 0.4 s, near the cardiac cycle flow minimum, in normotensive carotid model.

Inlet velocity (red) is a blunt power law profile as described, and develops into Womersley solution just before the stent (blue). Profiles are shown for half of the stent diameter, from center position 0 to full radius R at 0.00275 m. Although overall flow is positive, velocity near the wall is negative, contributing to a non-zero OSI for the normotensive simulation.

Although the shear stress is not greatly changed on stent surfaces from normotensive to hypertensive conditions, the OSI changes much more. The overall integrated flow is very similar, and the magnitude of the peak systole is similar between the two waveforms. The biggest difference then is in the shape of the two waveforms. In particular the range or fluctuation between the post-sytole global flow minimum and the local maximum in diastole is much smaller in hypertension, representing a lesser degree of oscillation.

Wall shear stress levels are also expected to impact function and gene expression of any endothelium seeded onto stent surfaces. Sustained "high" WSS of 10 Pa promotes a different phenotype than normal WSS (~2 Pa) or low WSS (<0.4 Pa)[164]. Specifically, sustained high wall shear stress promotes expression of an anti-coagulant and anti-inflammatory phenotype, and promotes EC proliferation. A proliferative phenotype could be advantageous for the described application of endothelial seeding for a vascular stent, as EC proliferation could help seeded ECs compensate for any incomplete stent coverage and local vessel denudation following pre-stenting balloon angioplasty. Anti-coagulant and anti-inflammatory factors secreted by the cells would further the desired outcome of EC seeding, which is reducing stent thrombosis and hyperplastic restenosis.

The degree of flow reversal impacts endothelial function[165]. OSI is correlated with intimal thickening[154] and *in vivo* measures of EC inflammatory phenotype such as

NF-κB expression[166], expression of monocyte chemoattractant protein-1[167], and expression of platelet-derived growth factors which promote EC turnover and smooth muscle cell infiltration of the subintimal space[168]. However, OSI alone has been found not to be highly predictive of EC inflammatory activation *in vitro*[163]. While an OSI threshold that may represent activation of an inflammatory phenotype or intimal thickening has not been identified, cells on stent surfaces with high OSI may have higher levels of inflammatory markers and be more likely to exhibit an inflammatory phenotype than ECs on a normal artery of similar dimensions.

The presented study has some limitations and inherent assumptions. The stented vessel is modeled as being rigid with a constant radius; we do not model 'pillowing' of the vessel protruding into the lumen between stent segments[102], or local minor dilation of the stented portion of vessel, as might be expected by typical oversizing of self-expanding stents. While arteries exhibit compliance, the assumption of rigid vessel walls for modeling likely resulted in a moderate overestimation of wall shear stresses compared with a distensible wall model[169] but was highly advantageous for practical concerns of computational time. Vessel elastic expansion is expected to be limited by an implanted stent and is known to decrease with age[170], but any distension could potentially alter shear stresses and increase the degree of flow reversal, through the Windkessel effect. The relationship between the hypertensive and normotensive conditions served to estimate the effects of vessel compliance due to changes in the inlet

waveform alone. Despite these approximations and assumptions, the temporal changes within each waveform and the trends between healthy and hypertensive waveforms should still be representative of trends in the native environment. While the values calculated in this study are specific to the stent geometry and flow conditions studied here, the trends are expected to remain the same from normal to hypertensive conditions. Additionally, trends in the distribution of stresses among lateral and lumenal surfaces, and the higher shear stresses on struts near the stent inlet, are expected to be representative of and apply to many similar stent geometries.

Future studies could include different vessel sizes and flow rates, to account for a greater range of inter-individual variability and alternate implantation sites (i.e. iliac artery, coronary artery). Importantly, this study is the first to present information on hemodynamic conditions on a stent surface rather than only on the native vessel wall. This is important in predicting retention of ECs implanted onto stents, as well as making general predictions about expected phenotype of the ECs (inflammatory vs. healthy). The results also serve to predict differences in local conditions based on reduced vessel compliance in the hypertensive state, which apply to both the stent surface and the vessel surface.

3.6 Conclusions

In conclusion, our results show that the hemodynamic conditions on a carotid artery stent are expected to be conducive to retaining and supporting a seeded layer of

functional endothelium on an implanted stent surface, under both normal and hypertensive conditions. These findings provide new insight in shear stresses and oscillations directly on the surface of an implanted stent, and inform future efforts to seed endothelium onto stents.

3.7 Chapter acknowledgements

We gratefully acknowledge Cordis Corp for providing stents and Michael DeSoto for assistance with the solid modeling. This study was supported by NIH 1R21-HL109897-01 and AHA 12BGIA11070002 to HEA, as well as NSF Graduate Research Fellowship and AHA predoctoral fellowship 12PRE11180003 to AEJ.

4. Point-of-Care Seeding of Nitinol Stents with Blood-Derived Endothelial Cells

Portions of the text and figures included in Chapter 4 have been submitted to Circulation for publication. This article does not yet have a publication date; Circulation does not require permission for authors to reuse their own articles, but an optional grant of license may be obtained as soon as one was available via Rightslink®.

4.1 Chapter synopsis

This chapter describes the method proof of concept phase of developing a point of care method for seeding nitinol vascular stents with functional endothelium. Thrombotic and restenotic complications remain with vascular stents. To ameliorate these complications we sought to develop a method for seeding nitinol stents within the delivery system immediately before implantation. We machined hundreds of very small holes into the stent delivery system sheath surrounding a commercially made nitinol stent, to allow for exit of an infused cell suspension. Blood-derived endothelial cells (ECs) were flushed through the stent delivery system and adhered to the stent as the suspension medium flowed outward through the holes. ECs spread to cover the stent surface following 24 h culture *in vitro* under static or flow conditions. After flow, ECs exhibited increased nitric oxide production; expression of genes KLF-2 and COX2 trended upward from static baseline. After 48 hours *in vivo* in a porcine model, autologous seeded ECs spread to cover the stent surface (n = 4). ECs seeded onto commercial nitinol stents within minutes of expansion spread to form a functional layer

in vitro and *in vivo* after 2 days, providing proof of concept that the infusion method of ECs into modified stent systems can feasibly be used at the point-of-care to seed a functional autologous endothelium.

4.2 Introduction

Percutaneous transluminal angioplasty and stent placement have revolutionized the treatment of coronary artery disease and peripheral vascular disease; however, restenosis at the intervention site remains a significant problem. Stent failure is associated with thrombosis and intimal hyperplasia. Intimal hyperplasia after percutaneous intervention is especially problematic in the peripheral arteries. In the femoropopliteal arteries, approximately 50% of self-expanding stents occlude within two years[122,171]. Close to 20% of patients who receive carotid artery stents will suffer from re-occlusion of the stented vessels after only two years[123].

Drug-eluting stents in coronary arteries have reduced stent restenosis rates[16,38], and have recently been approved for peripheral vascular indications[33]. Drug-eluting stents, however, are associated with a risk of late-stage thrombosis once the drug coating has dissipated[39,40], related to a lack of endothelium[172,173]. As an alternative, biorebsorbable stents of various materials are in clinical trials in the US, and some are approved for use in Europe[174], but it is unclear how restenosis rates compare to conventional treatment when no structural support remains, following full absorption of the device[54,55]. In order to reduce long-term thrombosis and intimal hyperplasia,

several strategies have been investigated to recruit circulating endothelial progenitor cells (EPCs) to cover stents. Antibodies to CD34[73,74,175] and CD144[78], as well as RGD peptides[81], have been used to capture circulating EPCs. However, among all circulating cells, these markers are not specific for EPCs and no single antibody specific to EPCs has yet been identified. A capture strategy utilizing aptamers is under investigation but has not been tried *in vivo* and has not been shown to be specific to EPCs[85].

Our overall goal is, prior to deployment, to coat nitinol stents with the patients' own endothelial cells (ECs), derived from peripheral blood, to promote rapid endothelial coverage and thereby decrease the risks of stent thrombosis and in-stent restenosis. This approach is different from the current drug-eluting devices, which inhibit smooth muscle cell (SMC) proliferation, but also inhibit EC growth on the stent and therefore inhibit vessel healing[47,125,176-183]. If a methodology of rapid endothelialization can be developed, the intrinsic anti-coagulant mechanisms of ECs should reduce the risk of stent thrombosis, and paracrine factors released by endothelial cells (e.g. nitric oxide) would inhibit SMC proliferation and intimal hyperplasia[61]. A method of rapid endothelialization therefore would have the potential to address both major failure modes of stenting: thrombosis and intimal hyperplasia.

Previous approaches to directly seed metal stents with ECs prior to implantation have been limited by the use of immortalized or xenogeneic cell sources[63,64], pre-coating of the stent with potentially thrombogenic polymers or proteins, such as fibronectin[62,65-

[68], prohibitively long culture (>7 days) of the stent and cells together prior to stent deployment[64-67], and compression of an expanded stent back into a delivery catheter after seeding in its expanded state[64-66,71]. As such, these studies suffer from incomplete endothelial coverage, especially after recompression of the stent[64,71]. Furthermore, *ex vivo* culture in these studies proved to be impractical for translation of these methods into clinical practice. An alternative strategy, targeting using magnetically tagged cells with local injection[72], is not practical for nitinol stents because nitinol is not ferromagnetic.

As an alternative, we have invented a novel rapid seeding method (QuickSeeding™), in which an EC suspension is infused into the stent delivery system to coat compressed nitinol vascular stents with blood-derived ECs 10 minutes prior to deployment. This method eliminates the need to culture the stent and cells together for multiple days and manipulate the stent back into/onto a delivery catheter; instead, EPCs are isolated from peripheral blood, expanded as ECs *ex vivo* until needed, and then infused within minutes of deployment at the point-of-care. This method was developed based on the following results. We have shown that ECs attach to Ti without pre-coating[126]. Second, nitinol stents are typically electropolished such that the outer surface is comprised of titanium oxide (TiO_2) with no measurable nickel, and we established that ECs can also attach to nitinol stents without pre-coating[25,136]. Lastly, rapidly-seeded ECs spread quickly on Ti surfaces under fluid flow conditions *in vitro*

and *in vivo* to form a confluent lining that prevents thrombosis when implanted into the inferior vena cava of pigs[136]. Nitinol stents are used in the majority of peripheral cases because of the flexibility and shape memory of nitinol; superficial peripheral sites include carotid and femoral arteries[20]. The technology presented here applies to nitinol stents and therefore has the greatest potential for use in peripheral artery disease.

For QuickSeeding™ nitinol stents, we use ECs derived from colony-forming cells [79] or late-outgrowth ECs [184] isolated from blood. These ECs are phenotypically and functionally identical to vessel wall ECs[90] and can be derived from the blood of the patient who might need percutaneous angioplasty with stent placement[97]. We used ECs derived from human umbilical cord blood (hECs) for *in vitro* experiments because of their human origin. For *in vivo* experiments, we use ECs derived from porcine peripheral blood (pECs), so that cell implantation is autologous for each individual pig.

We test the following hypotheses: 1) modification of the sheath of a commercial stent delivery system with micropores enables rapid infusion seeding of compressed nitinol vascular stents with ECs at the point-of-care; 2) ECs remain adherent after stent deployment and under arterial fluid shear stress conditions; and 3) ECs are functional on the nitinol stent surface as measured by expression of anti-thrombotic genes and production of nitric oxide in response to fluid flow. To test these hypotheses, we performed *in vitro* and *in vivo* experiments with ECs seeded onto nitinol stents. Our

results support the feasibility of this method of personalized cell therapy at the point-of-care.

4.3 Materials and methods

4.3.1 Isolation and culture of human umbilical cord blood-derived ECs (hECs)

Umbilical cord blood samples were obtained from the Carolina Cord Blood Bank at Duke University per protocols approved by the Duke Institutional Review Board. The hECs for the study came from a total of three donors, and were cultured using standard practice in EBM-2 base medium plus EGM-2 SingleQuots (Lonza, Basel, Switzerland)[90]. Cells were used at passages 6-10 for *in vitro* studies.

4.3.2 Isolation and culture of porcine peripheral blood-derived ECs (pECs)

ECs for *in vivo studies* were isolated from porcine peripheral blood, as we described previously[136]. All experiments with swine were approved by the Duke University Institutional Animal Care and Use Committee (IACUC) and were conducted in accordance with the National Institute of Health Guidelines for the Care and Use of Laboratory Animals. Yorkshire swine (4 female, at an initial weight of approximately 35 kg) underwent a blood draw 4 weeks prior to stent implantation to allow sufficient time for EPC isolation and amplification in culture. The pigs were sedated with Acepromazine (1.1 mg/kg) and Ketamine (22 mg/kg) intramuscular. Intubation was achieved with an endotracheal tube (30 cm length, 8 mm ID), and the pigs were

anesthetized with Isofluorane by mask. The pigs' groins were cleaned and sterilized with DuraPrep, and femoral vein access was obtained with a 5 F micro-introducer kit (Galt Medical) using the Seldinger technique[133]. After discarding the first 5 ml of blood, 40 ml of blood were collected into syringes containing 20 USP/mL heparin. This was followed by 1:1 dilution with Hank's buffered salt solution (without $CaCl_2$, $MgCl_2$, $MgSO_4$) and layered on equal volumes of Histopaque to create well-defined layers. The mononuclear cell layer was collected as described previously[126] and plated into two 12-well plates in full porcine EPC growth medium: EBM-2 base medium plus EGM-2 SingleQuots without fetal bovine serum (Lonza) and 2% porcine serum (Gemini Bio-Products). Cells were used at passages 5-6 for *in vivo* studies.

4.3.3 Characterization of ECs

For flow cytometry, ECs were incubated with 0.025% trypsin (Lonza) for 3 min at 37°C, and the reaction was neutralized with Trypsin Neutralizing Solution (Lonza). Cells were incubated at room temperature with FITC-conjugated or AlexaFluor 488-conjugated antibodies for 30 min. For hECs, markers CD31 and CD105 were tested as well as monocyte markers CD14 and CD45 (Serotec and BioLegend). For pECs, porcine EC marker CD31 as well as porcine monocyte markers CD14 and CD45 were tested (Serotec and BioLegend). Isotype controls (mouse IgG1 and mouse IgG2a; Serotec, BioLegend, Antigenix America) were used for each condition as appropriate. Cells were rinsed and pelleted and fixed in 3.7% paraformaldehyde. Approximately 9000 cells

were counted for each antibody on a FACSCalibur flow cytometry machine at the Duke University Flow Cytometry Shared Resource.

4.3.4 Delivery system modification

To enable radial flow of media and cells, micropores were drilled in the outer sheath of commercial nitinol-stent delivery systems (Cordis S.M.A.R.T.® CONTROL Vascular Stent System with 30 mm long and 6 mm diameter stents, Cordis Corporation, Bridgewater Township, NJ) using a 193 nm ArF excimer laser light in collaboration with Fraunhofer CMI (Brookline, MA). Micropores were drilled in the sheath only in the area containing the stent, and four pores were clustered in each space between wire braid reinforcements of the sheath (Figure 4.2). Micropores were evenly spaced circumferentially and each delivery system had approximately 5000 pores. Representative measurements of the major and minor diameters were made at the sheath outer surface (n = 4 systems) using phase contrast images and ImageJ software. A minimum of 50 pores were measured on each stent and averaged to obtain each n.

4.3.5 Stent seeding

A schematic of the cell seeding within the delivery system is shown in Figure 4.1. Prior to seeding, the gap between the delivery system sheath and the atraumatic distal tip was blocked by a rubber cap, so that the cell suspension was forced to exit through the circumferential holes. Without this cap, the "path of least resistance" was the gap around the tip, and cell suspension passing through the specially designed micropores

was greatly reduced. To begin QuickSeeding™, air was removed from stent delivery systems by flushing 70% ethanol through the side-arm flushing port of the stent, which communicates with the stent but not the guidewire lumen of the device. Following, DPBS with calcium chloride and magnesium chloride was flushed extensively through the same side-arm port to rinse away all ethanol. The distal end of the delivery system was submerged in DPBS with calcium chloride and magnesium chloride until seeding to prevent any re-introduction of air.

For *in vitro* seeding experiments, adherent EPCs were labeled with the fluorescent dye Cell Tracker Orange CMRA (Invitrogen, Carlsbad, CA) in serum-free medium (15 min, 37°C). For *in vivo* experiments, adherent EPCs were labeled with the long-term fluorescent dye PKH26 (Sigma-Aldrich) at a concentration of 4 μM (4 min, room temperature), and the reaction was stopped with porcine serum (Gemini Bioproducts, West Sacramento, CA). Following labeling, cells were dissociated with 0.25% trypsin (Lonza), and after dissociation the trypsin was neutralized with Trypsin Neutralizing Solution (Lonza). Cells were counted, centrifuged for 5 minutes at 1500 RPM and resuspended to a concentration of 1.5-2 x 10^6 cells/mL in DPBS with calcium chloride and magnesium chloride (Lonza).

The 2 mL cell suspension was infused using a syringe and a syringe pump (0.4 mL/min) until the entire solution was introduced. Cell concentration was approximately 2.0 ± 0.5 x 10^6 cells/mL for *in vitro* experiments and 5.0 ± 1.1 x 10^6 cells/mL for *in vivo*

experiments. In both cases, we used the entire number of cells available, and similar flasks tend to hold more pECs than hECs due to cell size. Higher concentrations of pECs for *in vivo* experiments also helped to compensate against loss of cells during deployment in the moving bloodstream, which we have not quantified. After introduction of the entire solution, the delivery system sat stationary at room temperature for five minutes to enhance cell attachment prior to deployment. Depending on the experiment, stents were deployed into static medium, flow circuit tubing, or a porcine vessel.

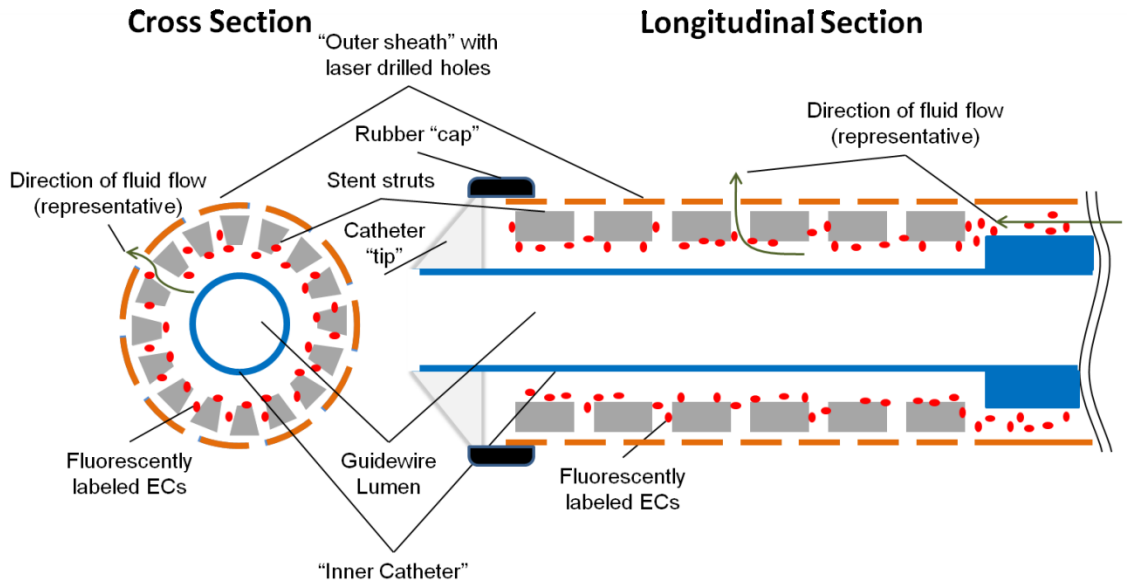

Figure 4.1: Schematic of in-catheter seeding of ECs.

Fluorescently labeled ECs (red) in a suspension are flushed through a stent delivery system from the proximal handle and adhere to a stent (gray) as the suspension medium flows outward through micropores in the delivery sheath (orange). The gap near the distal tip of the delivery system is closed with a rubber "cap" (black).

4.3.6 *In vitro* flow experiments

Stents for *in vitro* flow experiments were deployed into clear Tygon PVC tubing (McMaster-Carr, Elmhurst, IL) of 4 mm inner diameter. Tubing sections containing stents were filled with flow medium and connected to the flow circuit. The flow rate was increased gradually to the desired level over fifteen minutes. Stented tubes were exposed to steady laminar flow for 24 hours to simulate physiological shear stress of 15 dyn cm^{-2}, as we have done previously[126]. The applied shear stress of 15 dyn cm^{-2} was achieved by applying a flow rate of 160 mL/min. This imposed flow rate Q was calculated[185] according to

$$Q = (\tau \bullet \pi \bullet r\text{^}3) / (4 \bullet \mu) \quad (1)$$

where μ is the fluid viscosity at 37°C (0.035 g cm^{-1} s^{-1}), τ is the desired wall shear stress (15 dyn cm^{-2}), and r is the tubing radius (0.2 cm). Medium used for flow experiments was EBM-2 base medium plus EGM-2 SingleQuots (Lonza), with 3% (by weight) dextran added (Fisher Scientific), to increase the viscosity from standard medium and consequently reduce the flow rate while maintaining the desired shear stress. Medium was sterile filtered after addition of Dextran.

4.3.7 Nitric oxide quantification

To quantify nitric oxide (NO) production by ECs under flow and static conditions *in vitro*, we directly measured the primary oxidation product nitrite (NO_2^-) in 150μL medium samples collected from the static control flask and flow circuit reservoir

and 0 and 24 h in 5 experiments. Samples were frozen at -80°C after collection until analysis. Nitrite is a commonly used surrogate of NO availability[126] and has been shown to reflect changes in NO bioavailability following physical stimuli more effectively than measuring nitrate (NO_3^-) or the combined quantity of nitrite and nitrate (NOx)[186]. Nitrite concentration was measured by chemiluminescence with an Ionics/Sievers Nitric Oxide Analyzer (NOA280; Sievers Instruments, Boulder, CO) as described previously[126]. The total amount of nitrite produced was calculated as the product of concentration times the total volume of the medium (30 mL for flow circuit or 10 mL for static control), while adjusting for volume lost from taking samples.

4.3.8 Immunohistochemistry, fluorescent microscopy, and image analysis

EC-coated stents for imaging were fixed in 3.7% buffered formaldehyde (Ricca Chemical) and permeabilized with 0.1% TritonX-1000 (Sigma-Aldrich). Cells were blocked in 10% goat serum and incubated with mouse anti-human CD31 antibody (Invitrogen) diluted 1:100. Following, stents and cells were incubated with the secondary antibody goat anti-mouse IgG AlexaFluor 488 (Invitrogen), diluted 1:500. Nuclei were counterstained with Hoechst 34580 (Invitrogen), diluted 1:1000. Fluorescent microscopy was performed with an inverted microscope (Leica) with a monochrome digital camera (Qimaging, Surrey, BC).

4.3.9 Quantitative RT-PCR

Following 24 h flow or static culture, cells were released from stents with trypsin, and total RNA was isolated for gene expression analysis (RNeasy Plus Micro Kit, Qiagen). Quantitative RT-PCR was performed (iScript cDNA Synthesis Kit and iQ SYBR Green Supermix; Bio-Rad) as described previously[90,187] with the Bio-Rad MyIQ iCycler to evaluate expression of antithrombotic genes COX2 and eNOS, transcription factor KLF-2, and inflammatory marker VCAM-1. The housekeeping gene glyceraldehydes 3-phosphate dehydrogenase (GAPDH) served as endogenous control to target gene expression, and cells grown in culture flasks under normal conditions provided reference RNA. To determine relative gene expression the 2^ΔΔCt method was used, modified for primer efficiency[188]. Efficiency of each primer was measured and used to find ΔΔCt. Measured primer efficiencies were 86% for both KLF-2 and GAPDH, 80% for VCAM-1, and 100% for both eNOS and COX2. The forward and reverse primers used based on the gene sequence of interested were as follows for each gene respectively:

(a) COX2: 5′-TGA GCA TGT ACG GTT TGC TG-3′ and 5′-TGC TTG TCT GGA ACA ACT GC-3′;

(b) eNOS: 5′-GTG ATG GCG AAG CGA GTG AAG-3′ and 5′CCG AGC CCG AAC ACA CAG AAC-3′;

(c) KLF-2: 5′-GCA CGC ACA CAG GTC AGA AG-3′ and 5′-ACC AGT CAC AGT TTG GGA GGG-3′;

(d) VCAM-1: 5′-GGG CTT TCC TGC TGC GAA-3′ and 5′-AAG AGG CTG TAG CTC CCC G-3′

(e) GAPDH: 5′-GAC CCC TTC ATT GAC CTC AA-3′ and 5′-CAT GGA CTG TGG TCA TGA GC-3′

Melting curves were obtained after each reaction to verify that only the target cDNA was amplified.

4.3.10 Cleaning and re-compression of stents

To conserve the stents specially-machined stent delivery systems, stents and delivery systems were cleaned and re-used, for *in vitro* experiments only. All stents used for *in vivo* studies were new and were not re-used. After cells were released from each stent for RNA isolation as described below, stents were cleaned by sonication in Alconox soap solution, rinsed thoroughly in deionized water, then sonication in 70% ethanol. Delivery systems were cleaned by flushing through of Alconox soap solution, deionized water, then 70% ethanol. To allow re-use of the specially modified delivery system sheaths (for *in vitro* studies only), the tip of the delivery system was cut off to facilitate re-loading, and the inner catheter lumen was blocked with cyanoacrylate adhesive to prevent fluid escaping through the inner catheter rather than the higher-resistance infusion holes. Stents were recompressed to the delivery system diameter using a concentric stent compression device (model RMC, Blockwise Solutions) and pushed into an empty delivery system. The delivery system end was then closed off

around the outer sheath with a rubber cap, again to force the cell infusion to exit through the machined holes rather than the end of the sheath. Delivery systems were gas sterilized prior to use (18 h, 55°C)

4.3.11 Stent implantation in swine

All experiments with swine were approved by the Duke University Institutional Animal Care and Use Committee and were conducted in accordance with the National Institute of Health Guidelines for the Care and Use of Laboratory Animals. Pig weight at the time of the stenting procedure was 38.0 ± 2.0 kg. For pre-operative anticoagulation, each pig received a loading dose of 300 mg clopidogrel by mouth two days prior to the stent implantation procedure. On the day of implantation, Clopidogrel 75 mg was given orally and every day following until the explantation and sacrifice. Additionally, 325 mg aspirin was given to each pig by mouth beginning two days before surgery and continuing every day until explantation and sacrifice.

On the day of stent implantation, the pigs were sedated with Acepromazine (1.1 mg/kg) and Ketamine (22 mg/kg) intramuscular. Intubation was achieved with an endotracheal tube (30 cm length, 8 mm ID), and the pigs were anesthetized with Isofluorane by mask. The pigs' groins were cleaned and sterilized with DuraPrep, and right femoral artery access was obtained with a 5 F micro-introducer kit using the Seldinger technique[133]. An 8F introducer sheath was placed, and 200 IU heparing/kg administered. The anatomy was navigated using an 0.035" guidewire and 5F

angiographic catheter, under fluoroscopic visualization with a Siemens Siremobil Compact C-arm. The bicarotid artery was engaged and limited angiography was performed to verify anatomy with ISOVUE infused contrast agent (Bracco). A long sheath was exchanged for the short sheath to support subsequent balloon and stent delivery, and an additional 100 IU heparin/kg administered. An angioplasty balloon (6 mm diameter x 40 mm length) was inflated in the common carotid artery at a pressure of 1-4 atm for 30-60 sec. Following removal of the balloon catheter, the stent delivery catheter was advanced and the stent deployed by retraction of the outer sheath using the handle. Following deployment of each stent, angiography was performed to verify good stent apposition and placement. Each pig received both a bare control stent and a cell-seeded stent (6 mm diameter x 30 mm length), implanted in randomized fashion into right and left carotid arteries. Therefore, balloon angioplasty, stent deployment, and angiography were repeated for the opposite common carotid artery so that each pig received a total of one control stent and one stent seeded with its own autologous pECs. Following the stent procedure, devices and sheaths were removed and pressure held on the puncture site until hemostasis was achieved.

4.3.12 Safety of cell-seeding procedure

A gross neurological exam was performed before and after the procedure after the anesthesia had worn off. The exam was repeated every 24 hours until sacrifice. Each pig's alertness was assessed and spontaneous movements and gaze evaluated for

lateralizing behavior. Additionally, the pig's blink responses were tested and their reaction to tactile stimulation on their right and left sides.

4.3.13 Stent explantation

Two days after stent implantation, pigs were sedated, intubated, and anesthetized as described for stent implantation. The carotid arteries were exposed following sharp and blunt dissection and heparin was administered (200 IU/kg) waiting a minimum of 5 minutes before clamping and explanting the vessel. The vessels containing stents were explanted after clamping, in a randomized order (control vs. cell-seeded), and immediately rinsed with DPBS. A small portion of stent was removed with scissors and placed into culture medium to test for cell metabolism with the CCK-8 Assay (Sigma-Aldrich, St. Louis, MO). The remaining vessel and stent were then placed in 3.7% paraformaldehyde for fixation for 30 minutes. After fixation, the stent was cut with scissors and its inner surface examined for any gross clot before proceeding with fluorescent microscopy. After the devices were explanted, the pigs were euthanized with Euthasol euthanasia solution (390 mg/mL pentobarbital sodium and 50 mg/mL phenytoin sodium at 1 mL/10 lbs)

4.3.14 Cell viability on explanted stent segments

A 10% solution of CCK-8 (Sigma-Aldrich) was added to each well containing small segments of control or pEC-seeded stents, and incubated at 37°C, 5% CO_2. Absorbance was measured at 450 nm using a microplate reader (Thermo Scientific,

Waltham, MA) after 3 h and 21 h. The number of stent rows (a.k.a. crowns) was recorded for each piece to normalize for the size of the stent segment and associated surface area available to contain cells. Absorbance at 3 h was subtracted from absorbance at 21 h to measure the cell metabolism over time for both cell-seeded and control stents.

4.3.15 Fluorescent microscopy of explanted stent segments

Following explantation and paraformaldehyde fixation, the stents were cut longitudinally to visualize the inner surface as stated previously. The presence of PKH26-labeled ECs on stents was examined on an upright DMRB model microscope (Leica, Solms, Germany) with Qicam monochrome digital camera (Qimaging, Surrey, BC) and Image Pro Plus software (Leica). Stent segments were also subsequently imaged on a Zeiss 780 upright confocal microscope (Zeiss, Oberkochen, Germany).

4.3.16 Scanning electron microscopy (SEM)

Following stent explantation, paraformaldehyde fixing, and fluorescent imaging, stents were additionally fixed in glutaraldehyde 2%, then dehydrated in graded ethanol and hexamethyldisilazane (HMDS). Samples were sputter coated with gold for 30 sec and images taken with a XL30 Environmental SEM at 3-5 kV (FEI, Hillsboro, OR).

4.3.17 Statistical analysis

Since cells from the same source were used for a given flow experiment and static control, NO production was compared using a two-tailed paired t-test. RT-PCR

data was analyzed with a one-sample t-test vs. 1. CCK-8 metabolic activity assay was evaluated using a paired t-test. Statistical analyses were performed using GraphPad Prism 5 (GraphPad, La Jolla, CA) and JMP 8 software (SAS, Cary, NC). Values of $p < 0.1$ were considered to be statistically significant for the CCK-8 assay, with a limited sample size of three stents. Values of $p < 0.05$ were considered to be statistically significant for all other tests.

4.4 Results

4.4.1 EC isolation and characterization

The isolated hECs and pECs exhibited characteristic endothelial cell cobblestone morphology. Flow cytometry confirmed that the cell population was positive for EC markers CD31 and CD105. Cells were negative for leukocyte markers CD14 and CD45.

4.4.2 Delivery system micropore characterization

Micropores drilled into in the delivery system were observed with phase contrast microscopy and found to be evenly covering the stent (Figure 4.2) (approximately 5,000 pores per stent). Micropores were repeatably oriented in groups of 4 between braided wire reinforcements in the sheath, which could not easily be drilled through. Micropores were nearly circular at the sheath outer surface as visualized by light microscope, with major diameter of 39.4 ± 0.9 μm and minor diameter of 32.4 ± 0.4 μm (n = 4 systems). The minor diameter aligned along the direction of the stent axis.

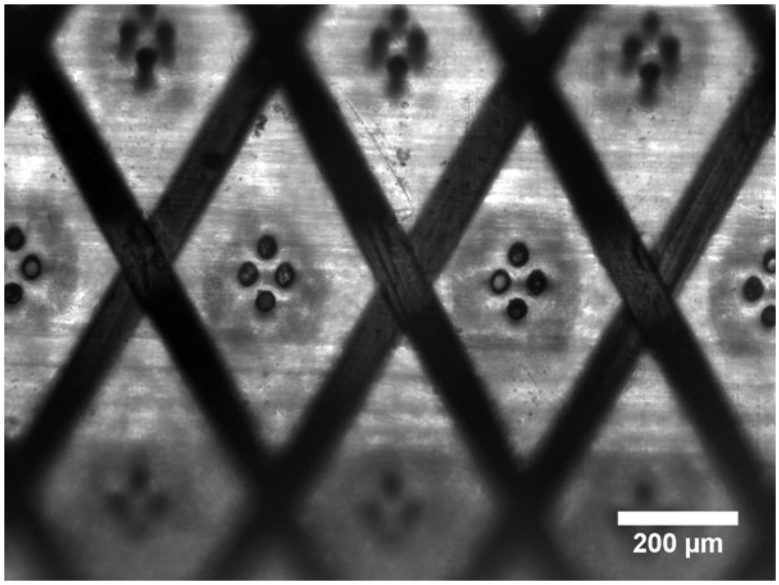

Figure 4.2: Light microscope image of holes machined in outer sheath of a commercial stent delivery system for the process of infusion seeding.

Each delivery system had approximately 5000 holes over the area of the stent.

4.4.3 hEC coverage and spreading inside nitinol stents *in vitro*

hECs QuickSeeded immediately before deployment were retained on the stent. Those hECs spread to cover the surface under both static and flow culture conditions. hEC surface coverage immediately after seeding (Figure 4.3A) was calculated as 55,000 ± 9,500 cells/cm^2 (n = 4). Large areas of the stent surface were covered with a confluent layer (Figure 4.3B,D) after 24 hours under both static and flow conditions. hEC confluence was confirmed by PECAM stain of cell junctions after 48 hours static culture (Figure 4.3C).

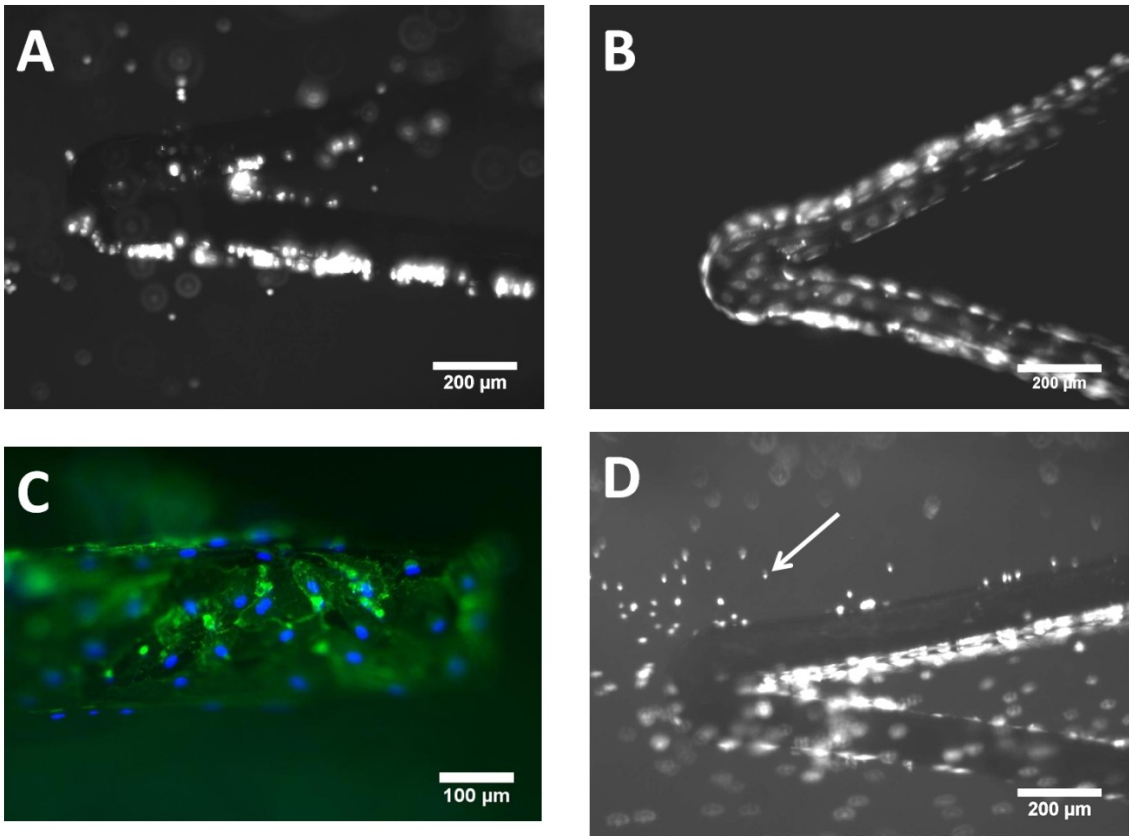

Figure 4.3: hEC coverage and spreading inside nitinol stents *in vitro*.

(A) Stent with hECs immediately following QuickSeeding™ *in vitro*. Stain: CellTracker Orange (LifeTechnologies, Carlsbad, CA). (B) Stent with hECs following QuickSeeding™ and 24 hours static culture viewed from the lumenal side. Stain: CellTracker Orange. (C) Stent with hECs following QuickSeeding™ and 48h static culture, pictured on lateral stent strut surface. Stain: PECAM (green); Hoechst 34580 (blue) (LifeTechnologies). Note that curved stent surface causes some areas to be out of focus while others are in focus. (D) Stent with hECs following QuickSeeding™ and 24 hours flow. Stent is viewed from outside through clear Tygon tubing of flow circuit (Stain: CellTracker Orange). Unspread hECs can be observed adherent to the tubing (arrow), whereas cells on nitinol stent are spread.

4.4.4 Nitric oxide production

We assessed NO levels by directly measuring nitrites in the cell culture medium and adjusting for respective fluid volume under flow and static conditions. Nitrite levels showed that there was a significant increase of NO production in the flow condition as compared to the static condition, after 24 hours time ($*p < 0.01$, $n = 5$). Total nitrite in the static condition was 0.41 ± 0.13 nmol, and total nitrite in the flow condition was 7.83 ± 1.97 nmol (Figure 4.4).

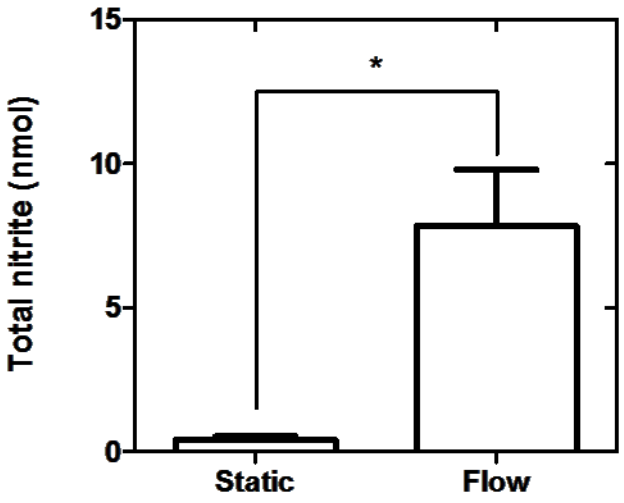

Figure 4.4: Nitrite production of ECs seeded onto nitinol stents, following 24 hours flow or static culture (*p < 0.01, n = 5).

4.4.5 Gene expression

ECs QuickSeeded™ onto stents were exposed to static or flow conditions for 24 hours and then evaluated for expression of several genes. Expression of inflammatory marker gene VCAM-1 was unchanged from static to flow conditions. In contrast, gene expression of eNOS was significantly downregulated in the flow condition ($p < 0.005$, one-sample t-test vs. 1). Although expression of anti-thrombotic genes KLF-2 and COX2 were upregulated, they did not reach statistical significance with a sample size of $n = 6$ (Figure 4.5).

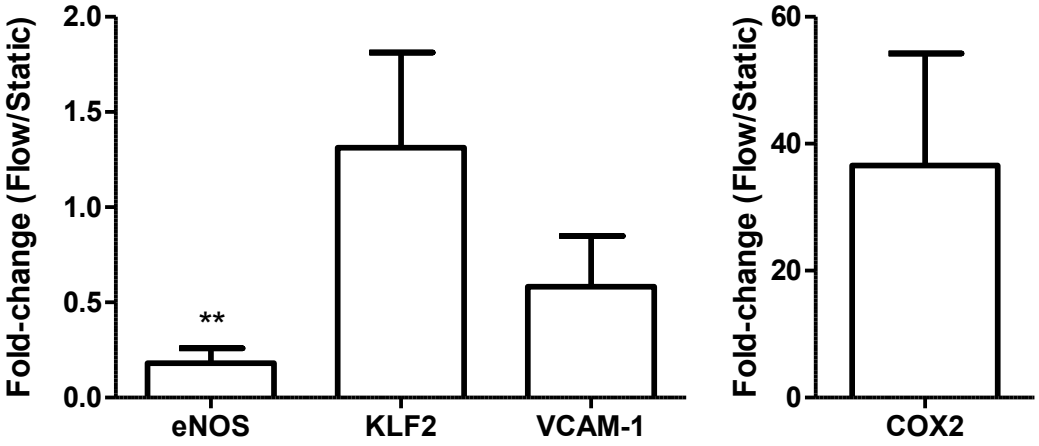

Figure 4.5: Gene expression of ECs on stents following 24 hours flow.

Values are normalized to static conditions (p < 0.005, n = 6, one-sample t-test vs. mean of 1).**

4.4.6 Safety of cell-seeding procedure *in vivo*

All pigs survived the procedure without complications. A neurological exam did not reveal any evidence of cerebrovascular accidents. The pigs were alert and oriented after the procedures; their gait was normal and symmetric; spontaneous movements were of similar magnitude on the right and left side. The pigs would blink to threat on the left and right and they did not exhibit gaze preference to either side. Further, the pigs reacted to tactile stimulation on their right and left sides.

4.4.7 pEC retention and spreading inside nitinol stents *in vivo*

The autologous fluorescent pECs, which were seeded onto the nitinol stents ten minutes before surgery, were visualized on every one of the four cell-seeded stents after two days *in vivo* and were found to have spread on the stent surfaces to form confluent monolayers (Figure 4.6). All pECs visualized on the cell-seeded nitinol stents were positive for fluorescent dye PKH26, supporting that these were the cells pre-seeded onto the stent and not colonized from the bloodstream or local vessel wall. Following staining with Hoechst 34580 for nuclei, selected samples were imaged again. Many extra nuclei were seen on both control and cell-seeded stents, but only cell-seeded stents were positive for EPC dye PKH26 (Figure 4.7). SEM images revealed these to be leukocytes. Both conditions had leukocytes visible on the surface; on the EC seeded stent these were on the ECs themselves. SEM images showed good coverage of ECs on the seeded stent, and fibrous covering on the bare metal stent (Figure 4.8).

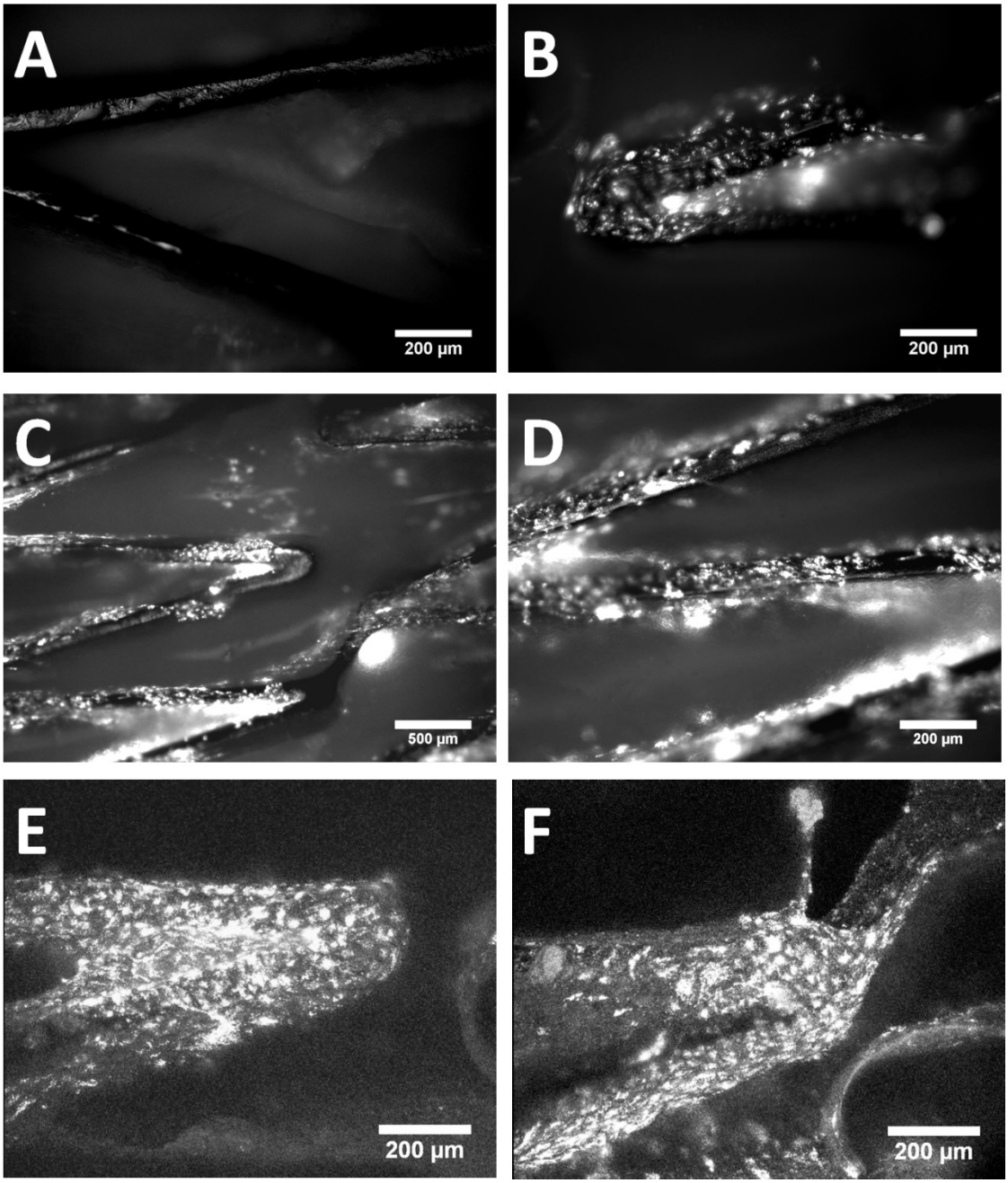

Figure 4.6: Stents following two days implantation in porcine carotid arteries, viewed from the lumenal (inner) side.

(A) Fluorescent microscope image of control (bare metal) stent. Variations in light are caused by reflections from the uneven metal surface. No endothelial cells are observed. (B-D) Fluorescent microscope image of cell-seeded stents. Stain: PKH26. (E-F) Confocal microscope image of cell-seeded stents. Stain: PKH26.

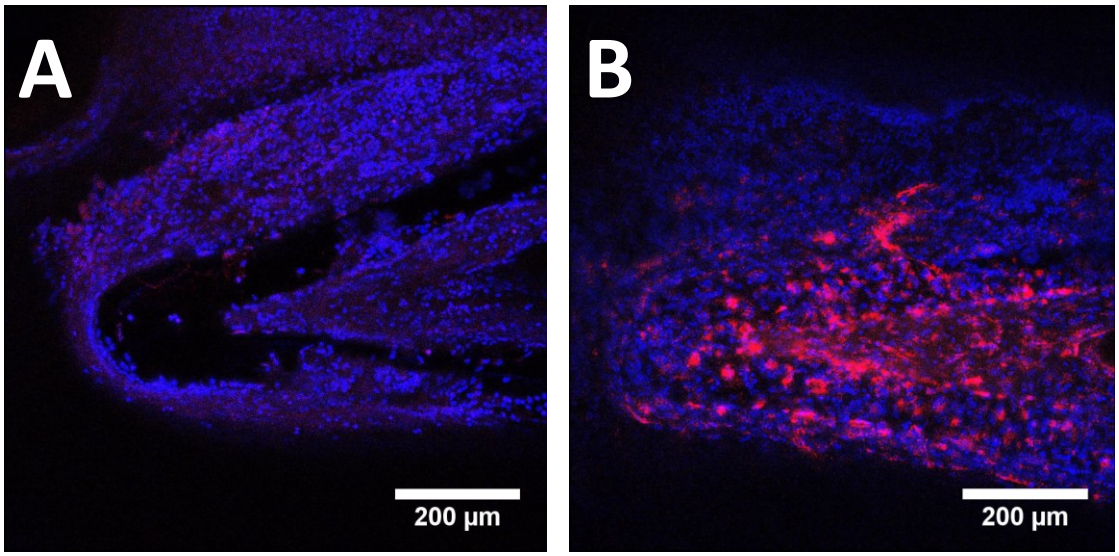

Figure 4.7: Confocal microscopy of stents following nuclear staining.

Stains: PKH26 (red), Hoechst34580 (blue). (A) Bare metal control stent. (B) pEC-seeded stent.

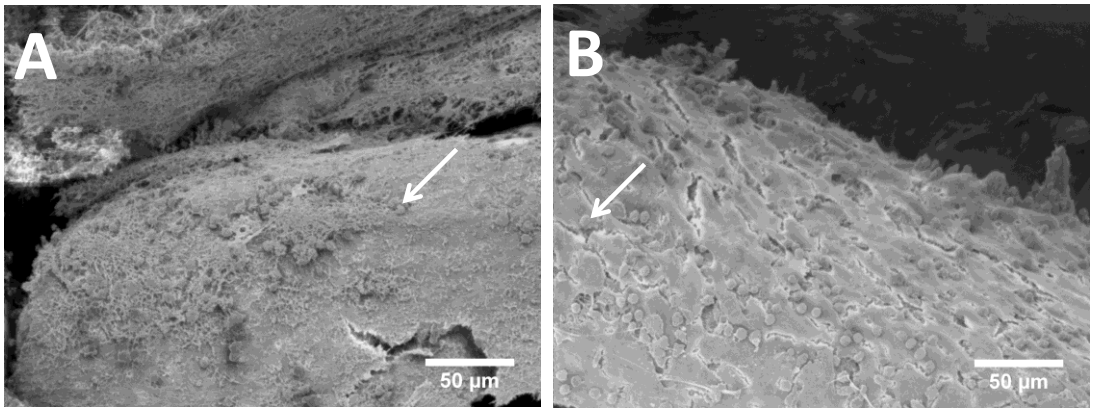

Figure 4.8: SEM image of stents following two days *in vivo* implantation.

Examples of leukocytes are indicated by arrows. (A) Bare metal control stent. (B) pEC-seeded stent with confluent endothelium seen on surface.

4.4.8 pEC viability inside nitinol stents *in vivo*

The CCK-8 metabolic assay suggested greater metabolic activity on the pEC-seeded stent segments than on the bare metal control stent segments ($p < 0.1$, $n = 3$), measured by a paired test of absorbance in the medium. Absorbance increased between 3 hours and 21 hours and was greater than the blank condition in both the control stents and pEC-seeded stents. However, the pEC-seeded stent showed a greater increase in absorbance than the control stent for every pair ($n = 3$), consistent with the hypothesis that pECs were covering the surface and were both viable and metabolically active (Figure 4.9).

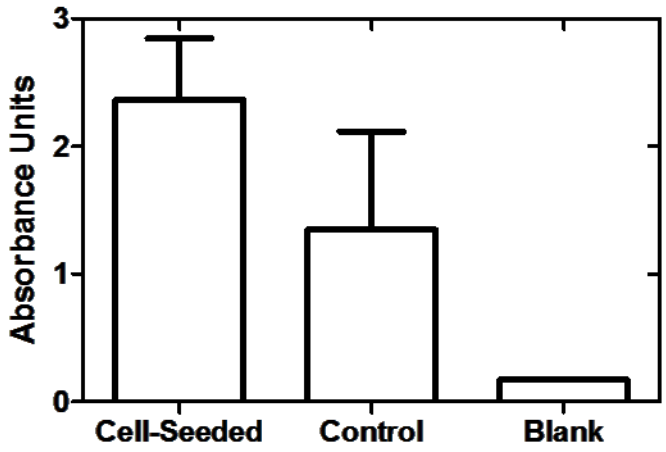

Figure 4.9: CCK-8 metabolic assay showing absorbance increase from 21 to 3 hours.

Cell-seeded samples showed more metabolic activity in every pair, consistent with the presence of metabolically active seeded ECs. (n = 3, cell-seeded and bare metal control; n = 1 blank).

4.5 Discussion

Rapid endothelialization of vascular stents is highly desirable to prevent thrombosis and ameliorate intimal hyperplasia. Especially in peripheral arterial disease, quick endothelialization may reduce the failure rates of the current standard of care. Ideally, stent seeding should utilize an autologous cell source so that immunosuppressive therapies are not required, and the cells are not immunogeneic. Blood-derived ECs as used in this study are an easily accessible source of autologous cells to each patient. The challenge of seeding cells quickly without re-compression of the stent was overcome using the QuickSeedingTM methodology.

The *ex vivo* results in this study show that hECs seeded onto a self-expanding nitinol stent with the QuickSeeding™ method remained adherent following stent deployment. Cells were retained under physiological flow conditions. Cells on the stent surface were functional, as demonstrated by the increase in nitrate production over 24 hours; this increase was significantly greater after exposure of the seeded stent to flow, as would be expected for a healthy layer of ECs. After QuickSeeding™, deployment, and flow, there was no evidence of EC "activation" to a pro-inflammatory phenotype, as demonstrated by the unchanged gene levels of VCAM-1 at 24 hours.

Antithrombotic genes COX2 and KLF-2 increased with flow but were not statistically significant. The analysis was confounded by the variability introduced by the very small amount of RNA collected from each single stent, though housekeeping

gene GAPDH helped to control for this. The coefficients of variation for KLF-2 and eNOS were much higher for ECs exposed to flow on the stent than on planar Ti surfaces [189]. Estimates of sample sizes required to evaluate the significance of COX2 and KLF-2 expression given the current mean and standard deviation were approximately 30 and 300, respectively. Levels of the eNOS gene were downregulated in the flow condition, which is surprising since nitrate levels, indicative of NO, increased. We have previously observed that nitrate levels can increase in the absence of an upregulation of the eNOS gene in hECs[189]; other factors such as phosphorylation of the eNOS enzyme, known to increase with shear stress, can increase enzyme activity and lead to more NO production[190-194].

Several factors influenced the variable levels of gene expression. Variations in shear stress over the stent surface likely contribute to the high variability of gene expression. Computational simulations of steady-state flow over identical stent geometry revealed large variations in shear stress experienced by different stent surfaces (Chapter 3, Figure 3.4). On lateral surfaces of the stent, a large shear stress gradient exists, and shear stresses vary by one order of magnitude along the width of the strut. Even under steady state conditions, the geometry of the stent was found to cause localized regions of flow reversal, equivalent to 3.6% of the fluid volume flowing through the stent. This steady-state simulation closely approximates the conditions of our *in vitro* flow circuit. The generalized collection of cells from a stent to assess gene

expression caused a pooling of cells from these different surfaces and introduced large additional variability. Collecting cells from the stent surfaces with trypsin was difficult with the complex geometry, and cell collection was likely only partially complete, adding to variability between experiments. Coefficients of variation for KLF-2 and eNOS were much higher on from the stent than from planar Ti surfaces[189]. Estimates of sample sizes required to evaluate the significance of COX2 and KLF-2 expression with these variation conditions were approximately 30 and 300, respectively. Time-varying flow conditions as those occurring *in vivo* further increase variation in shear stress across stent surfaces, as presented in Chapter 3.

Our *in vivo* and *in vitro* results demonstrate that pECs QuickSeeded™ onto a stent just minutes before implantation remain adherent even when deployed and then exposed to arterial shear stresses for 24 or 48 hours. Under these conditions, pECs spread on the stent surface and formed confluent monolayers. Although shear stresses during deployment are not precisely known, we estimate they are below 400 dyn/cm^2 based on the expected flow rates at the vessel center. At this level of shear stress for 15 min exposure, we found 20% detachment after a similar static cell attachment time of 15 min[126]. Some number of cells may be lost during deployment in the moving bloodstream, but sufficient cells remain to form a spread endothelial layer on the surface.

The cell seeding therapy presented in this study appears safe, as no adverse events or outcomes were observed in any animals. During the two-day duration of our *in vivo* studies, no gross thrombosis was observed in arteries stented with either cell-seeded or bare metal control stents. This was consistent with our expectations, based on the relatively short study duration and anticoagulant regimen (intraoperative heparin and daily aspirin and clopidogrel until sacrifice).

The *in vivo* study was designed to establish proof of principle and a longer-term study is needed to evaluate any differences in surface thrombosis on stents "protected" by an EC covering. Additionally, reducing the anticoagulant regimen would provide a greater "challenge" to the cell-seeded devices. For the purposes of this study, the bilateral placement of an EC-seeded stent and a bare metal control stent in the same animal controlled for inter-individual differences and also increased the number of stents compared to the number of animals; however, the bilateral placement in this study design did mean that we could not collect blood to probe for any differences in circulating coagulation factors between animals that received an EC-seeded stent vs. a bare metal control stent. In addition to thrombosis, the second major failure mode of stents is restenosis due to intimal hyperplasia and SMC hyperproliferation. We anticipate that the paracrine factors released by ECs would help to inhibit SMC proliferation and intimal hyperplasia, thus addressing this mode of restenosis. To properly assess intimal hyperplasia, longer-term studies are needed.

Explantation demonstrated endothelialization after two days on four out of four QuickSeeded™ stents implanted in porcine carotid arteries. In contrast, no ECs were observed on the bare metal control stents. In previous porcine studies, ECs are observed to "mostly" cover a stent implant after 7 days[195]. Cells observed on the QuickSeeded™ stent were the same pECs which we seeded onto the stent, and not "fall-out" cells from the adjacent vessel wall or circulation, as shown by the presence of the pre-implantation stain PKH26. The metabolic assay performed on the explanted stents suggests that the adherent pECs were alive and functional after two days. The bare metal stents showed metabolic activity, but to a lesser degree, consistent with the notion that both QuickSeeded™ and bare control stents had red blood cells and other cells on the surface after removal from blood circulation, and that the pECs account for the greater activity on seeded stents.

This study has the following limitations. One, the seeding parameters are not fully optimized. Therefore, we do not know exactly what optimal size, number, and spatial distribution of micropores in the delivery system wall will result in maximum EC coverage. Similarly, infusion parameters such as cell concentration, infusion rate, and "hold time" following infusion, can be changed and may be fine-tuned for increased EC coverage. Two, coverage itself is difficult to quantify; the geometry of the stent creates difficulty for bringing a large field into focus with conventional microscopy. The impact may be that some areas of the stent are covered with a lower density of cells, which do

not become fully confluent when spread. The small surface area of the stent limited the number of cells that could be removed and thus complicated interpretation of RT-PCR results. Three, the time required to isolate and expand cells is approximately 3-4 weeks. Although peripheral stenting procedures are more likely to be elective when compared to coronary procedures, future improvements in the isolation method are needed to increase initial yields[196] and decrease the culture time.

Nevertheless, this study provides an important first proof-of-concept that rapidly seeding ECs onto vascular stents at the point-of-care can lead to successful adhesion and survival after implantation. This study avoids many of the pitfalls of previous approaches such as thrombogenic pre-coatings, use of non-autologous cells, and cumbersome manipulation of a sterile endothelialized stent back into the delivery catheter. As such, the technology described here is the most clinically practical approach for endothelializing vascular stents that has been presented to date.

In conclusion, we have demonstrated the feasibility of seeding autologous endothelial cells onto nitinol vascular stents at the point-of-care just minutes before stent deployment. Stents implanted for two days into porcine carotid arteries retained seeded endothelium and showed no observable thrombus or safety problems. Future studies should examine longer periods of implantation in vivo to further characterize the technology; specifically, the ability of cells to remain on the stent long-term and the impact of the technology on intimal hyperplasia long-term.

4.6 Conclusions

We have demonstrated the feasibility of seeding autologous endothelial cells onto nitinol vascular stents at the point-of-care just minutes before stent deployment. Stents implanted for two days into porcine carotid arteries retained seeded endothelium and showed no observable thrombus or safety problems. Longer term studies with more implantations are needed to further characterize this new technology.

4.7 Chapter acknowledgements

We gratefully acknowledge Jason Allen and Thomas Stabler for nitrite measurement; Vrad Levering, Tracy Cheung, Cristina Fernandez for cell isolation; Melissa Ley for exceptional project support; Maria Noviani for surgical assistance. We are extremely grateful for financial support from the MORNINGSIDE FOUNDATION. This study was supported by NIH 1R21-HL109897-01 and AHA 12BGIA11070002 to HEA, as well as NSF Graduate Research Fellowship and AHA predoctoral fellowship 12PRE11180003 to AEJ, and grant 'Short term implantation of EPC-QuickSeeded stent,' from the MORNINGSIDE FOUNDATION.

5. Dissertation summary and future work

5.1 Dissertation summary

This project was motivated by the clinical need to improve the success rates of metal vascular stents, and reduce the incidence of thrombosis and intimal hyperplasia. The following hypotheses were tested: (1) ECs seeded onto Ti blood-contacting surfaces minutes before implantation will create a confluent cell layer *in vivo*; (2) This treatment will prevent thrombosis when inserted into the pro-thrombotic environment of the inferior vena cava (IVC) in swine; (3) Fluid stress conditions on the surfaces of an implanted carotid artery stent are amenable to supporting endothelial cell retention and antithrombotic function; (4) Modification of a commercial stent delivery system with micropores enables rapid infusion of ECs and adhesion to nitinol stents; and (5) ECs remain adherent and spread to form a functional layer after stent deployment and under arterial fluid shear stress conditions. The specific aims of the project were to: (1) optimize seeding of ECs onto Ti tube surfaces and characterize reduction of thrombus formation in swine; (2) determine fluid stresses on implanted carotid artery stent and predict suitability of surfaces for EC seeding; and (3) evaluate adhesion and function of seeded ECs on stents after deployment *in vitro* and *in vivo*.

In Chapter 2, the proof of concept was presented for using blood-derived ECs to cover Ti blood-contacting surfaces for reducing thrombosis *in vivo*. ECs were seeded onto solid Ti tubes by rotating a cell suspension and tube together for 30 min, prior to

static culture *in vitro* or implantation *in vivo* in the porcine inferior vena cava. All 4 cell-seeded *in vivo* implants were free of clot after 3 days, whereas 4 bare metal controls without ECs were either entirely occluded or partially thrombosed. Pre-labeled ECs had spread and were present on all 4 cell-seeded implants, while no endothelial cells were observed on control implants. ECs also spread on tubes cultured statically *in vitro,* and the degree of spreading was equal to the tubes seeded and implanted *in vivo.* These results suggest that blood-derived ECs represent a promising source of lining Ti implants to reduce thrombosis *in vivo.* Results from Chapter 2 supported the hypotheses that ECs seeded onto a Ti blood-contacting surface at the point of care could spread to create a confluent layer *in vivo*, and that the EC treatment could prevent thrombosis in the porcine vena cava. The results also supported progression from this materials proof of concept to a vascular stent application of EC seeding.

Shear stresses and oscillatory shear indices (OSI) on various surfaces of an implanted carotid artery stent were calculated and presented in Chapter 3. In both normotensive and hypertensive flow models, time-averaged shear stresses were <5 Pa on all stent surfaces. Transient shear stresses were <27.5 Pa on all stent surfaces, and were highest at peak systole and on the lumenal surface. Oscillatory shear stress was highest on lateral surfaces and lower lumenal surfaces. OSI was lower in the hypertensive flow model on all studied surfaces, corresponding to reduced vessel compliance and reduced fluctuation of the input waveform. Those regions that

exhibited flow reversal may alter endothelial cell function somewhat. Results from Chapter 3 supported the hypothesis that fluid stress conditions on the surfaces of an implanted carotid artery stent are amenable to supporting endothelial cell retention and antithrombotic function.

In Chapter 4, proof of concept studies for a new point-of-care EC seeding method of nitinol vascular stents were presented. Stent delivery systems which had been modified with small micropores allowed for the delivery of a cell suspension by infusion, so that ECs could be introduced to a stent minutes before its deployment *in vitro* or *in vivo.* ECs adhered to the stent, with coverage of 55,000 ± 9,500 cells/cm^2. ECs spread to c over the surface, following 24 hours culture *in vitro* under static or flow conditions. After flow, ECs exhibited increased production of the antithrombotic vasodilator nitric oxide. Additionally, after 24 hours flow, expression of genes KLF-2 and COX2 trended upward from their static baseline. After 48 hours *in vivo*, rapidly-seeded autologous ECs had spread to cover the surfaces of stents deployed in porcine carotid arteries (n = 4). A cell metabolism assay showed that EC-seeded stents had higher levels of cell metabolism after implantation, a difference which is attributed to the ECs on the surface and supports the idea that seeded ECs remained alive and functional *in vivo*. The results presented in Chapter 4 supported the hypotheses that modification of a commercial stent delivery system with micropores enables rapid infusion of ECs

and EC adhesion to nitinol stents, and that ECs remain adherent and spread to form a functional layer after stent deployment and under arterial fluid shear stress conditions.

Overall the results presented in this dissertation support the feasibility of a point-of-care method for stent seeding. Specifically, we found that ECs seeded onto Ti surfaces and nitinol stents minutes before introduction into the arterial or venous bloodstream *in vivo* remained adherent and spread to form a functional endothelial layer. We found that ECs seeded onto stents and exposed to steady flow *in vitro* released nitric oxide and expressed some of the anti-thrombotic genes typically upregulated under flow conditions. We also found that fluid shear stresses on the surface of a commercial nitinol stent implanted in a carotid artery are conducive to supporting EC adhesion and function, using a computational fluid dynamics model.

5.2 Future work to complete current studies

In Chapter 3, the shear stresses and oscillatory shear stresses on a deployed stent were determined and presented. Other commercial stent designs and other vessel sizes could be modeled to further expand and complete this study. Additionally, the shear stresses on the stent during deployment were not determined, but are expected to be non-negligible. Evaluating stent deployment in bloodflow as a moving boundary problem would give insight to the expected portion of cells lost during *in vivo* stent expansion to further complete this study.

In Chapter 4, feasibility studies for a point-of-care stent endothelialization method were presented. Input parameters for seeding could be further optimized, including: (1) cell infusion rate, (2) cell suspension concentration and volume, (3) size and distribution of micropores, and (4) "hold" time between cell infusion and stent deployment. These parameters were established for feasibility studies without systematic optimization, which could enhance cell coverage for subsequent studies. Additionally, pre-coating of the stent with an antibody or protein to enhance cell attachment remains as an option, though it would complicate the method concept.

To further complete the work presented in Chapter 4, longer term *in vivo* studies are recommended. A longer study duration is needed to assess the impact of EC seeding on thrombosis and intimal hyperplasia (with histological analysis). At a later time point, the initial inflammation from the stenting procedure would be reduced, allowing for better assessment of any sustained innate immunity response and leukocyte attachment to stents, as was observed in the short-term study of Chapter 4. While the studies in Chapter 2 presented strong differences in coagulation following EC seeding, these studies were conducted in the low-shear environment of the inferior vena cava. To assess effectiveness of the EC stent seeding on reducing surface thrombosis, a longer study is needed in the high-shear arterial implantation site.

To quantitatively assess the *in vivo* coverage with seeded ECs on implanted stents, a non-destructive visualization method would be required. We have proposed

an internal visualization device based on an endoscope platform with added fluorescent capability. Further work to develop this device to a working state would allow assessment of EC coverage to further complete the studies in Chapter 4.

5.3 Implications of this research

This work represents the first introduction of a point-of-care method for endothelializing metal stents with autologous cells. As discussed in Chapter 1, almost 1 million stents are placed each year in the United States alone, when considering both coronary and peripheral stenting procedures. These stents have the potential to fail because of thrombosis and intimal hyperplasia, and up to one quarter of these will require re-intervention, depending on the stent location and type (bare vs. drug-eluting). A new method and technology with the potential to improve restenosis rates could translate to years of improved patient quality of life, as well as reduced hospital costs because of a potentially reduced number of required re-interventions.

Results from Chapter 2 illustrate that autologous blood-derived ECs covering a Ti surface in contact with the bloodstream can prevent thrombosis at the metal surface. Application of this result to VADs, as mentioned in Chapter 1, or to stents, as we did in Chapter 4, has the potential to reduce embolic events with VADs and improve restenosis outcomes of stents, respectively. Further, the covering of a metal implant surface with ECs to prevent coagulation could reduce the need for long-term preventative anticoagulation therapy for patients with these implants. Because such therapies have

high risk of bleeding complications and sometimes require routine blood testing, a technology that could reduce the use of these anticoagulants without requiring immunosuppression could be very beneficial to these implant patients, and ultimately reduce medical costs.

In Chapter 3, our results indicated that shear stresses on a stent implanted into the carotid artery were likely conducive to the retention and desirable function of ECs seeded onto the surface. This study was the first to closely examine shear stresses or oscillatory shear index on the surfaces of the stent itself, and supports the feasibility of point-of-care stent seeding for both normotensive and hypertensive conditions. If a cell seeding therapy is proposed for clinical implementation in the future, such models would help to support feasibility and effectiveness claims. Examining fluid impacts on the surfaces of stent struts could also help to inform and direct design of a stent that may be prospectively and intentionally designed for point-of-care endothelialization. As others in the past have shown that stent geometry impacts shear stress on the intermediate vessel wall between struts, it is also expected that geometry would impact shear stresses on the surface of the stent itself. Modeling shear stresses on a stent surface for different potential geometries and designs represents a more efficient development strategy than testing a wide variety of stent designs with ECs experimentally.

Our results in Chapter 4 show the proof-of-concept of seeding ECs onto stents just ten minutes before the stents are deployed into the arterial bloodstream. Although

the ECs had a limited time to attach to the surface, and although the surface was untreated with any protein or substance to enhance adhesion, ECs were retained after deployment *in vivo* and spread to cover the surface after 2 days. Such a result may be surprising to those not familiar with our previous work with ECs and Ti, and represents a strategy for endothelializing stents with potential for clinical application. As described in Chapter 1, past work to seed stents with endothelium has been hampered by cell source, long culture times of stent and cells together, and the difficulty of manipulating stents back into a delivery catheter while maintaining sterility, and without loss of the endothelial layer. Balloon expandable stents suffered from large losses of pre-cultured cells on the lumenal surface after the abrasion of the balloon against the stent required for stent expansion. In contrast to those past studies, the work in Chapter 4 is more practical for clinical implementation. An individual's cells could be collected as described, and the stent and delivery system with micropore modifications for infusion could be used "off the shelf."

In total, the results in this dissertation suggest that point-of-care seeding of titanium blood-contacting surfaces with blood-derived ECs is both feasible and effective for preventing thrombosis.

5.4 Future directions for the point-of-care stent seeding project

This project was intended to investigate the feasibility of a point-of-care method for endothelializing nitinol stents and titanium cardiovascular implants with autologous

cells. While the results within this dissertation are promising as a first proof of concept, there are multiple directions in which the project could go to develop a clinically feasible strategy for point-of-care endothelialization of stents. Future work should first focus on (1) improving coverage of the stent after seeding, (2) long-term studies *in vivo*, and (3) improving the efficiency of EC isolation from blood, in order to shorten the time between initial blood draw and stent seeding. Finally, adoption of the technology to clinical use will also require attention to logistical details of the procedure and the connection between cell technician and clinician.

Improving coverage of the stent after seeding may be partly accomplished by optimizing seeding parameters as described above. Cell concentration, infusion rate, and "hold time" may all contribute to differences in EC coverage on deployed stents. User factors such as speed of sheath retraction during deployment may also impact cell retention. More involved methods for improving stent coverage may include technologies such as brief inflation of a proximal occlusion balloon during stent deployment to temporarily halt blood-flow and thus reduce the fluid shear stress from flowing blood experienced by the stent during deployment. Temporary occlusion has been suggested previously for local cell delivery to a magnetized stent[72]; the duration of occlusion required to accomplish stent deployment would be much less than the 5-10 min proposed in that study to deliver cells.

Long-term studies *in vivo* were described above as future work to complete the current studies. In order to translate the point-of-care stent seeding method to clinical practice, long-term animal studies with larger numbers of subjects will be required to support any application for first human use. In addition to establishing safety, such studies will investigate and establish the effectiveness of the proposed seeding method in reducing thrombosis and intimal hyperplasia.

To reduce the lead time between drawing blood to isolate ECs and the stenting procedure, it would be necessary to improve the efficiency of EC isolation from blood. We have proposed and begun to investigate methods to isolate ECs at the point-of-care. With sufficiently specific antibodies or capture molecules, circulating endothelial progenitor cells could be collected from blood in a procedure similar to apheresis. It is likely that the total numbers of ECs collected would still be less than the number obtained after isolation of a few colonies and subsequent multiple weeks culture *in vitro*. Therefore, point-of-care EC isolation would need to be married with the increase in seeding efficiency to be practical.

Finally, challenges exist to adoption of this endothelialization technology in clinical use. As described in this dissertation, preparation of the cell suspension is done in a laboratory environment using a sterile biological hood and other equipment such as a centrifuge. If the technology is applied using cells expanded in a laboratory culture

facility (vs. those isolated at the point-of-care), coordination between the culture facility and operating suite will be important, as well as close proximity between the spaces.

Adoption by clinicians will be an important piece of this roll-out, as the preparation of the stent delivery system and infusion of the cell suspension is closely tied to the timing of pre-stenting balloon angioplasty and the stent deployment itself. While the delivery system preparation and infusion of the cell suspension could be accomplished by ancillary personnel in the sterile field, it is unknown at this point how critical the timing of cell infusion is, or what consequences may result from completing the infusion too early and allowing the seeded stent to sit for an extended time. Clinicians may be resistant to the additional time of the cell infusion, if required to wait for it to finish in order to proceed with the stenting procedure. Still, similar hurdles in training and practice have been overcome previously, such as compression of endovascular heart valves by clinicians onto a delivery system at the point of care.

Appendix A: Protocols specific to this work

A.1 Protocol for Titanium Tube Seeding

Supplies/Equipment:
-Rotating Seeding Motor
-Cells (recommend 2xT150 or 4xT75 to have enough to seed and replate)
-Trypsin
-TNS
-DPBS (-/-)
-Cell Tracker Orange (CTO)
-Serum Free Medium – EBM-2+EGM-2
-Serum Medium – EGM-2+EGM-2+2% PS (for pEPC) or 10% FBS (for CBEPC)

Sterile Checklist:
-Sterile gloves x 3 or more pairs
-Black "Luer-Lok Tip cap"
-Sterile field towels (2)
-Reservoir [100 mL polycarbonate Erlenmeyer flask]
-Pulse Dampener with Large Inlet/Outlet Connections
-Silastic Tubing ½" diameter, approx. 18-22 inches in length
-Silastic Tubing ½" diameter, approx. 3 cm in length X2, TWO SECTIONS
-Silastic Tubing ½" diameter, approx. 5-6 cm in length
-Titanium machined inlet & outlet adapters
-COBE 3/8" x 3/32" SMARxT tubing, 5 foot long section (gas sterilize only)
-COBE 3/8" x 3/32" SMARxT tubing, 5-6 cm long section (gas sterilize only)
-3/8" to ½" adapter (gas sterilize only)

For seeding 5/8" Ti Tubing:
-10 mL syringe
-Assembled Titanium tube
-Cut 10 mL syringe (recommend cut at ~1.5 mL mark)
-2 sections of "large" Silastic tubing approx. 2-3 cm in length

For seeding ½" Ti Tubing:
-5 mL syringe
-Assembled Titanium tube
-Cut 5 mL syringe (recommend cut at 0.8mL mark)
-2 sections of "medium" Silastic tubing approx. 2-3 cm in length

Other Supplies:
-Lab tape & timer
-Hemacytometer

A. Cell Tracker Staining [written for use with Cell Tracker Orange – could use other]
   1. To make CTO 1mM stock solution, thaw vial of 50mg aliquot in light-protected container in hood and add 90 uL of sterile DMSO to vial.
   2. For CTO already made, thaw CTO to room temperature by placing under hood in light-protected conical tube.
   3. Warm up serum free medium (DMEM-F12+Antibiotic/Antimycotic) and DPBS(-/-) (without Calcium & Magnesium)
   4. Turn off fluorescent light in hood
   5. Aspirate regular medium off of cells
   6. Rinse cells twice with DPBS (-/-)
      Note: approx. 30 sec. each rinse; 6 mL will cover T-75 and 12 mL will cover T-150. Place DPBS (-/-) back into heat bath; will use again.
   7. To prepare CTO staining medium, aliquot 6mL serum free media for each T-75 and 12 mL for each T-150 flask to be stained.
   8. Add 2 uL CTO solution per 1mL of serum free medium to be used.
      Note: Serum free media is needed because serum media would cleave/interfere with CTO
   9. Add specified volume media with CTO to cells and incubate at 37*C for 15 minutes

B. Seeding Chamber Assembly
   1. While CTO is incubating with cells, use the available time to assemble the chamber for seeding of titanium tube. Fluorescent light may be on for these steps.
   2. Lay out sterile field towel in one side of hood (recommend opposite from the vacuum)
   3. Place the following sterile supplies onto sterile field:
      a. 10 mL syringe
      b. Assembled Titanium tube
      c. Cut 10 mL syringe (recommend cut at ~1.5 mL mark)
      d. 2 sections of Silastic tubing approx. 2-3 cm in length

e. Black "Luer-Lok Tip cap"

4. With sterile gloves, carefully push one piece of Silastic tubing onto each end of Titanium tube assembly.

   Note: Silastic tubing should be advanced onto Ti tube as far as it may easily go, and **must** be pushed past the beginning of the shrink tube holding Ti tube assembly together – otherwise cell solution will leak out between sections of Ti!

5. Push the cut 10 mL syringe, cut end first, into one of the open pieces of Silastic tubing, as far as it will go. (this should be able to be fully against Ti tube)

   Note: If there is a concern about temperature of tube, the entire assembly may be placed in a sterile screw-top container in incubator until just before cells are inserted.

6. The last step that may be done to prep the seeding chamber is to remove the plunger from the 10 mL syringe and set both pieces back in the field, (need to keep both), then add the syringe cap to the Luer end of the syringe.
7. Also while cells are staining with CTO, place rotating motor device into incubator where desired; it is not necessary to plug it in at this time.

C. Passaging and Cell Seeding

1. While cells are incubating with CTO, warm trypsin (.025%) and TNS aliquots (4 mL trypsin/T-75 and 8mL TNS/T-75).
2. Prepare other equipment – clean hemacytometer & coverslip as well as P20 pipet and place in hood.
3. When 15 minute incubation of cells with CTO is complete, turn off fluorescent hood light and retrieve cells.
4. Aspirate off media with CTO and rinse cells twice with DPBS (-/-)

   Note: approx. 30 sec. each rinse; 6 mL will cover T-75 and 12 mL will cover T-150. DPBS is done with use after this.

5. Add trypsin to cells in volumes stated above; Place flask in incubator for 3 minutes.
6. At 3 minutes, take flasks out and knock against bench. Look at cells under microscope to be sure that cells are detached and floating; if they are not, allow to incubate for another minute or so.
7. In hood, quickly add appropriate volumes of TNS to each flask.

8. Pipet the trypsin/TNS solution up and down and each flask and squirt it against the bottom surface of the flask a few times to detach any remaining adherent cells.
9. Pipet all solution in each flask up and place into conical tube for centrifuge.
10. Pipet solution up and down quickly to mix and then squirt 10uL of cell solution into one side of hemacytometer, change pipet tip, and repeat for the other side of hemacytometer.
11. Check volume of solution in conical tube for use in cell count, and then centrifuge cells (1400 RPM, 5 minutes) with appropriate counterbalance.
12. While cells are spinning, complete cell count as follows:
    a. Count one side (4 sets of 4x4 boxes) then count the other side. Add all together and divide by 8, multiply by 10000, then multiply by volume of liquid (mL) in the conical tube. This is the number of cells in conical.
13. When centrifuge cycle is over, remove cells and counterbalance from centrifuge, being careful not to disturb pellet at bottom of conical

    Note: Cells are still stained with CTO so be conscious to protect cells from excess light when reasonably possible.
14. In hood, gently aspirate supernatant solution by tilting the tube and aspirating liquid, not disturbing cell pellet.
15. Based on cell count, add appropriate amount of serum free medium (DMEM-F12+A/A) to reach desired cell concentration. Pipet up and down to mix cells well into suspension.

    Note: typical seeding density has been 1M/mL. Minimum volume needed is 9-10 mL; do not resuspend in smaller volume than that even if cell count is lower.
16. Pipet 9-10 mL of cell suspension into open syringe barrel with cap attached. Leave any remainder of cell suspension for replating a few steps later.
17. Insert plunger back into open end of syringe as far as possible

    Note: if possible, gently push plunger until it passes a ridge and snaps back into place – it is easier to do this while capped to avoid squirting out cell solution.
18. Invert syringe so that luer end points up and remove black cap. Carefully advance syringe past the 'snap ridge' if not done already, being careful to control plunger and avoid squirting cell solution everywhere. It is not

necessary/recommended to advance plunger and solution all the way to opening at this time.

19. Insert syringe luer end first into other open end of Silastic tubing attached to the titanium tube assembly. Advance syringe as far as it can go into Silastic tube to minimize volume needed to fill seeding chamber.
20. Onc e syringe is fully in place, hold assembly with open end of cut syringe up and slowly advance plunger with cell solution until cell solution can be seen coming into cut syringe. Continue advancing plunger until cell solution forms a nice bead at top, and add black cap on top of bead, so that no bubbles should be inside tube assembly.
21. Place sterile glove(s) inside hood and carefully insert tube/syringe assembly into inside of one glove and down one of the fingers. Use lab tape or rubber bands to close off glove at open cuff end, enclosing assembly inside.

    Note: this is done to maintain sterility of entire assembly while seeding in incubator.
22. Remove assembly in glove from hood and insert into prongs of rotating motor device (for 0.625" size) or fasten into syringe holder (for 0.500" size) in incubator, with the black cap end first and the lightweight syringe plunger end sticking out.

    Note: One shelf is in incubator for this step, and one should be out of the incubator, available for assembly of flow circuit if applicable.
23. Check to see that titanium tube is as level as possible by eye or using a level, and adjust if necessary by placing small items under either end of rotator.
24. Situate cord in incubator door and tape if necessary; plug in motor device and quickly observe to ensure that device is indeed rotating. Set timer to 30 minutes and start timer.
25. Return to hood to use remainder of cell suspension. Fluorescent light in hood may be turned on at this point.
26. Based on remaining volume of cell suspension, decide how many flasks to replate and prepare those flasks with appropriate volume of growth medium.

    Note: Growth medium used has been EBM-2+SQ+2%PS. Plate 13 mL medium into each T-75 and 25 mL into T-150.
27. Use P-1000 pipet to insert desired number of cells (1M/mL) into each flask. Gently slide flask on hood surface in Figure "8" pattern to evenly distribute cells in flask. Close flasks and return to incubator.

A.2 Protocol for Titanium Tube Culture in Flow

Assembly / Preparation of Large Flow Circuit for Large Stockert-Shiley Roller pump

1. While cells are seeding in rotational device, as much preparation of flow circuit as possible should be completed.
2. It is recommended to remove any unnecessary items from hood and remove sterile towel that was used for assembly of seeding chamber and lay out a new [large] sterile field towel on one side of hood for assembly of flow circuit.
3. Carefully place the following sterile supplies onto sterile field:
    a. Reservoir [100 mL polycarbonate Erlenmeyer flask]
    b. Pulse Dampener with Large Inlet/Outlet Connections
    c. Silastic Tubing ½" diameter, approx. 18-22 inches in length
    d. Silastic Tubing ½" diameter, approx. 3 cm in length X2, TWO SECTIONS
    e. Silastic Tubing ½" diameter, approx. 5-6 cm in length
    f. Titanium machined inlet & outlet adapters
    a. COBE 3/8" x 3/32" SMARxT tubing, 5 foot long section (gas sterilize only)
    g. COBE 3/8" x 3/32" SMARxT tubing, 5-6 cm long section (gas sterilize only)
    h. 3/8" to ½" adapter (gas sterilize only)
4. Spray down extra incubator shelf well and wipe off with Kimwipe, placing the incubator shelf into the hood next to sterile field towel. Orient shelf as it would sit in the incubator, with upturned lip out toward hood opening, and downturned lip in back of hood.
5. Complete steps 6-15, flow circuit assembly, with sterile gloves.
6. Place reservoir upright on front right corner of incubator shelf and securely tape in place with LOTS of lab tape.
7. Connect one end of 5' long 3/8" SMARxT tubing to pulse dampener; the other end may be placed in the reservoir to keep it out of the way if desired.
8. Connect the other end of pulse dampener to short (5-6cm) piece of SMARxT tubing.
9. Connect the open end of short SMARxT tubing to 3/8" to ½" adapter.
10. Connect the open end of 3/8" to ½" adapter to 5-6 cm long Silastic tubing.
11. Connect the open end of Silastic tubing to small/entry end of titanium inlet adapter.
12. Connect open end of titanium inlet adapter to 3 cm Silastic tubing.

Note: Tubing hanging off of titanium adapter should be short enough that you will be able to push it fully over tube with cells to fully abut the two pieces together; if tube looks too long, trim it now with sterile razor/scalpel.

13. Lay titanium inlet piece aside on sterile field.
14. Connect large end of titanium outlet adapter to the other 3 cm Silastic tubing.

    Note: Again, tubing hanging off of titanium adapter should be short enough that you will be able to push it fully over tube with cells to fully abut the two pieces together; if tube looks too long, trim it now with sterile razor/scalpel.
15. Connect small open end of titanium outlet adapter to the long Silastic tubing; the other end of Silastic tubing may be placed in the reservoir to keep it out of the way if desired. Lay open end of titanium outlet adapter aside on sterile field.
16. I recommend marking arrow(s) on the long section of 3/8" SMARxT tubing to show the direction of flow, from the reservoir forward to the pulse dampener. It is hard to tell which end is which when tubing is pushed through the small hole in incubator, and this will get the direction of flow correct.
17. Use zip ties and zip tie gun to snugly apply a total of 4 zip ties to secure circuit as follows:
    a. Tie Silastic tubing at both ends of titanium inlet adapter
    b. Tie Silastic tubing at both ends of titanium outlet adapter

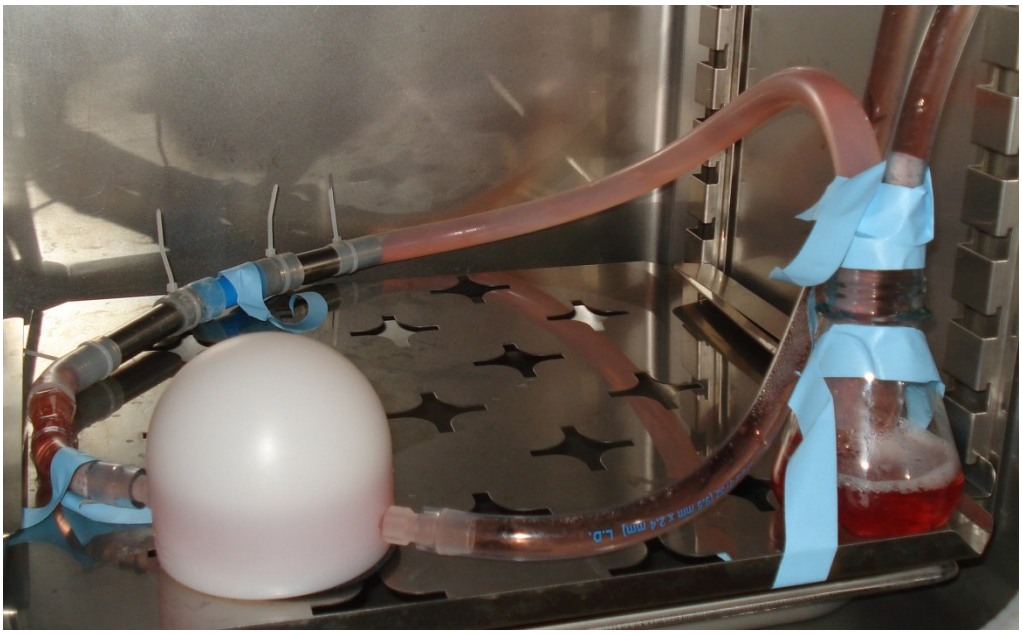

Figure 1. Suggested configuration for large flow circuit in incubator.

18. When the 30 minutes is up and it is time for the titanium tube to come out of the seeding device, remove the assembly in the glove from the prongs and remove the seeding device and its shelf from incubator, if flow circuit is to be placed in same space. Unplug rotating device.
19. Take glove and tube assembly back into hood and undo or cut tie from cuff end of glove, removing titanium & syringe assembly into sterile field.
20. Remove Silastic tubing from both ends of titanium tube containing cells, being careful not to scrape inner surface of titanium with inserted syringe other anything else.
    a. Note: If desired it is possible to uncap cut syringe first and withdraw liquid slowly into full syringe, to minimize mess. This should be done slowly to avoid detaching cells on titanium tube.
21. The next steps should be completed carefully but quickly to avoid the cells drying out; Insert the open Silastic tubes on titanium adapters over both ends of the titanium tube containing the cells. As when assembling the seeding chamber, the Silastic tubing must be pushed on far enough to be over shrink tubing and avoid leakage of fluid through tube.
22. When circuit is fully assembled and sealed off, hold the open ends of circuit that will go in the reservoir upright and quickly begin filling the circuit with serum medium (DMEM-F12+2%PS+A/A) by carefully and slowly pouring medium into the Silastic tubing (as this is the largest and easiest to pour into).
23. Try to fill the pulse dampener as desired so that the liquid level is a bit above the inlet and outlet and move the long tubing around to work any bubbles in the tubes up the open ends of the tubing, so that no large bubbles are in the circuit. Continue filling tubes with medium within 1-2 cm of the open ends.
24. Quickly (to avoid spilling) insert the open tubing ends into the open mouth of the reservoir. Tubing fits closely in the reservoir mouth; remember that the 3/8" SMARxT tubing is the inlet and should be pushed further down into the reservoir than the ½" Silastic outlet tubing.
25. Some liquid will flow from the tubes into the reservoir, leaving empty gaps in the tubing. This is acceptable because when the flow begins, bubbles before the sample will go to the bubble trap / pulse dampener, and bubbles after the sample will be pushed back to reservoir.

26. With a 25 mL pipet, fill the reservoir to just below the level where the threads for the cap begin. This will look very full, but some of this volume will fill the spaces that just formed in the tubing.

    Note: The volume of medium required to fill the circuit and reservoir has been approximately 400 mL in my experience (3 setups)
27. If you have not already done so, tape the pulse dampener, adapters, and sample into place on the incubator shelf so that they will not come apart and fall over when placed into the incubator. Place the long section of 3/8" SMARxT tubing on top so that it is easy to access to insert into pump.
28. Remove shelf and attached flow circuit carefully from the hood and carefully carry to incubator. Place shelf into incubator and make one fold in 3/8" tubing to push it through the hole in the incubator wall.
29. Push or pull through as much of the 3/8" tubing as possible without displacing the other circuit components.
30. If all components are stable, close the incubator door and move to the large pump.
31. ENSURE THE PUMP IS SWITCHED OFF and open the cover above the roller.
32. Open both tubing clamps and identify the end of the tubing that is the inlet (from your previous marks on the tubing). Lay this end into the first tubing clamp (at bottom) and secure tubing.

    Note: Pump is currently set up to rotate counter-clockwise. Inlet should be the bottom end.
33. Roll the pump by hand around onto tubing, laying tubing in between the white guides.
34. When tubing is fully in the "raceway," push the free end of tubing so that sits tightly against the curved wall of the pump and secure that outlet end of tubing in the top tubing clamps.
35. Close the cover and ensure that the pump speed is set to zero.
36. Turn on pump and switch the dial from zero to counter-clockwise flow.
37. Turn the pump up to a fraction of the desired experimental flow; flow should be ramped up over a period of approximately 15 minutes, in about 4 increments.
38. Look at the flow circuit in the incubator and ensure that there are no leaks. The bubbles in the tubes may remain stationary until higher flow rates (1LPM) are reached, when they will be pushed into the bubble traps.
39. If the pulse dampener level is not sufficient, hold it so that a little bit more liquid goes into it and then lay it down flat again.

40. Tape to the shelf again any components that seem unstable.
41. Continue ramping the flow to the desired level over the first 15 minutes and make a note of the time zero of the experiment. Clean up the hood and you are done!

A.3 Protocol for Titanium Tube Tube seeding for Surgical Implant

Supplies/Equipment:
-Rotating Seeding Motor 10 RPH – In O.R.
-Machined holder to connect tube to Motor – Attached to motor in O.R.
-Incubator for Seeding/Rotation – In O.R.
-Cells (recommend 3xT75 confluent to have enough to seed)
-Trypsin (.025%) (4 mL each T-75)
-TNS Trypsin Neutralizing Solution (8 mL each T-75)
-DPBS (-/-)
-PKH26 kit for fluorescent labeling
-Serum (PS or FBS)to use with PKH26 kit (3 mL for each T75)
-Serum Free Medium – EBM-2+EGM-2
-Serum Medium – EGM-2+EGM-2+2% PS (for pEPC)

Clean/Sterile Checklist:
-Sterile gloves x 3 or more pairs
-Black "Luer-Lok Tip cap"
-Sterile field towels (2)
-5 mL syringe
-Assembled Titanium tube, enough for control and cell use
-Cut 5 mL syringe (recommend cut at 0.8mL mark)
-2 sections of "medium" Silastic tubing ½" diameter, approx. 3-4 cm in length

Other Supplies:
-Lab tape & timer
-Hemacytometer

A. PKH26 Staining – Long-term membrane dye kit from Sigma; protocol approximates kit instructions.

Note: The morning that surgery is scheduled, complete the PKH26 staining in advance, then the cells will be placed back in normal medium until it is time to passage them.

1. Wash/rinse cells in **serum free media** 2 times (for about a minute each).
    a. 4 mL each T75; 4x3x2 = 24 mL to warm
2. Per the PKH26 kit protocol, mix the PKH26 red dye and the "Diluent C" component in a 15 mL conical, to a concentration of 4uM:

a. 3 mL of mixture is needed for each T75; Total is 9 mL Diluent C and 36 uL of dye.

3. Gently invert the capped conical to mix, then add 3 mL of dye mixture to each T75.
4. Allow the dye mixture to incubate flat on the cells in the hood at room temperature, **4 minutes.**
5. After 4 minutes, stop the reaction with an equal volume of serum(FBS or PS).
    a. 3 mL each T-75 for 9 mL total to warm up
6. After 1 minute, dilute this with full medium 1:1. Add a total of 6 mL full medium to each T75 (6x3 = 18 mL to warm up)
7. Aspirate all liquid from cells and wash 2x, possibly 3x, with full medium.
    a. 4 mL each T75 x 3 x 2 = 24 mL to warm up
8. Cover each T75 with a normal volume of full medium and return flasks to incubator, away from light, until it is time to start passaging.
    a. 13-15 mL each T75 x 3 = 45 mL to warm up.

B. Seeding Chamber Assembly

1. Lay out sterile field towel in one side of hood (recommend opposite from the vacuum)
2. Place the following sterile supplies onto sterile field:
    a. 5 mL syringe
    b. Assembled Titanium tube, including:
        A. Cut 5 mL syringe (recommend cut at ~0.8 mL mark)
        B. 2 sections of Silastic tubing approx. 3-4 cm in length
    c. Black "Luer-Lok Tip cap"
3. The last step that may be done to prep the seeding chamber is to remove the plunger from the 5 mL syringe and set both pieces back in the field, (need to keep both), then add the syringe cap to the Luer end of the syringe.

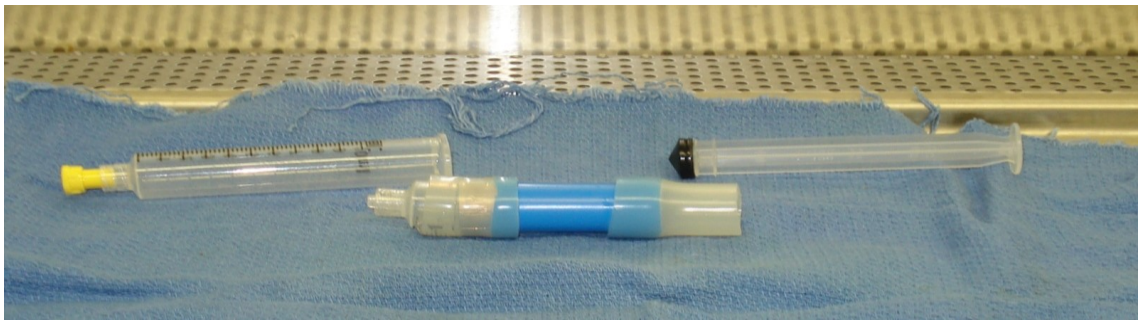

Figure 1. Assembled titanium tube system, shown here with yellow syringe cap instead of black pointed cap.

C. Passaging and Cell Seeding
   1. Prepare other equipment – clean hemacytometer & coverslip as well as P20 pipet and place in hood.
   2. When the go-ahead for cell seeding is given from the OR team, proceed to step 3.
   3. Aspirate off media from T75s and rinse cells twice with DPBS (-/-)
      Note: approx. 30-60 sec. each rinse; DPBS is done with use after this.
   4. Add trypsin to cells (4mL ea T75); Place flask in incubator for 3 minutes.
   5. At 3 minutes, take flasks out and knock against bench. Look at cells under microscope to be sure that cells are detached and floating; if they are not, allow to incubate for another minute or so.
   6. In hood, quickly add appropriate volumes of TNS (8mL ea T75) to each flask.
   7. Pipet the trypsin/TNS solution up and down and each flask and squirt it against the bottom surface of the flask a few times to detach any remaining adherent cells.
   8. Pipet all solution in each flask up and place all together into one conical tube for centrifuge.
   9. Pipet solution up and down quickly to mix and then squirt 10uL of cell solution into one side of hemacytometer, change pipet tip, and repeat for the other side of hemacytometer.
   10. Check volume of solution in conical tube for use in cell count, and then centrifuge cells (1400 RPM, 5 minutes) with appropriate counterbalance.
   11. While cells are spinning, complete cell count as follows:
       a. Count one side (4 sets of 4x4 boxes) then count the other side. Add all together and divide by 8, multiply by 10000, then multiply by volume

of liquid (mL) in the conical tube. This is the number of cells in conical.

12. When centrifuge cycle is over, remove cells and counterbalance from centrifuge, being careful not to disturb pellet at bottom of conical tube.
    Note: Cells are still stained with PKH so be conscious to protect cells from excess light when possible. Cell pellet should be a bright red-orange.
13. In hood, gently aspirate supernatant solution by tilting the tube and aspirating liquid, not disturbing cell pellet.
14. Based on cell count, add appropriate amount of serum free medium (DMEM-F12+A/A) to reach desired cell concentration. Pipet up and down to mix cells well into suspension.
    Note: typical seeding density has been 2-2.5M/mL. Minimum volume needed to fill chamber is 4.5 mL; do not resuspend in smaller volume than that even if cell count is lower. **Be sure to record cell count and seeding density!**
15. Pipet 4.5-5 mL of cell suspension into open syringe barrel with cap attached.
16. Insert plunger back into open end of syringe as far as possible. Note that the device should be only be handled with sterile gloves – 2 people may make this pipetting/assembly step easier.
    Note: if possible, gently push plunger until it passes a ridge and snaps back into place – it is easier to do this while capped to avoid squirting out cell solution.
17. Invert syringe so that luer end points up and remove black cap. Carefully advance syringe past the 'snap ridge' if not done already, being careful to control plunger and avoid squirting cell solution everywhere. It is not necessary/recommended to advance plunger and solution all the way to opening at this time.
18. Insert syringe luer end first into the open end of Silastic tubing attached to the titanium tube assembly. Advance syringe into Silastic tube, but not past the edge of the Titanium tube; this would displace cells from the space over the end of the tube.
19. Onc e syringe is fully in place, hold assembly with open end of cut syringe up and slowly advance plunger with cell solution until cell solution can be seen coming into cut syringe. Continue advancing plunger until cell solution

forms a nice bead at top, and add black cap on top of bead, so that no bubbles should be inside tube assembly.

20. Place sterile glove(s) inside hood and carefully insert tube/syringe assembly into inside of one glove and loosely down one of the fingers. Use lab tape or rubber bands to close off glove at open cuff end, enclosing assembly inside.
    Note: this is done to maintain sterility of entire assembly while transporting and seeding in incubator.
21. Remove assembly in glove from hood and quickly carry entire assembly to OR at Vivarium. It is advisable to continuously gently move or rotate the tube while it is being carried to the OR.
22. In the OR, insert into syringe holder in incubator and screw the syringe holder closed, with the black cap end first and the lightweight syringe plunger end sticking out.
23. Check to see that titanium tube is as level as possible, using a level, and adjust if necessary by turning knobs on motor holding apparatus.

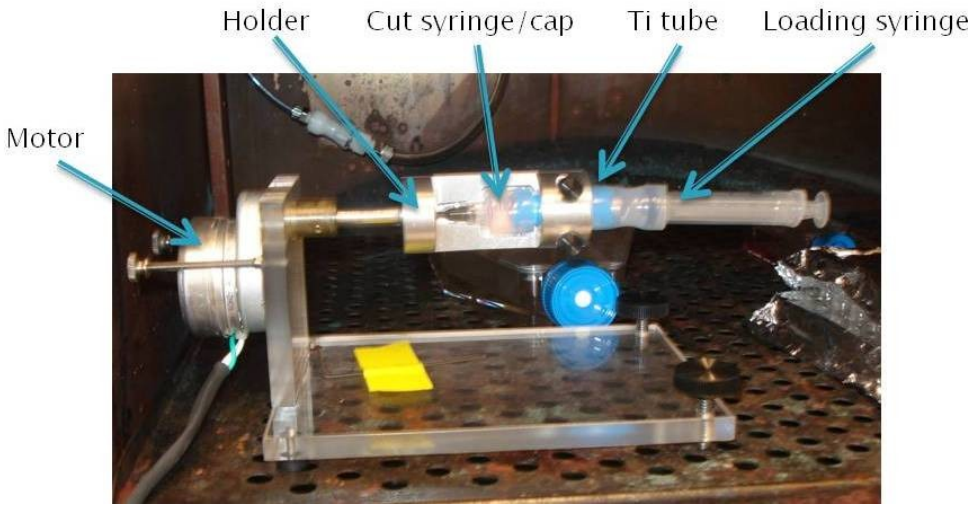

Figure 2. Titanium tube and motor assembly, pictured here without sterile glove covering.

24. Situate cord in incubator door and tape if necessary; plug in motor device and observe to ensure that device is indeed rotating. Set timer to 30 minutes and start timer.

25. At the end of the 30 minutes, as long as the OR Surgical team is ready, remove the syringe assembly from the syringe holder and carefully release the lab tape or rubber band holding the sterile glove closed.
26. WITHOUT TOUCHING THE INSIDE of the glove or the sterile surgical field, ease the syringe assembly out and present it to the surgical team.
27. The surgical team should remove the Silastic ends from the tube and quickly prepare the tube for implantation. It is helpful to keep the implantation field hydrated with saline while the implant is sutured into place.

A.4 Protocol for Titanium Tube Cleaning

Cleaning Protocol: Ti Tubing

1. Clean Ti tube with Alconox soap solution and soft sponge, rinse many times with DI H_2O
2. Submerge Ti pieces in Aqua Regia in very clean glass petri dishes for 5 minutes. (NOTE: THIS PART IS VERY DANGEROUS)
   Petri dishes must be very clean, usually clean as step 1
3. Submerge Ti pieces in DI H_2O to clean off Aqua Regia (approximately 1 L of H_2O per 21 pieces) and then rinse very thoroughly with a few more liters of DI H_2O
4. Proceed to next steps for soap and water sonication.

Cleaning Protocol: Plastic Parts, Flexible Tubing, Ti tubing Part II

1. Sonicate in Kendal sonicator for 2 cycles of 480 seconds in 1:1 Alconox, DI H_2O solution (use a Ziploc bag that has been cleaned with Alconox solution to hold the parts; fill remainder of sonicator chamber with DI H_2O to cover Ziploc bags)
2. Rinse contents of Ziploc bag with Ti pieces or plastic parts in DI H_2O 30 times
3. Sonicate again 2 cycles of 480 seconds in DI water in the same bag.
4. Rinse with a few more liters of DI H_2O in same Ziploc bag.
5. Let dry in Laminar flow head to prevent dust settling on surface.
6. Mark parts with the date as "cleaned" and store in conical tubes.

A.5 Protocol for Paraformaldehyde Preparation

Making Fresh Paraformaldehyde (3.7%) Solution

(This protocol yields 100ml of formaldehyde that can be stored in the refrigerator for up to two weeks.)

Equipment/Reagents:

- Paraformaldehyde, PBS (10X without Ca and Mg), distilled water.
- Pipettes, Erlenmeyer flask (about 100ml), graduated cylinders (10ml & 100ml), ice in bucket, 50ml Steriflip filters or similar.
- Hot plate/stirrer and bar, pH meter (1N HCl and 1N NaOH).

Reminders:

- Paraformaldehyde vapors are extremely toxic. Keep under the hood as constantly as possible, and only heat under the hood.

Protocol:

1. Weigh out 3.7g of paraformaldehyde.
2. Into the hood, bring the PBS, paraformaldehyde, water, NaOH, and hot plate/stirrer.
3. Into a clean Erlenmeyer flask (100ml), add 10ml of PBS and about 90ml water.
4. Place flask on hot plate/stirrer. Turn on stirrer and set heat at about 55-60°C.
5. Add paraformaldehyde to PBS, avoiding fumes.
6. Add 20µl of 1N NaOH to the solution.
7. Allow to stir. When nearly dissolved, remove from heat and put on ice.
    a. Note: it has been our experience that this dissolves poorly and a fair amount of solid will remain in the flask – the liquid should be poured off and the solid disposed of by vigorous rinsing into the formaldehyde waste container.
8. Calibrate pH meter and adjust pH of the solution to 7.2-7.4 by adding 1N HCl or 1N NaOH while stirring.
9. Return solution to hood and sterilize if desired, using a Steriflip filter (or similar filter device) into large conical tubes.
10. Label tube and refrigerate (4°C).
11. Clean area and equipment.

A.6 Protocol for Stent Seeding

The below protocol is for the in-catheter seeding of delivery systems which have been specially designed with holes or apertures over the stent area, with endothelial cells.

Supplies/Equipment:

- Loaded delivery system (gas sterilized if for long-term [>4hr] experiment)
- Cells (recommend 2xT75 to have enough to seed and replate)
- Trypsin and TNS
- DPBS (-/-) and DPBS (+/+), both sterile
- Cell Tracker Orange (CTO) or Cell Tracker Green (CTG)
- Serum Free Medium – EBM-2+EGM-2
- Serum Medium – EGM-2+EGM-2+A/A; +2% PS (for pEPC) or 2/10% FBS (for CBEPC)
- Syringe Pump
- Syringes (3cc, 5 or so)
- For flow: Tygon tubing (5/32" ID, McMaster-Carr Item 5114K15), long enough for stent + entrance length
- For flow: 2 ea. 2-way stopcocks, with male luer – to – barb adapters (see last photo below)
- Flow loop [with two pulse dampeners and larger reservoir, 250 mL] if completing flow experiment

Other Supplies:
-Lab tape & timer
-Hemacytometer

A. Cell Tracker Staining :

1. Note: Either Cell Tracker Orange or Cell Tracker Green may be used.
2. To make CTO 1mM stock solution, thaw vial of 50mg aliquot in light-protected container in hood and add 90 uL of sterile DMSO to vial.
3. For CTO already made, thaw CTO to room temperature by placing under hood in light-protected conical tube or otherwise protected from light.
4. Warm up serum free medium (6 mL per T-75)

5. Turn off fluorescent light in hood
6. To prepare CTO staining medium, aliquot 6mL serum free media for each T-75 and 12 mL for each T-150 flask to be stained.
7. Add 2 uL CTO solution per 1mL of serum free medium to be used.
    a. Note: Serum free media is needed because serum media would cleave/interfere with CTO
8. When CTO-medium is warm, aspirate regular medium off of cells and rinse twice with sterile DPBS (+/+ or -/-), about 1 minute per rinse.
9. Add specified volume CTO-media mix to cells and incubate at 37*C for 15 minutes

B. Delivery System Preparation :

1. Open sterile delivery system pouch inside the hood. If sterilized, tray substitutes as a bit of a sterile field towel; use care not to touch it more than is necessary.
2. Plug the distal end of delivery system as appropriate:
    a. For new delivery system with tip attached, use apparatus with rubber o-rings and screw it tightly, centered over the tip-sheath transition. Device can be autoclaved or sprayed/submerged in ethanol.


    b. For a re-utilized delivery system with tip cut off, cover sheath end with vinyl cap (McMaster #9753K11). This should ideally be done before sterilization. Care must be used not to damage end of sheath; cap can be slightly pre-stretched with SS mandrels.

3. Label a 3cc syringe for ethanol and fill it with 70% ethanol. Label a 3cc syringe for DPBS and fill it with sterile DPBS (+/+). Note: this should be done carefully to not contaminate DPBS bottle, perhaps from a conical of aliquoted DPBS.

4. Gently flush delivery system with full volume of 70% ethanol, into side flushing port (photo below). Liquid should be seen exiting in the stent area, and only minimally around sealing devices. Do not use excessive force, or vinyl caps may "blow off" the end. Flushing may be slow but is necessary to remove air pockets from inside delivery system.

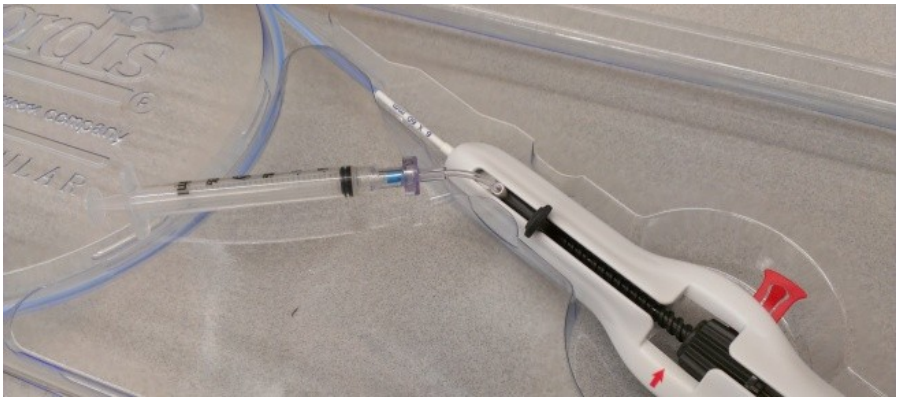

5. Following, flush delivery system with at least 1-1.5 cc of the sterile DPBS to replace ethanol. Submerge delivery system end in conical of DPBS (+/+) until stent seeding to prevent reintroduction of air.

C. Syringe Pump Preparation:

1. Place syringe pump into hood at far left side, plug in somewhere and turn on via switch at back.
    a. Note: if using outlet inside hood, "receptacle" switch atop hood must be switched on.

2. Press [Enter] to stop flashing. Press [Set] then [Diameter] and enter syringe diameter: 8.66 mm for 3 mL syringe. Press [Enter].
    a. (Note: if units are not as desired, press [Set] and parameter key again to change.)
    (http://www.harvardapparatus.com/hapdfs/HAI_DOCCAT_4/Syringe%20Selection%20Guide.pdf)
3. Press [Set], [Infuse Rate] and enter desired rate, then press [Enter]
    a. 0.4 mL/min to infuse 2 mL over 5 minutes.
4. Press [Set], [Refill Rate] and enter desired rate, then press [Enter]
    a. 5 mL/min or more is fine, this just backs up pump into position if needed.
5. Press [Set] , [Target Volume] and enter volume, then press [Enter]
    a. Probably 2 mL but can adjust up or down depending on # cells resulting from passaging.
6. With an empty syringe pulled back to the appropriate target volume, set pump to the right distance for plunger. Press [Infuse/Refill] and [Run/Stop] to move plunger holder as necessary.

D. Flow Loop Preparation:

1. While cells are incubating with CTO, prepare flow loop. Open package inside hood and add 150 mL of [warmed] medium to reservoir.
2. Secure cap onto reservoir. Ensure sampling tube and uptake tube are close to bottom but not flush with bottom of the reservoir. Return tube should also be as

far down as possible. Adjust tubes by pulling in/out with sterile tweezers if needed.

3. Connect rigid reservoir uptake tube to first pulse dampener. Connect two pulse dampeners with short section of tubing. Connect second pulse dampener to a placeholder connector, and connect the placeholder connector to tubing returning to reservoir (see photo below, with stent assembly in place of connector)

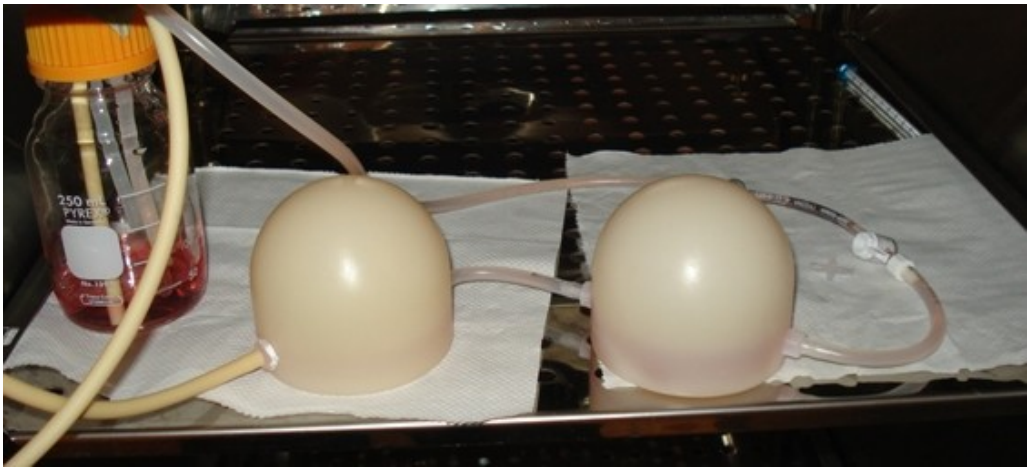

4. Carefully carry flow assembly to small incubator and put tubing into roller pump. Turn pump on to a low speed and ensure it is turning correct direction to move liquid from reservoir to first pulse dampener.
5. Turn flow up (60-80 mL/min) and fill both pulse dampeners by inverting them then turning them right side up again. Ensure flow is moving well and place paper towels beneath connector piece where stent will go. Turn flow back down to 15 mL/min or so.

E. Passaging & Stent Seeding:

1. While cells are incubating with CTO, warm trypsin (.025%) and TNS (will need 4 mL trypsin per T-75 and 8mL TNS per T-75).
2. Prepare other equipment – clean hemacytometer & coverslip as well as P20 pipet and place in hood.
3. When 15 minute incubation of cells with CTO is complete, turn off fluorescent hood light and retrieve cells.
4. Aspirate off media with CTO and rinse cells twice with DPBS (-/-)

a. Note: Approx. 30 sec. each rinse; 6 mL will cover T-75 and 12 mL will cover T-150. DPBS (-/-) is done with use after this.

5. Add trypsin to cells in volumes stated above; Place flask in incubator for 3 minutes.
6. At 3 minutes, take flasks out and knock against bench. Look at cells under microscope to be sure that cells are detached and floating; if they are not, allow to incubate for another minute or so.
7. In hood, quickly add appropriate volumes of TNS to each flask.
8. Pipet the trypsin/TNS solution up and down and each flask and squirt it against the bottom surface of the flask a few times to detach any remaining adherent cells.
9. Pipet all solution in each flask up and place into 50mL conical tube for centrifuge.
10. Pipet solution up and down quickly to mix and then squirt 10uL of cell solution into one side of hemacytometer, change pipet tip, and repeat for the other side of hemacytometer.
11. Check volume of solution in conical tube for use in cell count, and then centrifuge cells (1400 RPM, 5 minutes) with appropriate counterbalance.
12. While cells are spinning, complete cell count as follows:
    a. Count one side (4 sets of 4x4 boxes) then count the other side. Add all together and divide by 8, multiply by 10000, then multiply by volume of liquid (mL) in the conical tube. This is the number of cells in conical.
13. When centrifuge cycle is over, remove cells and counterbalance from centrifuge, being careful not to disturb pellet at bottom of conical.
    a. Note: Cells are still stained with CTO so be conscious to protect cells from excess light when reasonably possible.
14. In hood, gently aspirate supernatant solution by tilting the tube and aspirating liquid, not disturbing cell pellet.
    28. Based on cell count, add appropriate amount of **DPBS (+/+)** to reach desired cell concentration. Pipet up and down to mix cells well into suspension. We use DPBS instead of medium as in normal passaging, because it seems to increase quick adhesion.
15. Note: typical seeding density has been 1-2M/mL; Resuspend such that final volume matches or exceeds that input to the syringe pump previously.
16. Pipet appropriate volume of cell suspension into open syringe barrel with cap attached. Leave any remainder of cell suspension for replating a few steps later.

17. Insert plunger back into open end of syringe as far as possible.
    a. Note: If possible, gently push plunger until it passes a ridge and snaps back into place – it is easier to do this while capped to avoid squirting out cell solution.
18. Turn syringe open-end-up and remove black cap. Slowly advance plunger with cell solution until cell solution can be seen coming out top with no bubbles. Continue advancing plunger until cell solution forms a nice bead at top, and attach syringe to add to delivery system sideport previously used for flushing.
19. Put syringe into syringe pump and carefully hold stent delivery system next to syringe pump.
    a. Place distal end of delivery system into a large conical to capture flowthrough solution, for minimal mess as well as optional counting or replating.
20. Check that syringe pump is set to "INFUSE." If set to "REFILL" press [Infuse/Refill]. Once syringe is fit into plunger mechanism, press [Run/Stop] to begin infusion. Hold onto bulky stent system handle so that it does not "flop" out of machine along with the syringe.
21. After syringe pump has stopped, syringe may be removed from pump but should remain attached to stent delivery system. Allow delivery system to sit stationary for 5 minutes (for better cell attachment).
22. After 5 minutes, seeding process is complete. For immediate imaging, deploy stent into air or liquid as desired and protocol is complete. For beginning of flow, deploy stent into 4mm Tygon tubing and continue:
    a. Stent should be toward one end of tubing but enough room must be left distal to the stent to allow 3-way stopcock to fit completely inside Tygon tubing (leave approx. 2 cm).
23. Attach 3-way stopcocks to both ends of Tygon tubing, and use a syringe attached to one stopcock to completely fill tube with warm medium (see photo below).

24. When tubing is full of medium, close both stopcocks and transfer stent assembly into flow loop. Stop pump and wait 5-10 seconds for pressure to equalize and flow to stop completely.
25. Place stent assembly into flow circuit where placeholder connector is. Open both stopcocks.
26. Start pump again – it should be at a low flowrate (15 mL/min or so).
27. Continue ramping the flow to the desired calculated level over the first 15 minutes and make a note of the time zero of the experiment, flow rate, and record other experimental notes. Replate any leftover cells if desired. Clean up the hood and you are done!

A.7 Protocol for Stent Recompression & Reloading

The below protocol is tailored to the Cordis Smart stent in dimensions but will apply to most 6Fr self-expanding stents and delivery systems.

Supplies/Equipment:

- Blockwise Engineering Stent Recompression Device model RMC
- "Transfer Tube": Teflon/FEP tubing 1/16" (.0625") ID x 1/8" OD (McMaster 52355K41), cut to length 1-2 cm longer than stent of interest.
- Compression Pushing Cannula: 17 GRW Stainless steel tubing x 12" (McMaster 8988K416)
- Transfer Cannula: 16 GRW Stainless steel tubing x 12" (McMaster 8988K415)
- Stainless Steel support wires: 0.015" x 12" (McMaster 6517K64); 0.032" x 12" (McMaster 6517K66)
- Empty/deployed delivery systems to transfer stents

Procedure:

1. Begin with an expanded/deployed stent. Place a support wire (.015" or .032") through the lumen of the stent and place it into the Blockwise stent recompression device.

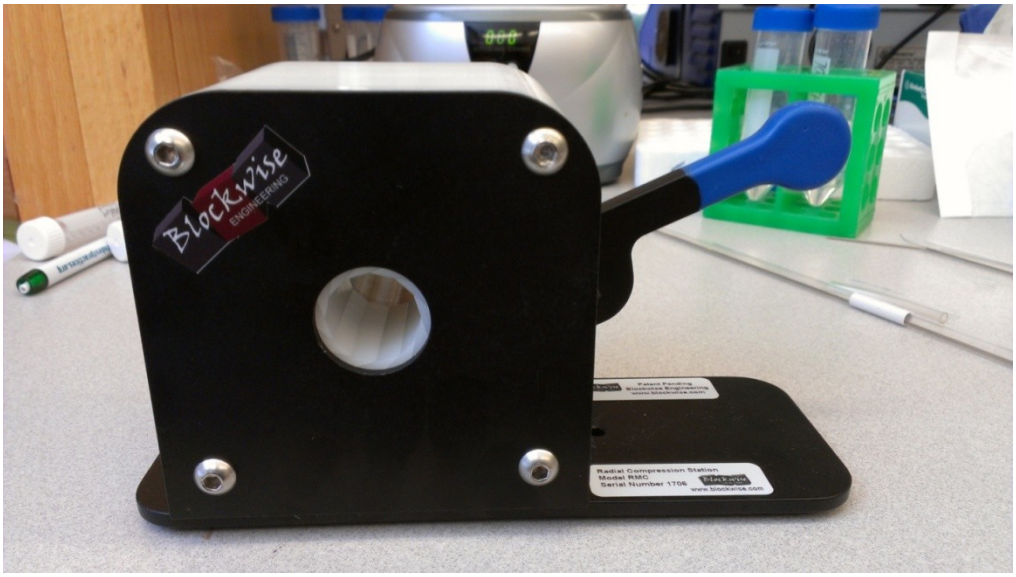

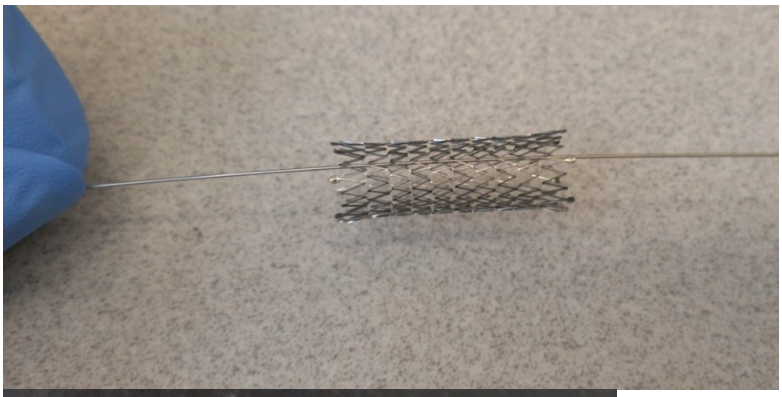

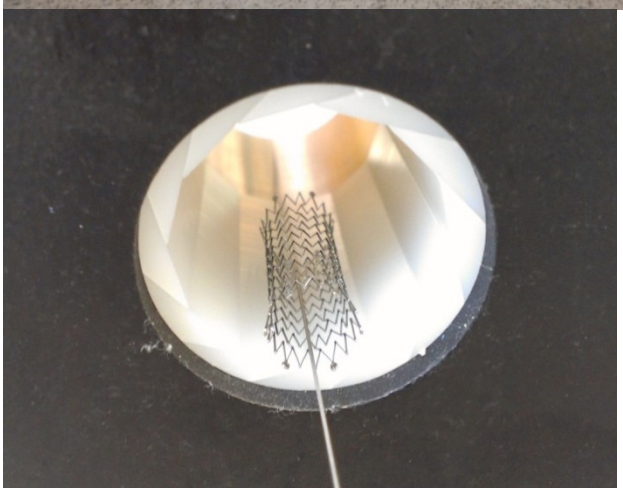

2. Compress handle of Blockwise device completely to pre-set positive stop (stop should be set at OD of 17GRW cannula). Adjust stent position until the end of stent just slightly protrudes from compression jaws: this will aid in alignment of the transfer tube to the stent jaws.

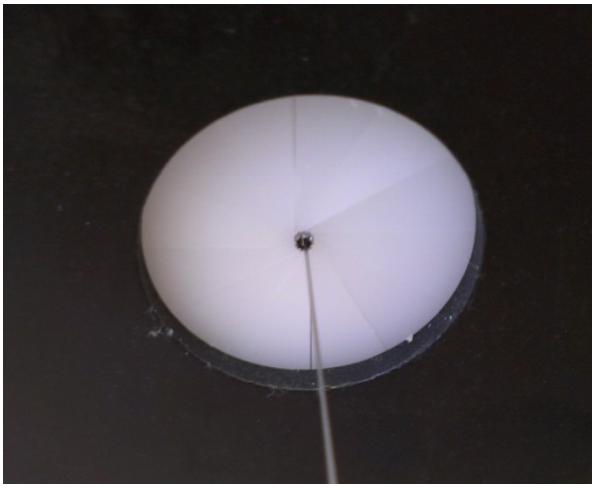

3. Insert 17GRW cannula into back of jaws until it can be felt to touch the back of the stent.

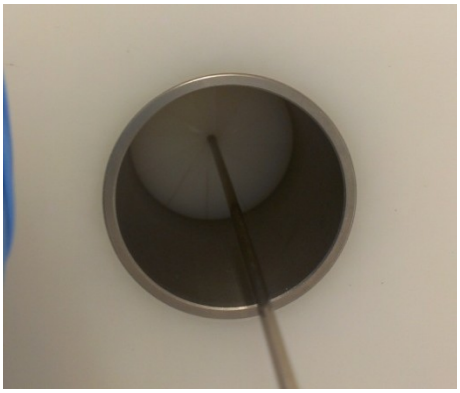

4. Position transfer tube over the eyelets slightly protruding from "front" side of compression jaws, and align transfer tube completely over these eyelets so that no segments "catch" on the outside of tubing.
5. While maintaining constant diameter on compression lever, hold tubing tightly against the jaws and push the cannula from behind slowly and smoothly to advance stent into transfer tube.

   Note: 2 operators / 3 hands may be preferred at this point. One operator can hold down lever with an elbow or knee while holding the transfer tube and pushing cannula with opposite hands.

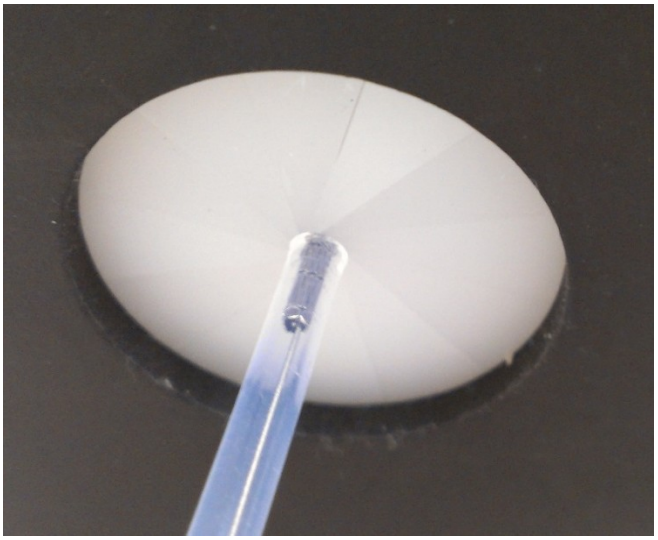

6. When stent is completely inside tube, compression lever may be released and the stent removed. The stent will now be completely contained inside the transfer tube. Stents may be stored in this configuration before reloading into delivery

systems. Stent should be inspected to make sure struts are not crossed, bent, or damaged.

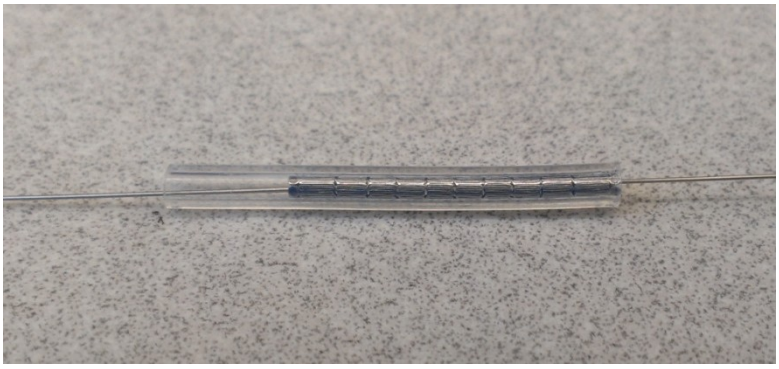

7. Select and prepare empty delivery system for stent transfer:
    a. Select a delivery system made for a stent of equal or greater length than the stent you wish to load. Stents longer than that of the original delivery system will not "fit."
    b. Cut off the atraumatic tip of the delivery system just proximal to that tip.

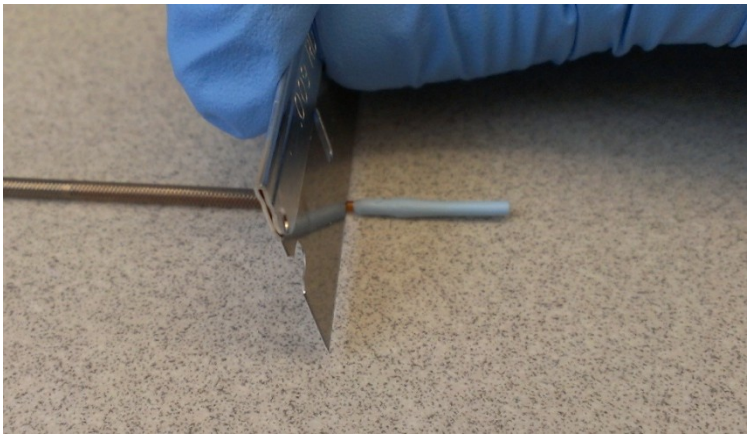

8. Using the delivery system handle, extend the "inner catheter" of the delivery system approximately the length of the stent to be loaded.
    a. Using 17GRW or 16GRW cannula, gently advance stent so that a partial segment is extending from the transfer tube. As before, this will help to align the stent inside the delivery system for loading. (See photo).

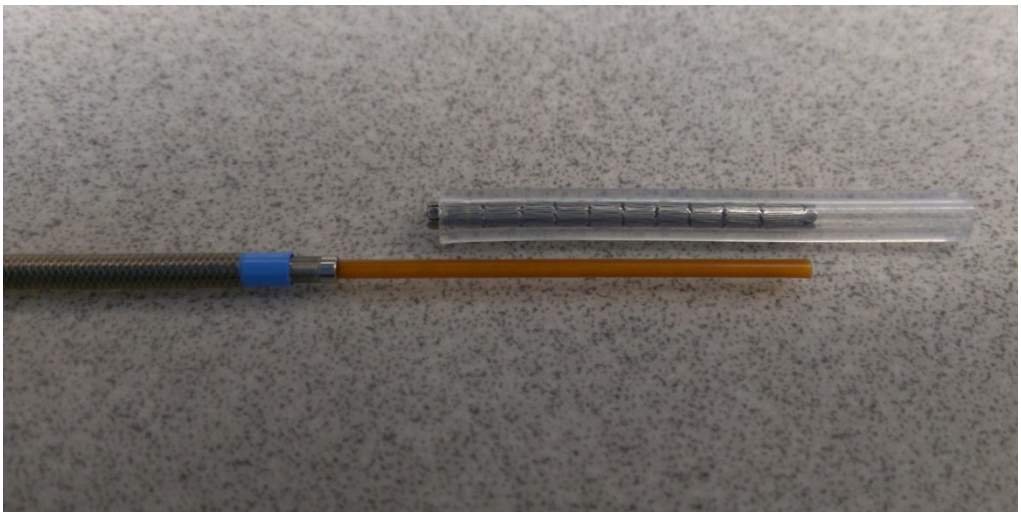

9. Gently insert the inner catheter (orange) through the open lumen of the stent. Take care not to catch the end of the inner catheter on any stent struts. Insert catheter in the direction shown above such that the stent struts extending from the transfer tube are next to the delivery sheath.

10. Gently insert the stent struts under and inside the end of the delivery system. The blue material is fragile and easily damaged, so this step must be done cautiously! Repeated damage will prevent delivery system from being reloaded at all. Following this step, the transfer tube should be abutted to delivery system sheath as in the photo below.

11. Using the 16GRW cannula (17GRW cannula cannot fit over the orange inner catheter), gently advance the stent into the delivery system. The transfer tube must be held tightly against the delivery sheath or segments will "escape" and expand, requiring stent compression to begin again at step 1.
    a. Note: For additional support, a 0.032" wire may be placed within the lumen of the orange inner catheter, but only if the catheter lumen has not been previously glued shut (see Appendix: Preparing Delivery System for Re-Use)

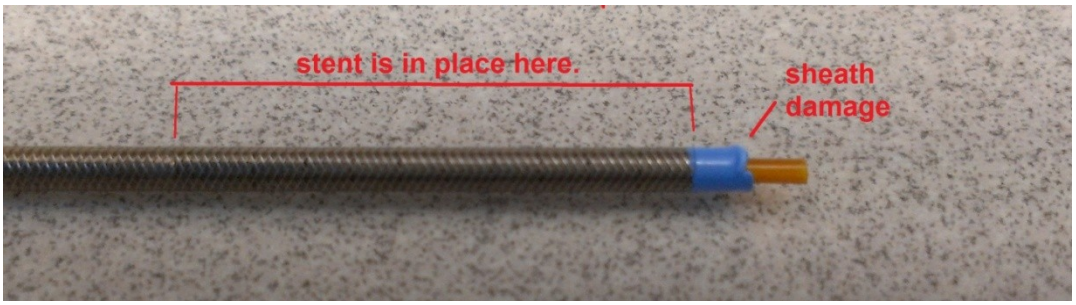

12. The stent is now fully inside the delivery system and can be deployed again.

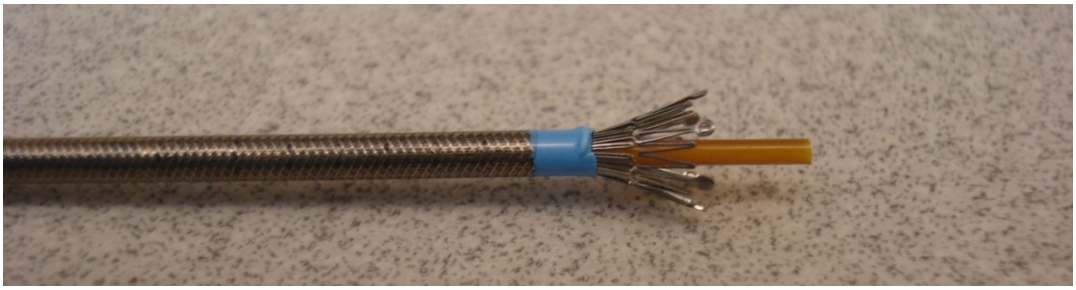

I. Appendix: Preparing Delivery System for Re-Use

Supplies/Equipment:

- Superglue
- Luer lock needle Size 20 ½ G or smaller (larger gauge #)
- 1cc syringe

Procedure:

1. To re-use a delivery system for seeding, the tip is cut off as shown above. Therefore it is necessary to plug both the inner catheter, and the distal end of the outer sheath for seeding. The outer sheath will be capped with a small vinyl cap, but the inner catheter should be plugged with glue or something similar.
2. Prepare delivery system for re-use by cutting off tip as shown above and fully extending inner catheter out past outer sheath.
3. Carefully attach luer needle to 1cc syringe and uncap. Uncap superglue and insert needle into superglue tip far enough so that glue can be drawn into the syringe through the needle.
4. Draw up a small volume of glue (0.3 cc or less) and remove needle from glue. Quickly and carefully insert needle into the lumen of orange inner catheter. Depress syringe to place glue into inner catheter lumen. Withdraw needle.
5. Before glue dries (very quick), wipe the outside of the inner catheter with a Kimwipe or paper towel to remove excess glue. Excess glue on the outside will create problems when trying to thread inner catheter through a compressed stent.
6. Glue should be seen inside translucent inner catheter as one or more bubbles or beads. Cyanoacrylates cure in the presence of air & moisture, which is limited inside the small space; catheter should be allowed to sit several hours or ideally overnight before use in seeding or even reloading.
7. Important – mark that the 'inner catheter has been glued' on delivery system handle to identify this. Gluing will not have to be repeated if catheter is re-used again.

Appendix B: License for previously published work

Permission to reuse portions of "Use of autologous blood-derived endothelial progenitor cells at point-of-care to protect against implant thrombosis in a large animal model" included in Chapter 2.

ELSEVIER LICENSE
TERMS AND CONDITIONS
Nov 06, 2013

This is a License Agreement between Alexandra E Jantzen ("You") and Elsevier ("Elsevier") provided by Copyright Clearance Center ("CCC"). The license consists of your order details, the terms and conditions provided by Elsevier, and the payment terms and conditions.

All payments must be made in full to CCC. For payment instructions, please see information listed at the bottom of this form.

Supplier	Elsevier Limited The Boulevard,Langford Lane Kidlington,Oxford,OX5 1GB,UK
Registered Company Number	1982084
Customer name	Alexandra E Jantzen
Customer address	170 Grey Elm Trail DURHAM, NC 27713
License number	3263210466856
License date	Nov 06, 2013
Licensed content publisher	Elsevier
Licensed content publication	Biomaterials
Licensed content title	Use of autologous blood-derived endothelial progenitor cells at point-of-care to protect against implant thrombosis in a large animal model
Licensed content author	Alexandra E. Jantzen,Whitney O. Lane,Shawn M. Gage,Ryan M. Jamiolkowski,Justin M. Haseltine,Lauren J. Galinat,Fu-Hsiung Lin,Jeffrey H. Lawson,George A. Truskey,Hardean E. Achneck
Licensed content date	November 2011

Licensed content volume number	32
Licensed content issue number	33
Number of pages	8
Start Page	8356
End Page	8363
Type of Use	reuse in a thesis/dissertation
Portion	full article
Format	both print and electronic
Are you the author of this Elsevier article?	Yes
Will you be translating?	No
Order reference number	0001
Title of your thesis/dissertation	Seeding of Titanium Surfaces and Nitinol Stents with Blood-Derived Endothelial Cells
Expected completion date	Apr 2014
Estimated size (number of pages)	150
Elsevier VAT number	GB 494 6272 12
Permissions price	0.00 USD
VAT/Local Sales Tax	0.0 USD / 0.0 GBP
Total	0.00 USD

Terms and Conditions

INTRODUCTION

1. The publisher for this copyrighted material is Elsevier. By clicking "accept" in connection with completing this licensing transaction, you agree that the following terms and conditions apply to this transaction (along with the Billing and Payment terms and conditions established by Copyright Clearance Center, Inc. ("CCC"), at the time that you opened your Rightslink account and that are available at any time at http://myaccount.copyright.com).

GENERAL TERMS

2. Elsevier hereby grants you permission to reproduce the aforementioned

material subject to the terms and conditions indicated.

3. Acknowledgement: If any part of the material to be used (for example, figures) has appeared in our publication with credit or acknowledgement to another source, permission must also be sought from that source. If such permission is not obtained then that material may not be included in your publication/copies. Suitable acknowledgement to the source must be made, either as a footnote or in a reference list at the end of your publication, as follows:

"Reprinted from Publication title, Vol /edition number, Author(s), Title of article / title of chapter, Pages No., Copyright (Year), with permission from Elsevier [OR APPLICABLE SOCIETY COPYRIGHT OWNER]." Also Lancet special credit - "Reprinted from The Lancet, Vol. number, Author(s), Title of article, Pages No., Copyright (Year), with permission from Elsevier."

4. Reproduction of this material is confined to the purpose and/or media for which permission is hereby given.

5. Altering/Modifying Material: Not Permitted. However figures and illustrations may be altered/adapted minimally to serve your work. Any other abbreviations, additions, deletions and/or any other alterations shall be made only with prior written authorization of Elsevier Ltd. (Please contact Elsevier at permissions@elsevier.com)

6. If the permission fee for the requested use of our material is waived in this instance, please be advised that your future requests for Elsevier materials may attract a fee.

7. Reservation of Rights: Publisher reserves all rights not specifically granted in the combination of (i) the license details provided by you and accepted in the course of this licensing transaction, (ii) these terms and conditions and (iii) CCC's Billing and Payment terms and conditions.

8. License Contingent Upon Payment: While you may exercise the rights licensed immediately upon issuance of the license at the end of the licensing process for the transaction, provided that you have disclosed complete and accurate details of your proposed use, no license is finally effective unless and until full payment is received from you (either by publisher or by CCC) as provided in CCC's Billing and Payment terms and conditions. If full payment is not received on a timely basis, then any license preliminarily granted shall be deemed automatically revoked and shall be void as if never granted. Further, in the event that you breach any of these terms and conditions or any of CCC's Billing and Payment terms and conditions, the license is automatically revoked and shall be void as if never granted. Use of materials as described in a revoked license, as well as any use of the materials beyond the scope of an unrevoked license, may

constitute copyright infringement and publisher reserves the right to take any and all action to protect its copyright in the materials.

9. Warranties: Publisher makes no representations or warranties with respect to the licensed material.

10. Indemnity: You hereby indemnify and agree to hold harmless publisher and CCC, and their respective officers, directors, employees and agents, from and against any and all claims arising out of your use of the licensed material other than as specifically authorized pursuant to this license.

11. No Transfer of License: This license is personal to you and may not be sublicensed, assigned, or transferred by you to any other person without publisher's written permission.

12. No Amendment Except in Writing: This license may not be amended except in a writing signed by both parties (or, in the case of publisher, by CCC on publisher's behalf).

13. Objection to Contrary Terms: Publisher hereby objects to any terms contained in any purchase order, acknowledgment, check endorsement or other writing prepared by you, which terms are inconsistent with these terms and conditions or CCC's Billing and Payment terms and conditions. These terms and conditions, together with CCC's Billing and Payment terms and conditions (which are incorporated herein), comprise the entire agreement between you and publisher (and CCC) concerning this licensing transaction. In the event of any conflict between your obligations established by these terms and conditions and those established by CCC's Billing and Payment terms and conditions, these terms and conditions shall control.

14. Revocation: Elsevier or Copyright Clearance Center may deny the permissions described in this License at their sole discretion, for any reason or no reason, with a full refund payable to you. Notice of such denial will be made using the contact information provided by you. Failure to receive such notice will not alter or invalidate the denial. In no event will Elsevier or Copyright Clearance Center be responsible or liable for any costs, expenses or damage incurred by you as a result of a denial of your permission request, other than a refund of the amount(s) paid by you to Elsevier and/or Copyright Clearance Center for denied permissions.

LIMITED LICENSE

The following terms and conditions apply only to specific license types:

15. **Translation**: This permission is granted for non-exclusive world **English**

rights only unless your license was granted for translation rights. If you licensed translation rights you may only translate this content into the languages you requested. A professional translator must perform all translations and reproduce the content word for word preserving the integrity of the article. If this license is to re-use 1 or 2 figures then permission is granted for non-exclusive world rights in all languages.

16. **Website**: The following terms and conditions apply to electronic reserve and author websites:
Electronic reserve: If licensed material is to be posted to website, the web site is to be password-protected and made available only to bona fide students registered on a relevant course if:
This license was made in connection with a course,
This permission is granted for 1 year only. You may obtain a license for future website posting,
All content posted to the web site must maintain the copyright information line on the bottom of each image,
A hyper-text must be included to the Homepage of the journal from which you are licensing at http://www.sciencedirect.com/science/journal/xxxxx or the Elsevier homepage for books at http://www.elsevier.com , and
Central Storage: This license does not include permission for a scanned version of the material to be stored in a central repository such as that provided by Heron/XanEdu.

17. **Author website** for journals with the following additional clauses:

All content posted to the web site must maintain the copyright information line on the bottom of each image, and the permission granted is limited to the personal version of your paper. You are not allowed to download and post the published electronic version of your article (whether PDF or HTML, proof or final version), nor may you scan the printed edition to create an electronic version. A hyper-text must be included to the Homepage of the journal from which you are licensing at http://www.sciencedirect.com/science/journal/xxxxx . As part of our normal production process, you will receive an e-mail notice when your article appears on Elsevier's online service ScienceDirect (www.sciencedirect.com). That e-mail will include the article's Digital Object Identifier (DOI). This number provides the electronic link to the published article and should be included in the posting of your personal version. We ask that you wait until you receive this e-mail and have the DOI to do any posting.

Central Storage: This license does not include permission for a scanned version of the material to be stored in a central repository such as that provided by Heron/XanEdu.

18. **Author website** for books with the following additional clauses:
Authors are permitted to place a brief summary of their work online only.
A hyper-text must be included to the Elsevier homepage at http://www.elsevier.com . All

content posted to the web site must maintain the copyright information line on the bottom of each image. You are not allowed to download and post the published electronic version of your chapter, nor may you scan the printed edition to create an electronic version.

Central Storage: This license does not include permission for a scanned version of the material to be stored in a central repository such as that provided by Heron/XanEdu.

19. **Website** (regular and for author): A hyper-text must be included to the Homepage of the journal from which you are licensing at http://www.sciencedirect.com/science/journal/xxxxx. or for books to the Elsevier homepage at http://www.elsevier.com

20. **Thesis/Dissertation**: If your license is for use in a thesis/dissertation your thesis may be submitted to your institution in either print or electronic form. Should your thesis be published commercially, please reapply for permission. These requirements include permission for the Library and Archives of Canada to supply single copies, on demand, of the complete thesis and include permission for UMI to supply single copies, on demand, of the complete thesis. Should your thesis be published commercially, please reapply for permission.

21. **Other Conditions**:

v1.6

If you would like to pay for this license now, please remit this license along with your payment made payable to "COPYRIGHT CLEARANCE CENTER" otherwise you will be invoiced within 48 hours of the license date. Payment should be in the form of a check or money order referencing your account number and this invoice number RLNK501153150.
Once you receive your invoice for this order, you may pay your invoice by credit card. Please follow instructions provided at that time.

Make Payment To:
Copyright Clearance Center
Dept 001
P.O. Box 843006
Boston, MA 02284-3006

For suggestions or comments regarding this order, contact RightsLink Customer Support: customercare@copyright.com or +1-877-622-5543 (toll free in the US) or +1-978-646-2777.

Gratis licenses (referencing $0 in the Total field) are free. Please retain this printable license for your reference. No payment is required.

References

1. Lloyd-Jones D, Adams RJ, Brown TM, Carnethon M, Dai S, De Simone G, Ferguson TB, Ford E, Furie K, Gillespie C and others. Heart Disease and Stroke Statistics—2010 Update. Circulation 2010;121(7):e46-e215.

2. Go AS, Mozaffarian D, Roger VL, Benjamin EJ, Berry JD, Blaha MJ, Dai S, Ford ES, Fox CS, Franco S and others. Heart Disease and Stroke Statistics-2014 Update a Report from the American Heart Association. Circulation 2014;129(3):E28-E292.

3. Michael TT, Abdel-karim A-rR, Papayannis A, Lichtenwalter C, de Lemos JA, Obel O, Addo T, Roesle M, Haagen D, Rangan BV and others. Recurrent Cardiovascular Events with Paclitaxel-Eluting Versus Bare-Metal Stents in Saphenous Vein Graft Lesions: Insights from the Sos (Stenting of Saphenous Vein Grafts) Trial. Journal of Invasive Cardiology 2011;23(6):216-219.

4. The Sage Group. New Estimates for Prevalence of Peripheral Artery Disease (Pad) in U.S. http://heartheavy.com/new-estimates-for-prevalence-of-peripheral-artery-disease-pad-in-u-s/. Accessed 08 Nov 2011.

5. Highland Capital Partners. Pervasis to Present Interim Data from Phase 1/2 Clinical Study of Novel Cell Therapy Targeting Peripheral Artery Disease at International Conference on Cell Therapy for Cardiovascular Diseases. http://www.hcp.com/news/newsdetails.php/id/87812. Accessed April 27, 2012.

6. Kroger K, Buss C, Goyen M, Santosa F, Rudofsky G. Diameter of Occluded Superficial Femoral Arteries Limits Percutaneous Recanalization: Preliminary Results. Journal of Endovascular Therapy 2002;9(3):369-374.

7. Duda SH, Bosiers M, Lammer J, Scheinert D, Zeller T, Oliva V, Tielbeek A, Anderson J, Wiesinger B, Tepe G and others. Drug-Eluting and Bare Nitinol Stents for the Treatment of Atherosclerotic Lesions in the Superficial Femoral Artery: Long-Term Results from the Sirocco Trial. Journal of Endovascular Therapy 2006;13(6):701-710.

8. Chorny M, Fishbein I, Yellen BB, Alferiev IS, Bakay M, Ganta S, Adamo R, Amiji M, Friedman G, Levy RJ. Targeting Stents with Local Delivery of Paclitaxel-Loaded Magnetic Nanoparticles Using Uniform Fields. Proceedings of the National Academy of Sciences of the United States of America 2010;107(18):8346-8351.

9. Polyak B, Fishbein I, Chorny M, Alferiev I, Williams D, Yellen B, Friedman G, Levy RJ. High Field Gradient Targeting of Magnetic Nanoparticle-Loaded Endothelial Cells to the Surfaces of Steed Stents. Proceedings of the National Academy of Sciences of the United States of America 2008;105(2):698-703.

10. Stoeckel D, Pelton A, Duerig T. Self-Expanding Nitinol Stents: Material and Design Considerations. European Radiology 2004;14(2):292-301.

11. Lloyd-Jones DM, Larson MG, Beiser A, Levy D. Lifetime Risk of Developing Coronary Heart Disease. Lancet 1999;353(9147):89-92.

12. Auerbach D, Meada JL, Steiner C. Hospital Stays with Cardiac Stents, 2009; Statistical Brief #128. Healthcare Cost and Utilization Project 2012.

13. Lee TH, Hillis LD, Nabel EG. Cabg Vs. Stenting--Clinical Implications of the Syntax Trial. The New England journal of medicine 2009;360(8):e10.

14. Buszman PE, Kiesz SR, Bochenek A, Peszek-Przybyla E, Szkrobka I, Debinski M, Bialkowska B, Dudek D, Gruszka A, Zurakowski A and others. Acute and Late Outcomes of Unprotected Left Main Stenting in Comparison with Surgical Revascularization. Journal of the American College of Cardiology 2008;51(5):538-545.

15. Brilakis ES, Lichtenwalter C, Abdel-karim A-rR, de Lemos JA, Obel O, Addo T, Roesle M, Haagen D, Rangan BV, Saeed B and others. Continued Benefit from Paclitaxel-Eluting Compared with Bare-Metal Stent Implantation in Saphenous Vein Graft Lesions During Long-Term Follow-up of the Sos (Stenting of Saphenous Vein Grafts) Trial. Jacc-Cardiovascular Interventions 2011;4(2):176-182.

16. Pfisterer M, Brunner-La Rocca HP, Rickenbacher P, Hunziker P, Mueller C, Nietlispach F, Leibundgut G, Bader F, Kaiser C, Investigators B. Long-Term Benefit-Risk Balance of Drug-Eluting Vs. Bare-Metal Stents in Daily Practice: Does Stent Diameter Matter? Three-Year Follow-up of Basket. European Heart Journal 2009;30(1):16-24.

17. Kauffman GB, Mayo I. The Story of Nitinol: The Serendipitous Discovery of the Memory Metal and Its Applications. The Chemical Educator 1997;2(2):1-21.

18. Duerig T, Pelton A, Stockel D. An Overview of Nitinol Medical Applications. Materials Science and Engineering a-Structural Materials Properties Microstructure and Processing 1999;273:149-160.

19. Lombardi S, Poncet P. Metallurgical Principles of Nitinol and Its Use in Interventional Devices. Controversies and Consensus in Imaging and Intervention (C2I2) 2004((Autumn):24-26.

20. Vogel TR, Shindelman LE, Nackman GB, Graham AM. Efficacious Use of Nitinol Stents in the Femoral and Popliteal Arteries. Journal of Vascular Surgery 2003;38(6):1178-1183.

21. Smouse HB, Nikanorov A, LaFlash D. Biomechanical Forces in the Femoropopliteal Arterial Segment. Endovascular Today 2005;4(6):60-66.

22. Amoroso G, Geuns R-Jv, Spaulding C, Manzo-Silberman S, Hauptmann KE, Spaargaren R, Garcia-Garcia HM, Serruys PW, Verheye S. Assessment of the Safety and Performance of the Stentys Self-Expanding Coronary Stent in Acute Myocardial Infarction: Results from the Apposition I Study. EuroIntervention 2011;7(4):428-436.

23. Giacchi G, La Manna A, Tamburino C, Capodanno D, Capranzano P. Self-Apposing Stentys® Stent in Acute Myocardial Infarction. Minerva cardioangiologica 2014;62(1):59-70.

24. Plant SD, Grant DM, Leach L. Behaviour of Human Endothelial Cells on Surface Modified Niti Alloy. Biomaterials 2005;26(26):5359-5367.

25. Trepanier C, Tabrizian M, Yahia L, Bilodeau L, Piron DL. Effect of Modification of Oxide Layer on Niti Stent Corrosion Resistance. Journal of Biomedical Materials Research 1998;43(4):433-440.

26. Achneck HE, Jamiolkowski RM, Jantzen AE, Haseltine JM, Lane WO, Huang JK, Galinat LJ, Serpe MJ, Lin FH, Li M and others. The Biocompatibility of Titanium Cardiovascular Devices Seeded with Autologous Blood-Derived Endothelial Progenitor Cells Epc-Seeded Antithrombotic Ti Implants. Biomaterials 2011;32(1):10-18.

27. Jantzen AE, Lane WO, Gage SM, Jamiolkowski RM, Haseltine JM, Galinat LJ, Lin F-H, Lawson JH, Truskey GA, Achneck HE. Use of Autologous Blood-Derived

Endothelial Progenitor Cells at Point-of-Care to Protect against Implant Thrombosis in a Large Animal Model. Biomaterials 2011;32(33):8356-63.

28. Minar E, Pokrajac B, Maca T, Ahmadi R, Fellner C, Mittlbock M, Seitz W, Wolfram R, Potter R. Endovascular Brachytherapy for Prophylaxis of Restenosis after Femoropopliteal Angioplasty - Results of a Prospective Randomized Study. Circulation 2000;102(22):2694-2699.

29. Dormandy JA, Rutherford RB. Management of Peripheral Arterial Disease (Pad). Tasc Working Group. Transatlantic Inter-Society Consensus (Tasc). Journal of vascular surgery : official publication, the Society for Vascular Surgery [and] International Society for Cardiovascular Surgery, North American Chapter 2000;31(1 Pt 2):S1-S296.

30. Johnston KW. Femoral and Popliteal Arteries - Reanalysis of Results of Balloon Angioplasty. Radiology 1992;183(3):767-771.

31. Capek P, McLean GK, Berkowitz HD. Femoropopliteal Angioplasty - Factors Influencing Long-Term Success. Circulation 1991;83(2):70-80.

32. Duda SH, Bosiers M, Lammer J, Scheinert D, Zeller T, Tielbeek A, Anderson J, Wiesinger B, Tepe G, Lansky A and others. Sirolimus-Eluting Versus Bare Nitinol Stent for Obstructive Superficial Femoral Artery Disease: The Sirocco Ii Trial. Journal of Vascular and Interventional Radiology 2005;16(3):331-338.

33. Dake MD, Ansel GM, Jaff MR, Ohki T, Saxon RR, Smouse HB, Zeller T, Roubin GS, Burket MW, Khatib Y and others. Paclitaxel-Eluting Stents Show Superiority to Balloon Angioplasty and Bare Metal Stents in Femoropopliteal Disease Twelve-Month Zilver Ptx Randomized Study Results. Circulation-Cardiovascular Interventions 2011;4(5):495-504.

34. Schuhlen H, Kastrati A, Mehilli J, Hausleiter J, Pache J, Dirschinger J, Schomig A. Restenosis Detected by Routine Angiographic Follow-up and Late Mortality after Coronary Stent Placement. American Heart Journal 2004;147(2):317-322.

35. Elezi S, Kastrati A, Hadamitzky M, Dirschinger J, Neumann FJ, Schomig A. Clinical and Angiographic Follow-up after Balloon Angioplasty with Provisional Stenting for Coronary in-Stent Restenosis. Catheterization and Cardiovascular Interventions 1999;48(2):151-156.

36. Kastrati A, Mehilli J, Dirschinger J, Pache J, Ulm K, Schuhlen H, Seyfarth M, Schmitt C, Blasini R, Neumann FJ and others. Restenosis after Coronary Placement of Various Stent Types. American Journal of Cardiology 2001;87(1):34-39.

37. Pfisterer M, Brunner-La Rocca HP, Buser PT, Rickenbacher P, Hunziker P, Mueller C, Jeger R, Bader F, Osswald S, Kaiser C and others. Late Clinical Events after Clopidogrel Discontinuation May Limit the Benefit of Drug-Eluting Stents - an Observational Study of Drug-Eluting Versus Bare-Metal Stents. Journal of the American College of Cardiology 2006;48(12):2584-2591.

38. Moses JW, Leon MB, Popma JJ, Fitzgerald PJ, Holmes DR, O'Shaughnessy C, Caputo RP, Kereiakes DJ, Williams DO, Teirstein PS and others. Sirolimus-Eluting Stents Versus Standard Stents in Patients with Stenosis in a Native Coronary Artery. New England Journal of Medicine 2003;349(14):1315-1323.

39. Venkatraman S, Boey F. Release Profiles in Drug-Eluting Stents: Issues and Uncertainties. Journal of Controlled Release 2007;120(3):149-160.

40. McFadden EP, Stabile E, Regar E, Cheneau E, Ong ATL, Kinnaird T, Suddath WO, Weissman NJ, Torguson R, Kent KM and others. Late Thrombosis in Drug-Eluting Coronary Stents after Discontinuation of Antiplatelet Therapy. The Lancet;364(9444):1519-1521.

41. Cragg GM, Newman DJ. Plants as a Source of Anti-Cancer Agents. Journal of Ethnopharmacology 2005;100(1-2):72-79.

42. Groth CG, Backman L, Morales JM, Calne R, Kreis H, Lang P, Touraine JL, Claesson K, Campistol JM, Durand D and others. Sirolimus (Rapamycin)-Based Therapy in Human Renal Transplantation - Similar Efficacy and Different Toxicity Compared with Cyclosporine. Transplantation 1999;67(7):1036-1042.

43. Campistol JM, Eris J, Oberbauer R, Friend P, Hutchison B, Morales JM, Claesson K, Stallone G, Russ G, Rostaing L and others. Sirolimus Therapy after Early Cyclosporine Withdrawal Reduces the Risk for Cancer in Adult Renal Transplantation. Journal of the American Society of Nephrology 2006;17(2):581-589.

44. Falotico R, Zhao J. Polymers and Drug-Eluting Stents. Textbook of Interventional Cardiovascular Pharmacology 2007:289.

45. Virmani R, Guagliumi G, Farb A, Musumeci G, Grieco N, Motta T, Mihalcsik L, Tespili M, Valsecchi O, Kolodgie FD. Localized Hypersensitivity and Late Coronary Thrombosis Secondary to a Sirolimus-Eluting Stent Should We Be Cautious? Circulation 2004;109(6):701-705.

46. Nebeker JR, Virmani R, Bennett CL, Hoffman JM, Samore MH, Alvarez J, Davidson CJ, McKoy JM, Raisch DW, Whisenant BK and others. Hypersensitivity Cases Associated with Drug-Eluting Coronary Stents - a Review of Available Cases from the Research on Adverse Drug Events and Reports (Radar) Project. Journal of the American College of Cardiology 2006;47(1):175-181.

47. Finn AV, Nakazawa G, Joner M, Kolodgie FD, Mont EK, Gold HK, Virmani R. Vascular Responses to Drug Eluting Stents - Importance of Delayed Healing. Arteriosclerosis Thrombosis and Vascular Biology 2007;27(7):1500-1510.

48. Stone GW, Midei M, Newman W, Sanz M, Hermiller JB, Williams J, Farhat N, Mahaffey KW, Cutlip DE, Fitzgerald PJ and others. Comparison of an Everolimus-Eluting Stent and a Paclitaxel-Eluting Stent in Patients with Coronary Artery Disease - a Randomized Trial. Jama-Journal of the American Medical Association 2008;299(16):1903-1913.

49. Kandzari DE, Leon MB, Popma JJ, Fitzgerald PJ, O'Shaughnessy C, Ball MW, Turco M, Applegate RJ, Gurbel PA, Midei MG and others. Comparison of Zotarolimus-Eluting and Sirolimus-Eluting Stents in Patients with Native Coronary Artery Disease - a Randomized Controlled Trial. Journal of the American College of Cardiology 2006;48(12):2440-2447.

50. Meredith IT, Ormiston J, Whitbourn R, Kay IP, Muller D, Popma JJ, Cutlip DE, Fitzgerald PJ, Investigators EI. Four-Year Clinical Follow-up after Implantation of the Endeavor Zotarolimus-Eluting Stent: Endeavor I, the First-in-Human Study. American Journal of Cardiology 2007;100(8B):56M-61M.

51. Middleton JC, Tipton AJ. Synthetic Biodegradable Polymers as Orthopedic Devices. Biomaterials 2000;21(23):2335-2346.

52. Dake MD, Scheinert D, Tepe G, Tessarek J, Fanelli F, Bosiers M, Ruhlmann C, Kavteladze Z, Lottes AE, Ragheb AO and others. Nitinol Stents with Polymer-Free Paclitaxel Coating for Lesions in the Superficial Femoral and Popliteal Arteries above the Knee: Twelve-Month Safety and Effectiveness Results from

the Zilver Ptx Single-Arm Clinical Study. Journal of Endovascular Therapy 2011;18(5):613-623.

53. Minami Y, Kaneda H, Inoue M, Ikutomi M, Morita T, Nakajima T. Endothelial Dysfunction Following Drug-Eluting Stent Implantation: A Systematic Review of the Literature. International Journal of Cardiology 2013;165(2):222-228.

54. Erbel R, Di Mario C, Bartunek J, Bonnier J, de Bruyne B, Eberli FR, Erne P, Haude M, Heublein B, Horrigan M and others. Temporary Scaffolding of Coronary Arteries with Bioabsorbable Magnesium Stents: A Prospective, Non-Randomised Multicentre Trial. The Lancet;369(9576):1869-1875.

55. Ormiston JA, Serruys PW, Regar E, Dudek D, Thuesen L, Webster MWI, Onuma Y, Garcia-Garcia HM, McGreevy R, Veldhof S. A Bioabsorbable Everolimus-Eluting Coronary Stent System for Patients with Single De-Novo Coronary Artery Lesions (Absorb): A Prospective Open-Label Trial. The Lancet;371(9616):899-907.

56. Serruys PW, Onuma Y, Dudek D, Smits PC, Koolen J, Chevalier B, de Bruyne B, Thuesen L, McClean D, van Geuns R-J and others. Evaluation of the Second Generation of a Bioresorbable Everolimus-Eluting Vascular Scaffold for the Treatment of De Novo Coronary Artery Stenosis 12-Month Clinical and Imaging Outcomes. Journal of the American College of Cardiology 2011;58(15):1578-1588.

57. Bezerra H, Chamie D, Kanaya T, Fujino Y, Kuang Y, Naimark W, Palasis M, Tanaka K, Attizzani G, Costa M. Serial Optical Coherence Tomography Morphometric Assessment of the Novel Stanza™ Bioresorbable Vascular Scaffold Implanted in Superficial Femoral Arteries in a Pre–Clinical Sheep Model. Journal of the American College of Cardiology 2013;61(10_S).

58. Karanasos A, van Geuns R-J, Zijlstra F, Regar E. Very Late Bioresorbable Scaffold Thrombosis after Discontinuation of Dual Antiplatelet Therapy. European Heart Journal 2014.

59. Sigwart U, Puel J, Mirkovitch V, Joffre F, Kappenberger L. Intravascular Stents to Prevent Occlusion and Restenosis after Trans-Luminal Angioplasty. New England Journal of Medicine 1987;316(12):701-706.

60. Baxter TJ, Bennett RC, Obrien BM, Henderso.Pn. Histopathology of Small Vessels Following Microvascular Repair. British Journal of Surgery 1972;59(8):617-&.

61. Zhu S, Malhotra A, Zhang L, Deng S, Zhang T, Freedman NJ, Storms R, Peppel K, Goldschmidt-Clermont PJ, Dong C. Human Umbilical Cord Blood Endothelial Progenitor Cells Decrease Vein Graft Neointimal Hyperplasia in Scid Mice. Atherosclerosis 2010;212(1):63-69.

62. Giessen WVd, Serruys P, Visser W, Verdouw P, Schalkwijk Wv, Jongkind J. Endothelialization of Intravascular Stents. Journal of Interventional Cardiology 1988;1:109-120.

63. Kutryk MJ, van Dortmont LM, de Crom RP, van der Kamp AW, Verdouw PD, van der Giessen WJ. Seeding of Intravascular Stents by the Xenotransplantation of Genetically Modified Endothelial Cells. Seminars in interventional cardiology : SIIC 1998;3(3-4):217-20.

64. Scott NA, Candal FJ, Robinson KA, Ades EW. Seeding of Intracoronary Stents with Immortalized Human Microvascular Endothelial-Cells. American Heart Journal 1995;129(5):860-866.

65. Zhu W, Tian Y, Zhou L-F, Wang Y, Song D, Mao Y, Yang G-Y. Development of a Novel Endothelial Cell-Seeded Endovascular Stent for Intracranial Aneurysm Therapy. Journal of Biomedical Materials Research Part A 2008;85A(3):715-721.

66. Shirota T, Yasui H, Shimokawa H, Matsuda T. Fabrication of Endothelial Progenitor Cell (Epc)-Seeded Intravascular Stent Devices and in Vitro Endothelialization on Hybrid Vascular Tissue. Biomaterials 2003;24(13):2295-2302.

67. Shi HJ, Cao AH, Teng GJ. Seeding Endothelial Progenitor Cells on a Self-Expanding Metal Stent: An in Vitro Study. Journal of Vascular and Interventional Radiology 2010;21(7):1061-1065.

68. Dichek DA, Neville RF, Zwiebel JA, Freeman SM, Leon MB, Anderson WF. Seeding of Intravascular Stents with Genetically Engineered Endothelial-Cells. Circulation 1989;80(5):1347-1353.

69. Fine E, Zhang L, Fenniri H, Webster TJ. Enhanced Endothelial Cell Functions on Rosette Nanotube-Coated Titanium Vascular Stents. International Journal of Nanomedicine 2009;4(1):91-97.

70. Wang GX, Deng XY, Tang CJ, Liu LS, Xiao L, Xiang LH, Quan XJ, Legrand AP, Guidoin R. The Adhesive Properties of Endothelial Cells on Endovascular Stent Coated by Substrates of Poly-L-Lysine and Fibronectin. Artificial Cells Blood Substitutes and Biotechnology 2006;34(1):11-25.

71. Flugelman MY, Virmani R, Leon MB, Bowman RL, Dichek DA. Genetically Engineered Endothelial-Cells Remain Adherent and Viable after Stent Deployment and Exposure to Flow Invitro. Circulation Research 1992;70(2):348-354.

72. Pislaru SV, Harbuzariu A, Gulati R, Witt T, Sandhu NP, Simari RD, Sandhu GS. Magnetically Targeted Endothelial Cell Localization in Stented Vessels. Journal of the American College of Cardiology 2006;48(9):1839-1845.

73. van Beusekom HMM, Ertas G, Sorop O, Serruys PW, van der Giessen WJ. The Genous (Tm) Endothelial Progenitor Cell Capture Stent Accelerates Stent Re-Endothelialization but Does Not Affect Intimal Hyperplasia in Porcine Coronary Arteries. Catheterization and Cardiovascular Interventions 2012;79(2):231-242.

74. Garg S, Duckers HJ, Serruys PW. Endothelial Progenitor Cell Capture Stents: Will This Technology Find Its Niche in Contemporary Practice? European Heart Journal 2010;31(9):1032-1035.

75. Simper D, Stalboerger PG, Panetta CJ, Wang SH, Caplice NM. Smooth Muscle Progenitor Cells in Human Blood. Circulation 2002;106(10):1199-1204.

76. Beijk MAM, Klomp M, van Geloven N, Koch KT, Henriques JPS, Baan J, Vis MM, Tijssen JGP, Piek JJ, de Winter RJ. Two-Year Follow-up of the Genous (Tm) Endothelial Progenitor Cell Capturing Stent Versus the Taxus Liberte Stent in Patients with De Novo Coronary Artery Lesions with a High-Risk of Restenosis: A Randomized, Single-Center, Pilot Study. Catheterization and Cardiovascular Interventions 2011;78(2):189-195.

77. Haude M, Lee SWL, Worthley SG, Silber S, Verheye S, Erbs S, Rosli MA, Botelho R, Meredith I, Sim KH and others. The Remedee Triala Randomized Comparison of a Combination Sirolimus-Eluting Endothelial Progenitor Cell Capture Stent with a Paclitaxel-Eluting Stent. JACC: Cardiovascular Interventions 2013;6(4):334-343.

78. Lim W-H, Seo W-W, Choe W, Kang C-K, Park J, Cho H-J, Kyeong S, Hur J, Yang H-M, Cho H-J and others. Stent Coated with Antibody against Vascular Endothelial-Cadherin Captures Endothelial Progenitor Cells, Accelerates Re-Endothelialization, and Reduces Neointimal Formation. Arteriosclerosis Thrombosis and Vascular Biology 2011;31(12):2798-U141.

79. Yoder MC, Mead LE, Prater D, Krier TR, Mroueh KN, Li F, Krasich R, Temm CJ, Prchal JT, Ingram DA. Redefining Endothelial Progenitor Cells Via Clonal Analysis and Hematopoietic Stem/Progenitor Cell Principals. Blood 2007;109(5):1801-1809.

80. Matsuda T, Kuwana M, Aomizu T, Yamagishi M, Ohtake H, Watanabe G. Surface Design for in Situ Capture of Endothelial Progenitor Cells: Vegf-Bound Surface Architecture and Behaviors of Cultured Mononuclear Cells. Journal of Biomedical Materials Research Part B-Applied Biomaterials 2013;101B(1):50-60.

81. Blindt R, Vogt F, Astafieva I, Fach C, Hristov M, Krott N, Seitz B, Kapurniotu A, Kwok C, Dewor M and others. A Novel Drug-Eluting Stent Coated with an Integrin-Binding Cyclic Arg-Gly-Asp Peptide Inhibits Neointimal Hyperplasia by Recruiting Endothelial Progenitor Cells. Journal of the American College of Cardiology 2006;47(9):1786-1795.

82. Avci-Adali M, Ziemer G, Wendel HP. Induction of Epc Homing on Biofunctionalized Vascular Grafts for Rapid in Vivo Self-Endothelialization - a Review of Current Strategies. Biotechnology Advances 2010;28(1):119-129.

83. Wei Y, Ji Y, Xiao L-L, Lin Q-k, Xu J-p, Ren K-f, Ji J. Surface Engineering of Cardiovascular Stent with Endothelial Cell Selectivity for in Vivo Re-Endothelialisation. Biomaterials 2013;34(11):2588-2599.

84. Suuronen EJ, Zhang P, Kuraitis D, Cao X, Melhuish A, McKee D, Li F, Mesana TG, Veinot JP, Ruel M. An Acellular Matrix-Bound Ligand Enhances the Mobilization, Recruitment and Therapeutic Effects of Circulating Progenitor Cells in a Hindlimb Ischemia Model. Faseb Journal 2009;23(5):1447-1458.

85. Hoffmann J, Paul A, Harwardt M, Groll J, Reeswinkel T, Klee D, Moeller M, Fischer H, Walker T, Greiner T and others. Immobilized DNA Aptamers Used as Potent Attractors for Porcine Endothelial Precursor Cells. Journal of Biomedical Materials Research Part A 2008;84A(3):614-621.

86. Kunz GA, Liang G, Cuculi F, Gregg D, Vata KC, Shaw LK, Goldschmidt-Clermont PJ, Dong C, Taylor DA, Peterson ED. Circulating Endothelial Progenitor Cells Predict Coronary Artery Disease Severity. American Heart Journal 2006;152(1):190-195.

87. Asahara T, Murohara T, Sullivan A, Silver M, vanderZee R, Li T, Witzenbichler B, Schatteman G, Isner JM. Isolation of Putative Progenitor Endothelial Cells for Angiogenesis. Science 1997;275(5302):964-967.

88. Ingram DA, Mead LE, Tanaka H, Meade V, Fenoglio A, Mortell K, Pollok K, Ferkowicz MJ, Gilley D, Yoder MC. Identification of a Novel Hierarchy of Endothelial Progenitor Cells Using Human Peripheral and Umbilical Cord Blood. Blood 2004;104(9):2752-2760.

89. Jantzen AE, Lane WO, Gage SM, Haseltine JM, Galinat LJ, Jamiolkowski RM, Lin F-H, Truskey GA, Achneck HE. Autologous Endothelial Progenitor Cell-Seeding Technology and Biocompatibility Testing for Cardiovascular Devices in Large Animal Model. Journal of visualized experiments : JoVE 2011(55):N/A.

90. Brown MA, Wallace CS, Angelos M, Truskey GA. Characterization of Umbilical Cord Blood-Derived Late Outgrowth Endothelial Progenitor Cells Exposed to Laminar Shear Stress. Tissue Engineering Part A 2009;15(11):3575-3587.

91. Povsic TJ, Goldschmidt-Clermont PJ. Endothelial Progenitor Cells: Markers of Vascular Reparative Capacity. Therapeutic advances in cardiovascular disease 2008;2(3):199-213.

92. Farb A, Weber DK, Kolodgie FD, Burke AP, Virmani R. Morphological Predictors of Restenosis after Coronary Stenting in Humans. Circulation 2002;105(25):2974-2980.

93. Tiwari A, Salacinski HJ, Hamilton G, Seifalian AM. Tissue Engineering of Vascular Bypass Grafts: Role of Endothelial Cell Extraction. European Journal of Vascular and Endovascular Surgery 2001;21(3):193-201.

94. Jarrell BE, Williams SK, Stokes G, Hubbard FA, Carabasi RA, Koolpe E, Greener D, Pratt K, Moritz MJ, Radomski J and others. Use of Freshly Isolated Capillary Endothelial-Cells for the Immediate Establishment of a Monolayer on a Vascular Graft at Surgery. Surgery 1986;100(2):392-399.

95. Shi Z, Neoh K, Kang E. In Vitro Endothelialization of Cobalt Chromium Alloys with Micro/Nanostructures Using Adipose-Derived Stem Cells. Journal of Materials Science: Materials in Medicine 2013;24(4):1067-1077.

96. Schreml S, Babilas P, Fruth S, Orso E, Schmitz G, Mueller MB, Nerlich M, Prantl L. Harvesting Human Adipose Tissue-Derived Adult Stem Cells: Resection Versus Liposuction. Cytotherapy 2009;11(7):947-957.

97. Stroncek JD, Grant BS, Brown MA, Povsic TJ, Truskey GA, Reichert WM. Comparison of Endothelial Cell Phenotypic Markers of Late-Outgrowth Endothelial Progenitor Cells Isolated from Patients with Coronary Artery Disease and Healthy Volunteers. Tissue Engineering Part A 2009;15(11):3473-3486.

98. Shepherd RM, Capoccia BJ, Devine SM, DiPersio J, Trinkaus KM, Ingram D, Link DC. Angiogenic Cells Can Be Rapidly Mobilized and Efficiently Harvested from the Blood Following Treatment with Amd3100. Blood 2006;108(12):3662-3667.

99. Migliavacca F, Petrini L, Montanari V, Quagliana I, Auricchio F, Dubini G. A Predictive Study of the Mechanical Behaviour of Coronary Stents by Computer Modelling. Medical Engineering & Physics 2005;27(1):13-18.

100. Zunino P, D'Angelo C, Petrini L, Vergara C, Capelli C, Migliavacca F. Numerical Simulation of Drug Eluting Coronary Stents: Mechanics, Fluid Dynamics and Drug Release. Computer Methods in Applied Mechanics and Engineering 2009;198(45-46):3633-3644.

101. Rebelo N, Fu R, Lawrenchuk M. Study of a Nitinol Stent Deployed into Anatomically Accurate Artery Geometry and Subjected to Realistic Service Loading. Journal of Materials Engineering and Performance 2009;18(5-6):655-663.

102. Berry JL, Santamarina A, Moore JE, Jr., Roychowdhury S, Routh WD. Experimental and Computational Flow Evaluation of Coronary Stents. Annals of Biomedical Engineering 2000;28(4):386-398.

103. LaDisa JF, Guler I, Olson LE, Hettrick DA, Kersten JR, Warltier DC, Pagel PS. Three-Dimensional Computational Fluid Dynamics Modeling of Alterations in Coronary Wall Shear Stress Produced by Stent Implantation. Annals of Biomedical Engineering 2003;31(8):972-980.

104. Gundert TJ, Marsden AL, Yang W, LaDisa JJF. Optimization of Cardiovascular Stent Design Using Computational Fluid Dynamics. Journal of Biomechanical Engineering 2012;134(1):011002-8.

105. Theriault P, Terriault P, Brailovski V, Gallo R. Finite Element Modeling of a Progressively Expanding Shape Memory Stent. Journal of Biomechanics 2006;39(15):2837-2844.

106. Gong X-Y, Pelton AR, Duerig TW, Rebelo N, Perry K. Finite Element Analysis and Experimental Evaluation of Superelastic Nitinol Stent. In: Pelton A, Duerig T, editors; 2003; Pacific Grove, California, USA. p 453-462.

107. Pelton AR, Schroeder V, Mitchell MR, Gong X-Y, Barney M, Robertson SW. Fatigue and Durability of Nitinol Stents. Journal of the Mechanical Behavior of Biomedical Materials 2008;1(2):153-164.

108. Jaff MR. The Nature of Sfa Disease. Endovascular Today 2004;2004(October):3-5.

109. LaDisa JF, Olson LE, Guler I, Hettrick DA, Audi SH, Kersten JR, Warltier DC, Pagel PS. Stent Design Properties and Deployment Ratio Influence Indexes of Wall Shear Stress: A Three-Dimensional Computational Fluid Dynamics Investigation within a Normal Artery. Journal of Applied Physiology 2004;97(1):424-430.

110. LaDisa JF, Jr., Olson LE, Hettrick DA, Warltier DC, Kersten JR, Pagel PS. Axial Stent Strut Angle Influences Wall Shear Stress after Stent Implantation: Analysis Using 3d Computational Fluid Dynamics Models of Stent Foreshortening. Biomedical engineering online 2005;4:59.

111. Liu SQ, Goldman J. Role of Blood Shear Stress in the Regulation of Vascular Smooth Muscle Cell Migration. Ieee Transactions on Biomedical Engineering 2001;48(4):474-483.

112. LaDisa JF, Olson LE, Molthen RC, Hettrick DA, Pratt PF, Hardel MD, Kersten JR, Warltier DC, Pagel PS. Alterations in Wall Shear Stress Predict Sites of Neointimal Hyperplasia after Stent Implantation in Rabbit Iliac Arteries. American Journal of Physiology-Heart and Circulatory Physiology 2005;288(5):H2465-H2475.

113. Wentzel JJ, Krams R, Schuurbiers JCH, Oomen JA, Kloet J, van der Giessen WJ, Serruys PW, Slager CJ. Relationship between Neointimal Thickness and Shear Stress after Wallstent Implantation in Human Coronary Arteries. Circulation 2001;103(13):1740-1745.

114. Sprague EA, Luo J, Palmaz JC. Endothelial Cell Migration onto Metal Stent Surfaces under Static and Flow Conditions. Journal of Long-Term Effects of Medical Implants 2000;10(1-2):97-110.

115. Frank AO, Walsh PW, Moore JE. Computational Fluid Dynamics and Stent Design. Artificial Organs 2002;26(7):614-621.

116. Frangos JA, Huang TY, Clark CB. Steady Shear and Step Changes in Shear Stimulate Endothelium Via Independent Mechanisms - Superposition of Transient and Sustained Nitric Oxide Production. Biochemical and Biophysical Research Communications 1996;224(3):660-665.

117. White CR, Haidekker M, Bao X, Frangos JA. Temporal Gradients in Shear, but Not Spatial Gradients, Stimulate Endothelial Cell Proliferation. Circulation 2001;103(20):2508-2513.

118. Bao XP, Lu CY, Frangos JA. Temporal Gradient in Shear but Not Steady Shear Stress Induces Pdgf-a and Mcp-1 Expression in Endothelial Cells - Role of No, Nf Kappa B, and Egr-1. Arteriosclerosis Thrombosis and Vascular Biology 1999;19(4):996-1003.

119. Lietz K, Miller LW. Destination Therapy: Current Results and Future Promise. Seminars in thoracic and cardiovascular surgery 2008;20(3):225-33.

120. Selgrade BP, Truskey GA. Computational Fluid Dynamics Analysis to Determine Shear Stresses and Rates in a Centrifugal Left Ventricular Assist Device. Artificial Organs 2012:E89-E96.

121. Achneck HE, Sileshi B, Parikh A, Milano CA, Welsby IJ, Lawson JH. Pathophysiology of Bleeding and Clotting in the Cardiac Surgery Patient from Vascular Endothelium to Circulatory Assist Device Surface. Circulation 2010;122(20):2068-2077.

122. Schillinger M, Sabeti S, Dick P, Amighi J, Mlekusch W, Schlager O, Loewe C, Cejna M, Lammer J, Minar E. Sustained Benefit at 2 Years of Primary

Femoropopliteal Stenting Compared with Balloon Angioplasty with Optional Stenting. Circulation 2007;115(21):2745-2749.

123. Maleux G, Marrannes J, Heye S, Daenens K, Verhamme P, Thijs V. Outcome of Carotid Artery Stenting at 2 Years Follow-Up: Comparison of Nitinol Open Cell Versus Stainless Steel Closed Cell Stent Design. Journal of Cardiovascular Surgery 2009;50(5):669-675.

124. Dick P, Wallner H, Sabeti S, Loewe C, Mlekusch W, Lammer J, Koppensteiner R, Minar E, Schillinger M. Balloon Angioplasty Versus Stenting with Nitinol Stents in Intermediate Length Superficial Femoral Artery Lesions. Catheterization and Cardiovascular Interventions 2009;74(7):1090-1095.

125. Slottow TLP, Waksman R. Drug-Eluting Stent Safety. American Journal of Cardiology 2007;100(8B):10M-17M.

126. Achneck HE, Jamiolkowski RM, Jantzen AE, Haseltine JM, Lane WO, Huang JK, Galinat LJ, Serpe MJ, Lin F-H, Li M and others. The Biocompatibility of Titanium Cardiovascular Devices Seeded with Autologous Blood-Derived Endothelial Progenitor Cells Epc-Seeded Antithrombotic Ti Implants. Biomaterials 2011;32(1):10-18.

127. Velik-Salchner C, Schnurer C, Fries D, Mussigang PR, Moser PL, Streif W, Kolbitsch C, Lorenz IH. Normal Values for Thrombelastography (Rotem (R)) and Selected Coagulation Parameters in Porcine Blood. Thrombosis Research 2006;117(5):597-602.

128. Kang C, Bonneau M, Brouland JP, Sollier CBD, Drouet L. In Vivo Pig Models of Venous Thrombosis Mimicking Human Disease. Thrombosis and Haemostasis 2003;89(2):256-263.

129. Dal Nogare AR, Toews GB. Characteristics of Alveolar Macrophages in an Animal Model of Resolving Pulmonary Inflammation. American Review of Respiratory Disease 1990;142(3):660-667.

130. Ueberrueck T, Tautenhahn J, Meyer L, Kaufmann O, Lippert H, Gastinger I, Wahlers T. Comparison of the Ovine and Porcine Animal Models for Biocompatibility Testing of Vascular Prostheses. Journal of Surgical Research 2005;124(2):305-311.

131. Achneck HE, Serpe MJ, Jamiolkowski RM, Eibest LM, Craig SL, Lawson JH. Regenerating Titanium Ventricular Assist Device Surfaces after Gold/Palladium Coating for Scanning Electron Microscopy. Microscopy Research and Technique 2010;73(1):71-76.

132. DeGarmo P, Black J, Kohser R. Materials and Processes in Manufacturing. 9th Ed. Wiley 2003;223.

133. Seldinger SI. Catheter Replacement of the Needle in Percutaneous Arteriography: A New Technique. Acta Radiologica [Old Series] 1953;39(5):368-376.

134. Truskey GA, Yuan F, Katz DF. Transport Phenomena in Biological Systems. Upper Saddle River, N.J.: Pearson/Prentice Hall; 2009.

135. Raymond MA, Smith ER, Liesegang J. The Physical Properties of Blood - Forensic Considerations. Science & Justice 1996;36(3):153-160.

136. Jantzen AE, Lane WO, Gage SM, Jamiolkowski RM, Haseltine JM, Galinat LJ, Lin F-H, Lawson JH, Truskey GA, Achneck HE. Use of Autologous Blood-Derived Endothelial Progenitor Cells at Point-of-Care to Protect against Implant Thrombosis in a Large Animal Model. Biomaterials 2011;32(33):8356-8363.

137. Wegener J, Janshoff A, Galla HJ. Cell Adhesion Monitoring Using a Quartz Crystal Microbalance: Comparative Analysis of Different Mammalian Cell Lines. European Biophysics Journal with Biophysics Letters 1998;28(1):26-37.

138. Rameis M-T, Cei S, Bernardi J, Watzek G, Gruber R. Development of an in Vitro Model on Cellular Adhesion on Granular Natural Bone Mineral under Dynamic Seeding Conditions - a Pilot Study. Journal of Biomedical Materials Research Part B-Applied Biomaterials 2009;91B(2):766-771.

139. Fisher RA. Statistical Methods for Research Workers. 10th Edn. Revised & Enlarged; 1946. 1-354 p.

140. Moulder J, Stickle W, Sobol P, editors. Handbook of X Ray Photoelectron Spectroscopy (P/N 624755). Perkin-Elmer, Physical Electronics Division;; 1992.

141. Samaroo HD, Lu J, Webster TJ. Enhanced Endothelial Cell Density on Niti Surfaces with Sub-Macron to Nanometer Roughness. International Journal of Nanomedicine 2008;3(1):75-82.

142. Nappo F, Esposito K, Cioffi M, Giugliano G, Molinari AM, Paolisso G, Marfella R, Giugliano D. Postprandial Endothelial Activation in Healthy Subjects and in Type 2 Diabetic Patients: Role of Fat and Carbohydrate Meals. Journal of the American College of Cardiology 2002;39(7):1145-1150.

143. Li H, Cybulsky MI, Gimbrone MA, Libby P. An Atherogenic Diet Rapidly Induces Vcam-1, a Cytokine-Regulatable Mononuclear Leukocyte Adhesion Molecule, in Rabbit Aortic Endothelium. Arteriosclerosis and Thrombosis 1993;13(2):197-204.

144. Rashid ST, Salacinski HJ, Hamilton G, Seifalian AM. The Use of Animal Models in Developing the Discipline of Cardiovascular Tissue Engineering: A Review. Biomaterials 2004;25(9):1627-1637.

145. Achneck HE, Sileshi B, Lawson JH. Review of the Biology of Bleeding and Clotting in the Surgical Patient. Vascular 2008;16:S6-S13.

146. Jaffer AK, Barsoum WK, Krebs V, Hurbanek JG, Morra N, Brotman DJ. Duration of Anesthesia and Venous Thromboembolism after Hip and Knee Arthroplasty. Mayo Clinic Proceedings 2005;80(6):732-738.

147. Ellsworth WA, Basu CB, Iverson RE. Perioperative Considerations for Patient Safety During Cosmetic Surgery - Preventing Complications. Canadian Journal of Plastic Surgery 2009;17(1):9-16.

148. Forbes TJ, Rosenthal GL, Reul GR, Ott DA, Feltes TF. Risk Factors for Life-Threatening Cavopulmonary Thrombosis in Patients Undergoing Bidirectional Superior Cavopulmonary Shunt: An Exploratory Study. American Heart Journal 1997;134(5):865-871.

149. Zhao T, Zhang Z-N, Rong Z, Xu Y. Immunogenicity of Induced Pluripotent Stem Cells. Nature 2011;474(7350):212-U251.

150. Hsiao H-M, Chiu Y-H, Lee K-H, Lin C-H. Computational Modeling of Effects of Intravascular Stent Design on Key Mechanical and Hemodynamic Behavior. Computer-Aided Design 2012;44(8):757-765.

151. Hyre M, Pulliam R, Squire J. Modeling Stent Expansion Dynamics and Blood Flow Patterns in a Stenotic Artery. Modelling in Medicine and Biology 2011:115.

152. McVeigh GE, Burns DE, Johnston GD, Finkelstein SM, Cohn JN. Reduced Arterial Vascular Compliance as a Marker for Essential-Hypertension. British Journal of Clinical Pharmacology 1990;29(5):P587-P587.

153. Gundert TJ, Shadden SC, Williams AR, Koo B-K, Feinstein JA, LaDisa JF, Jr. A Rapid and Computationally Inexpensive Method to Virtually Implant Current and Next-Generation Stents into Subject-Specific Computational Fluid Dynamics Models. Annals of Biomedical Engineering 2011;39(5):1423-1437.

154. Ku DN, Giddens DP, Zarins CK, Glagov S. Pulsatile Flow and Atherosclerosis in the Human Carotid Bifurcation Positive Correlation between Plaque Location and Low and Oscillating Shear Stress. Arteriosclerosis 1985;5(3):293-302.

155. Augst AD, Ariff B, Thom SAGM, Xu XY, Hughes AD. Analysis of Complex Flow and the Relationship between Blood Pressure, Wall Shear Stress, and Intima-Media Thickness in the Human Carotid Artery. American Journal of Physiology-Heart and Circulatory Physiology 2007;293(2):H1031-H1037.

156. Holdsworth DW, Norley CJD, Frayne R, Steinman DA, Rutt BK. Characterization of Common Carotid Artery Blood-Flow Waveforms in Normal Human Subjects. Physiological Measurement 1999;20(3):219-240.

157. Masuda M, Emoto T, Suzuki A, Akutagawa M, Kitawaki T, Kitaoka K, Tanaka H, Obara S, Yoshizaki K, Konaka S and others. Evaluation of Blood Flow Velocity Waveform in Common Carotid Artery Using Multi-Branched Arterial Segment Model of Human Arteries. Biomedical Signal Processing and Control 2013;8(6):509-519.

158. Weissler AM, Peeler RG, Roehll WH. Relationships between Left Ventricular Ejection Time, Stroke Volume, and Heart Rate in Normal Individuals and Patients with Cardiovascular Disease. American Heart Journal 1961;62(3):367-378.

159. Gelfand BD, Epstein FH, Blackman BR. Spatial and Spectral Heterogeneity of Time-Varying Shear Stress Profiles in the Carotid Bifurcation by Phase-Contrast. Journal of Magnetic Resonance Imaging 2006;24(6):1386-1392.

160. Avolio AP, Deng FQ, Li WQ, Luo YF, Huang ZD, Xing LF, Orourke MF. Effects of Aging on Arterial Distensibility in Populations with High and Low Prevalence of Hypertension - Comparison between Urban and Rural Communities in China. Circulation 1985;71(2):202-210.

161. Vaitkevicius PV, Fleg JL, Engel JH, Oconnor FC, Wright JG, Lakatta LE, Yin FCP, Lakatta EG. Effects of Age and Aerobic Capacity on Arterial Stiffness in Healthy-Adults. Circulation 1993;88(4):1456-1462.

162. Pearson AC, Guo RQ, Orsinelli DA, Binkley PF, Pasierski TJ. Transesophageal Echocardiographic Assessment of the Effects of Age, Gender, and Hypertension on Thoracic Aortic-Wall Size, Thickness, and Stiffness. American Heart Journal 1994;128(2):344-351.

163. Feaver RE, Gelfand BD, Blackman BR. Human Haemodynamic Frequency Harmonics Regulate the Inflammatory Phenotype of Vascular Endothelial Cells. Nature Communications 2013;4.

164. Dolan JM, Sim FJ, Meng H, Kolega J. Endothelial Cells Express a Unique Transcriptional Profile under Very High Wall Shear Stress Known to Induce Expansive Arterial Remodeling. American Journal of Physiology-Cell Physiology 2012;302(8):C1109-C1118.

165. Chiu J-J, Chien S. Effects of Disturbed Flow on Vascular Endothelium: Pathophysiological Basis and Clinical Perspectives. Physiological Reviews 2011;91(1):327-387.

166. Brooks AR, Lelkes PI, Rubanyi GM. Gene Expression Profiling of Human Aortic Endothelial Cells Exposed to Disturbed Flow and Steady Laminar Flow. Physiological Genomics 2002;9(1):27-41.

167. Hsiai TK, Cho SK, Reddy S, Hama S, Navab M, Demer LL, Honda HM, Ho CM. Pulsatile Flow Regulates Monocyte Adhesion to Oxidized Lipid-Induced Endothelial Cells. Arteriosclerosis Thrombosis and Vascular Biology 2001;21(11):1770-1776.

168. Thomas JA, Deaton RA, Hastings NE, Shang Y, Moehle CW, Eriksson U, Topouzis S, Wamhoff BR, Blackman BR, Owens GK. Pdgf-Dd, a Novel Mediator of Smooth Muscle Cell Phenotypic Modulation, Is Upregulated in Endothelial

Cells Exposed to Atherosclerosis-Prone Flow Patterns. American Journal of Physiology-Heart and Circulatory Physiology 2009;296(2):H442-H452.

169. Zhao SZ, Xu XY, Hughes AD, Thom SA, Stanton AV, Ariff B, Long Q. Blood Flow and Vessel Mechanics in a Physiologically Realistic Model of a Human Carotid Arterial Bifurcation. Journal of Biomechanics 2000;33(8):975-984.

170. Nagai Y, Helwegen J, Fleg JL, Beemer MK, Earley CJ, Metter EJ. Associations of Aortic Windkessel Function with Age, Gender and Cardiovascular Risk Factors. Ultrasound in medicine & biology 2001;27(9):1207-1210.

171. Wu T-Y, Chou H-H, Chang S-H, Tsai Y-J, Hsieh C-A, Cheng S-T, Yeh K-H, Chang H-J, Ko Y-L, Huang H-L. Comparison of Immediate and 2-Year Outcomes between Excimer Laser-Assisted Angioplasty with Spot Stent and Primary Stenting in Intermediate to Long Femoropopliteal Disease. Scientific World Journal 2013.

172. Finn AV, Joner M, Nakazawa G, Kolodgie F, Newell J, John MC, Gold HK, Virmani R. Pathological Correlates of Late Drug-Eluting Stent Thrombosis - Strut Coverage as a Marker of Endothelialization. Circulation 2007;115(18):2435-2441.

173. Farb A, Burke AP, Kolodgie FD, Virmani R. Pathological Mechanisms of Fatal Late Coronary Stent Thrombosis in Humans. Circulation 2003;108(14):1701-1706.

174. O'Riordan M. Medscape. First Bioabsorbable Stent Approved in Europe. http://www.medscape.com/viewarticle/735561. Accessed March 3, 2014.

175. Granada JF, Inami S, Aboodi MS, Tellez A, Milewski K, Wallace-Bradley D, Parker S, Rowland S, Nakazawa G, Vorpahl M and others. Development of a Novel Prohealing Stent Designed to Deliver Sirolimus from a Biodegradable Abluminal Matrix / Clinical Perspective. Circulation: Cardiovascular Interventions 2010;3(3):257-266.

176. Ichikawa M, Yutani C, Hayashi T, Nakata T, Iwata A, Lim Y-J, Mishima M. Angioscopic Findings of Delayed Healing at Sites of Sirolimus-Eluting Stent Overlap after 21-Month Implantation. International Journal of Cardiology 2008;129(1):E10-E11.

177. van Beusekom HMM, Saia F, Zindler JD, Lemos PA, Hoor SLS-t, Leeuwen MAHv, de Feijter PJ, Serruys PW, van der Giessen WJ. Drug-Eluting Stents Show

Delayed Healing: Paclitaxel More Pronounced Than Sirolimus. European Heart Journal 2007;28(8):974-979.

178. Rodriguez AE, Rodriguez-Granillo GA, Palacios IF. Late Stent Thrombosis: The Damocle's Sword of Drug Eluting Stents? EuroIntervention : journal of EuroPCR in collaboration with the Working Group on Interventional Cardiology of the European Society of Cardiology 2007;2(4):512-7.

179. Luescher TF, Steffel J, Eberli FR, Joner M, Nakazawa G, Tanner FC, Virmani R. Drug-Eluting Stent and Coronary Thrombosis - Biological Mechanisms and Clinical Implications. Circulation 2007;115(8):1051-1058.

180. Grumann T, Diehl P, Bode C, Moser M. Is Stent Thrombosis the New Achilles Heel of Interventional Cardiology? State of the Art Clinical Trials, Causes and Approaches for Prevention. Hamostaseologie 2007;27(5):344-50.

181. Hofma SH, van der Giessen WJ, van Dalen BM, Lemos PA, McFadden EP, Sianos G, Ligthart JMR, van Essen D, de Feyter PJ, Serruys PW. Indication of Long-Term Endothelial Dysfunction after Sirolimus-Eluting Stent Implantation. European Heart Journal 2006;27(2):166-170.

182. Togni M, Raber L, Cocchia R, Wenaweser P, Cook S, Windecker S, Meier B, Hess OM. Local Vascular Dysfunction after Coronary Paclitaxel-Eluting Stent Implantation. International Journal of Cardiology 2007;120(2):212-220.

183. Joner M, Finn AV, Farb A, Mont EK, Kolodgie FD, Ladich E, Kutys R, Skorija K, Gold HK, Virmani R. Pathology of Drug-Eluting Stents in Humans - Delayed Healing and Late Thrombotic Risk. Journal of the American College of Cardiology 2006;48(1):193-202.

184. Tura O, Skinner EM, Barclay GR, Samuel K, Gallagher RCJ, Brittan M, Hadoke PWF, Newby DE, Turner ML, Mills NL. Late Outgrowth Endothelial Cells Resemble Mature Endothelial Cells and Are Not Derived from Bone Marrow. Stem Cells 2013;31(2):338-348.

185. Truskey GA, Yuan F, Katz DF. Transport Phenomena in Biological Systems. In: MJ H, editor. Upper Saddle River, N.J.: Pearson/Prentice Hall; 2009.

186. Lauer T, Preik M, Rassaf T, Strauer BE, Deussen A, Feelisch M, Kelm M. Plasma Nitrite Rather Than Nitrate Reflects Regional Endothelial Nitric Oxide Synthase

Activity but Lacks Intrinsic Vasodilator Action. Proceedings of the National Academy of Sciences 2001;98(22):12814-12819.

187. Wallace CS, Strike SA, Truskey GA. Smooth Muscle Cell Rigidity and Extracellular Matrix Organization Influence Endothelial Cell Spreading and Adhesion Formation in Coculture. American Journal of Physiology-Heart and Circulatory Physiology 2007;293(3):H1978-H1986.

188. Livak KJ, Schmittgen TD. Analysis of Relative Gene Expression Data Using Real-Time Quantitative Pcr and the 2(T)(-Delta Delta C) Method. Methods 2001;25(4):402-408.

189. Jantzen AE, Achneck HE, Truskey GA. Surface Projections of Titanium Substrates Increase Antithrombotic Endothelial Function in Response to Shear Stress. Journal of Biomedical Materials Research Part A 2013;101(11):3181-3191.

190. Perez de Prado A, Perez-Martinez C, Cuellas-Ramon C, Manuel Gonzalo-Orden J, Regueiro-Purrinos M, Martinez B, Garcia-Iglesias MJ, Ajenjo JM, Altonaga JR, Diego-Nieto A and others. Time Course of Reendothelialization of Stents in a Normal Coronary Swine Model: Characterization and Quantification. Veterinary Pathology 2011;48(6):1109-1117.

191. Kang S, Carlon T, Jantzen A, Lin F-H, Ley M, Allen J, Stabler T, Haley NR, Truskey G, Achneck H. Isolation of Functional Human Endothelial Cells from Small Volumes of Umbilical Cord Blood. Annals of Biomedical Engineering 2013;41(10):2181-2192.

Biography

Alexandra Elizabeth Jantzen was born on August 7, 1984 in Louisville, KY to Charles and Margaret Jantzen. Alexandra received her Bachelor of Science degree in Biomedical Engineering from Rose-Hulman Institute of Technology in Terre Haute, IN in May of 2006. Shortly after graduating from Rose-Hulman, Alexandra relocated to Bloomington, IN and worked for several years in product development of vascular stents at Cook Medical. Her work led to multiple product launches and several published patents and patent applications. Alexandra left to pursue her graduate studies at Duke University in August 2009. While at Duke, Alexandra received the National Science Foundation Graduate Research Fellowship, James B. Duke Fellowship, and American Heart Association Predoctoral Research Fellowship. Alexandra received her Master of Science degree in Biomedical Engineering from Duke University in 2012. In 2014, Alexandra completed the Certificate in Biomolecular and Tissue Engineering at Duke. Her publications include:

Alexandra E. Jantzen, Hardean E. Achneck, George A. Truskey, Calculated Shear Stresses on Implanted Carotid Stent Surfaces Are Conducive to Endothelial Cell Seeding and Retention. (submitted to Journal of Biomechanics, March 2014).

Alexandra E. Jantzen, Katherine M. Baker, James S. Mills, Fu-Hsiung Lin, George A. Truskey, Hardean E. Achneck. Point-of-Care Seeding of Nitinol Stents with Blood-Derived Endothelial Cells. (submitted to Circulation, March 2014).

Alexandra E. Jantzen, Hardean E. Achneck, George A. Truskey. Surface Projections of Titanium Substrates Increase Antithrombotic Endothelial Function in Response to Shear Stress. Journal of Biomedical Materials: Part A, 2013. 101(11): p.3181-3191.

Sa Do Kang, Tim A. Carlon, Alexandra E. Jantzen, Fu-Hsiung Lin, M. Ley, Jason D. Allen, Thomas V. Stabler, Nancy Rebecca Haley, George A. Truskey, Hardean E. Achneck. Isolation of Functional Human Endothelial Cells from Small Volumes of Umbilical Cord Blood. Annals of Biomedical Engineering, 2013. 41(10): p.2181-2192.

Alexandra E. Jantzen, Whitney O. Lane, Shawn M. Gage, Ryan M. Jamiolkowski, Justin M. Haseltine, Lauren J. Galinat, Fu-Hsiung Lin, Jeffrey H. Lawson, George A. Truskey, Hardean E. Achneck. . Use of autologous blood-derived endothelial progenitor cells at point-of-care to protect against implant thrombosis in a large animal model. Biomaterials, 2011. 32(33): p. 8356-63.

Alexandra E. Jantzen, Whitney O. Lane, Shawn M. Gage, Justin M. Haseltine, Lauren J. Galinat, Ryan M. Jamiolkowski, Fu-Hsiung Lin, George A. Truskey, Hardean E. Achneck. Autologous Endothelial Progenitor Cell-Seeding Technology and Biocompatibility Testing For Cardiovascular Devices in Large Animal Model. Journal of Visualized Experiments, 2011: 3197.

Hardean E. Achneck, Ryan M. Jamiolkowski, Alexandra E. Jantzen, Justin M. Haseltine, Whitney O. Lane, Jessica K. Huang, Lauren J. Galinat, Michael J. Serpe, Fu-Hsiung Lin, Madison Li, Amar Parikh, Liqiao Ma, Tao Chen, Bantayehu Sileshi, Carmelo A. Milano, Charles S. Wallace, Thomas V. Stabler, Jason D. Allen, George A. Truskey, Jeffrey H. Lawson. The biocompatibility of titanium cardiovascular devices seeded with autologous blood-derived endothelial progenitor cells: EPC-seeded antithrombotic Ti Implants. Biomaterials, 2011. 32(1): p. 10-18.

1. Lloyd-Jones D, Adams RJ, Brown TM, Carnethon M, Dai S, De Simone G, Ferguson TB, Ford E, Furie K, Gillespie C and others. Heart Disease and Stroke Statistics—2010 Update. Circulation 2010;121(7):e46-e215.

2. Go AS, Mozaffarian D, Roger VL, Benjamin EJ, Berry JD, Blaha MJ, Dai S, Ford ES, Fox CS, Franco S and others. Heart Disease and Stroke Statistics-2014 Update a Report from the American Heart Association. Circulation 2014;129(3):E28-E292.

3. Michael TT, Abdel-karim A-rR, Papayannis A, Lichtenwalter C, de Lemos JA, Obel O, Addo T, Roesle M, Haagen D, Rangan BV and others. Recurrent Cardiovascular Events with Paclitaxel-Eluting Versus Bare-Metal Stents in

Saphenous Vein Graft Lesions: Insights from the Sos (Stenting of Saphenous Vein Grafts) Trial. Journal of Invasive Cardiology 2011;23(6):216-219.

4. The Sage Group. New Estimates for Prevalence of Peripheral Artery Disease (Pad) in U.S. http://heartheavy.com/new-estimates-for-prevalence-of-peripheral-artery-disease-pad-in-u-s/. Accessed 08 Nov 2011.

5. Highland Capital Partners. Pervasis to Present Interim Data from Phase 1/2 Clinical Study of Novel Cell Therapy Targeting Peripheral Artery Disease at International Conference on Cell Therapy for Cardiovascular Diseases. http://www.hcp.com/news/newsdetails.php/id/87812. Accessed April 27, 2012.

6. Kroger K, Buss C, Goyen M, Santosa F, Rudofsky G. Diameter of Occluded Superficial Femoral Arteries Limits Percutaneous Recanalization: Preliminary Results. Journal of Endovascular Therapy 2002;9(3):369-374.

7. Duda SH, Bosiers M, Lammer J, Scheinert D, Zeller T, Oliva V, Tielbeek A, Anderson J, Wiesinger B, Tepe G and others. Drug-Eluting and Bare Nitinol Stents for the Treatment of Atherosclerotic Lesions in the Superficial Femoral Artery: Long-Term Results from the Sirocco Trial. Journal of Endovascular Therapy 2006;13(6):701-710.

8. Chorny M, Fishbein I, Yellen BB, Alferiev IS, Bakay M, Ganta S, Adamo R, Amiji M, Friedman G, Levy RJ. Targeting Stents with Local Delivery of Paclitaxel-Loaded Magnetic Nanoparticles Using Uniform Fields. Proceedings of the National Academy of Sciences of the United States of America 2010;107(18):8346-8351.

9. Polyak B, Fishbein I, Chorny M, Alferiev I, Williams D, Yellen B, Friedman G, Levy RJ. High Field Gradient Targeting of Magnetic Nanoparticle-Loaded Endothelial Cells to the Surfaces of Steed Stents. Proceedings of the National Academy of Sciences of the United States of America 2008;105(2):698-703.

10. Stoeckel D, Pelton A, Duerig T. Self-Expanding Nitinol Stents: Material and Design Considerations. European Radiology 2004;14(2):292-301.

11. Lloyd-Jones DM, Larson MG, Beiser A, Levy D. Lifetime Risk of Developing Coronary Heart Disease. Lancet 1999;353(9147):89-92.

12. Auerbach D, Meada JL, Steiner C. Hospital Stays with Cardiac Stents, 2009; Statistical Brief #128. Healthcare Cost and Utilization Project 2012.

13. Lee TH, Hillis LD, Nabel EG. Cabg Vs. Stenting--Clinical Implications of the Syntax Trial. The New England journal of medicine 2009;360(8):e10.

14. Buszman PE, Kiesz SR, Bochenek A, Peszek-Przybyla E, Szkrobka I, Debinski M, Bialkowska B, Dudek D, Gruszka A, Zurakowski A and others. Acute and Late Outcomes of Unprotected Left Main Stenting in Comparison with Surgical Revascularization. Journal of the American College of Cardiology 2008;51(5):538-545.

15. Brilakis ES, Lichtenwalter C, Abdel-karim A-rR, de Lemos JA, Obel O, Addo T, Roesle M, Haagen D, Rangan BV, Saeed B and others. Continued Benefit from Paclitaxel-Eluting Compared with Bare-Metal Stent Implantation in Saphenous Vein Graft Lesions During Long-Term Follow-up of the Sos (Stenting of Saphenous Vein Grafts) Trial. Jacc-Cardiovascular Interventions 2011;4(2):176-182.

16. Pfisterer M, Brunner-La Rocca HP, Rickenbacher P, Hunziker P, Mueller C, Nietlispach F, Leibundgut G, Bader F, Kaiser C, Investigators B. Long-Term Benefit-Risk Balance of Drug-Eluting Vs. Bare-Metal Stents in Daily Practice: Does Stent Diameter Matter? Three-Year Follow-up of Basket. European Heart Journal 2009;30(1):16-24.

17. Kauffman GB, Mayo I. The Story of Nitinol: The Serendipitous Discovery of the Memory Metal and Its Applications. The Chemical Educator 1997;2(2):1-21.

18. Duerig T, Pelton A, Stockel D. An Overview of Nitinol Medical Applications. Materials Science and Engineering a-Structural Materials Properties Microstructure and Processing 1999;273:149-160.

19. Lombardi S, Poncet P. Metallurgical Principles of Nitinol and Its Use in Interventional Devices. Controversies and Consensus in Imaging and Intervention (C2I2) 2004((Autumn):24-26.

20. Vogel TR, Shindelman LE, Nackman GB, Graham AM. Efficacious Use of Nitinol Stents in the Femoral and Popliteal Arteries. Journal of Vascular Surgery 2003;38(6):1178-1183.

21. Smouse HB, Nikanorov A, LaFlash D. Biomechanical Forces in the Femoropopliteal Arterial Segment. Endovascular Today 2005;4(6):60-66.

22. Amoroso G, Geuns R-Jv, Spaulding C, Manzo-Silberman S, Hauptmann KE, Spaargaren R, Garcia-Garcia HM, Serruys PW, Verheye S. Assessment of the Safety and Performance of the Stentys Self-Expanding Coronary Stent in Acute Myocardial Infarction: Results from the Apposition I Study. EuroIntervention 2011;7(4):428-436.

23. Giacchi G, La Manna A, Tamburino C, Capodanno D, Capranzano P. Self-Apposing Stentys® Stent in Acute Myocardial Infarction. Minerva cardioangiologica 2014;62(1):59-70.

24. Plant SD, Grant DM, Leach L. Behaviour of Human Endothelial Cells on Surface Modified Niti Alloy. Biomaterials 2005;26(26):5359-5367.

25. Trepanier C, Tabrizian M, Yahia L, Bilodeau L, Piron DL. Effect of Modification of Oxide Layer on Niti Stent Corrosion Resistance. Journal of Biomedical Materials Research 1998;43(4):433-440.

26. Achneck HE, Jamiolkowski RM, Jantzen AE, Haseltine JM, Lane WO, Huang JK, Galinat LJ, Serpe MJ, Lin FH, Li M and others. The Biocompatibility of Titanium Cardiovascular Devices Seeded with Autologous Blood-Derived Endothelial Progenitor Cells Epc-Seeded Antithrombotic Ti Implants. Biomaterials 2011;32(1):10-18.

27. Jantzen AE, Lane WO, Gage SM, Jamiolkowski RM, Haseltine JM, Galinat LJ, Lin F-H, Lawson JH, Truskey GA, Achneck HE. Use of Autologous Blood-Derived Endothelial Progenitor Cells at Point-of-Care to Protect against Implant Thrombosis in a Large Animal Model. Biomaterials 2011;32(33):8356-63.

28. Minar E, Pokrajac B, Maca T, Ahmadi R, Fellner C, Mittlbock M, Seitz W, Wolfram R, Potter R. Endovascular Brachytherapy for Prophylaxis of Restenosis after Femoropopliteal Angioplasty - Results of a Prospective Randomized Study. Circulation 2000;102(22):2694-2699.

29. Dormandy JA, Rutherford RB. Management of Peripheral Arterial Disease (Pad). Tasc Working Group. Transatlantic Inter-Society Consensus (Tasc). Journal of vascular surgery : official publication, the Society for Vascular Surgery [and]

International Society for Cardiovascular Surgery, North American Chapter 2000;31(1 Pt 2):S1-S296.

30. Johnston KW. Femoral and Popliteal Arteries - Reanalysis of Results of Balloon Angioplasty. Radiology 1992;183(3):767-771.

31. Capek P, McLean GK, Berkowitz HD. Femoropopliteal Angioplasty - Factors Influencing Long-Term Success. Circulation 1991;83(2):70-80.

32. Duda SH, Bosiers M, Lammer J, Scheinert D, Zeller T, Tielbeek A, Anderson J, Wiesinger B, Tepe G, Lansky A and others. Sirolimus-Eluting Versus Bare Nitinol Stent for Obstructive Superficial Femoral Artery Disease: The Sirocco Ii Trial. Journal of Vascular and Interventional Radiology 2005;16(3):331-338.

33. Dake MD, Ansel GM, Jaff MR, Ohki T, Saxon RR, Smouse HB, Zeller T, Roubin GS, Burket MW, Khatib Y and others. Paclitaxel-Eluting Stents Show Superiority to Balloon Angioplasty and Bare Metal Stents in Femoropopliteal Disease Twelve-Month Zilver Ptx Randomized Study Results. Circulation-Cardiovascular Interventions 2011;4(5):495-504.

34. Schuhlen H, Kastrati A, Mehilli J, Hausleiter J, Pache J, Dirschinger J, Schomig A. Restenosis Detected by Routine Angiographic Follow-up and Late Mortality after Coronary Stent Placement. American Heart Journal 2004;147(2):317-322.

35. Elezi S, Kastrati A, Hadamitzky M, Dirschinger J, Neumann FJ, Schomig A. Clinical and Angiographic Follow-up after Balloon Angioplasty with Provisional Stenting for Coronary in-Stent Restenosis. Catheterization and Cardiovascular Interventions 1999;48(2):151-156.

36. Kastrati A, Mehilli J, Dirschinger J, Pache J, Ulm K, Schuhlen H, Seyfarth M, Schmitt C, Blasini R, Neumann FJ and others. Restenosis after Coronary Placement of Various Stent Types. American Journal of Cardiology 2001;87(1):34-39.

37. Pfisterer M, Brunner-La Rocca HP, Buser PT, Rickenbacher P, Hunziker P, Mueller C, Jeger R, Bader F, Osswald S, Kaiser C and others. Late Clinical Events after Clopidogrel Discontinuation May Limit the Benefit of Drug-Eluting Stents - an Observational Study of Drug-Eluting Versus Bare-Metal Stents. Journal of the American College of Cardiology 2006;48(12):2584-2591.

38. Moses JW, Leon MB, Popma JJ, Fitzgerald PJ, Holmes DR, O'Shaughnessy C, Caputo RP, Kereiakes DJ, Williams DO, Teirstein PS and others. Sirolimus-Eluting Stents Versus Standard Stents in Patients with Stenosis in a Native Coronary Artery. New England Journal of Medicine 2003;349(14):1315-1323.

39. Venkatraman S, Boey F. Release Profiles in Drug-Eluting Stents: Issues and Uncertainties. Journal of Controlled Release 2007;120(3):149-160.

40. McFadden EP, Stabile E, Regar E, Cheneau E, Ong ATL, Kinnaird T, Suddath WO, Weissman NJ, Torguson R, Kent KM and others. Late Thrombosis in Drug-Eluting Coronary Stents after Discontinuation of Antiplatelet Therapy. The Lancet;364(9444):1519-1521.

41. Cragg GM, Newman DJ. Plants as a Source of Anti-Cancer Agents. Journal of Ethnopharmacology 2005;100(1-2):72-79.

42. Groth CG, Backman L, Morales JM, Calne R, Kreis H, Lang P, Touraine JL, Claesson K, Campistol JM, Durand D and others. Sirolimus (Rapamycin)-Based Therapy in Human Renal Transplantation - Similar Efficacy and Different Toxicity Compared with Cyclosporine. Transplantation 1999;67(7):1036-1042.

43. Campistol JM, Eris J, Oberbauer R, Friend P, Hutchison B, Morales JM, Claesson K, Stallone G, Russ G, Rostaing L and others. Sirolimus Therapy after Early Cyclosporine Withdrawal Reduces the Risk for Cancer in Adult Renal Transplantation. Journal of the American Society of Nephrology 2006;17(2):581-589.

44. Falotico R, Zhao J. Polymers and Drug-Eluting Stents. Textbook of Interventional Cardiovascular Pharmacology 2007:289.

45. Virmani R, Guagliumi G, Farb A, Musumeci G, Grieco N, Motta T, Mihalcsik L, Tespili M, Valsecchi O, Kolodgie FD. Localized Hypersensitivity and Late Coronary Thrombosis Secondary to a Sirolimus-Eluting Stent Should We Be Cautious? Circulation 2004;109(6):701-705.

46. Nebeker JR, Virmani R, Bennett CL, Hoffman JM, Samore MH, Alvarez J, Davidson CJ, McKoy JM, Raisch DW, Whisenant BK and others. Hypersensitivity Cases Associated with Drug-Eluting Coronary Stents - a Review of Available Cases from the Research on Adverse Drug Events and Reports (Radar) Project. Journal of the American College of Cardiology 2006;47(1):175-181.

47. Finn AV, Nakazawa G, Joner M, Kolodgie FD, Mont EK, Gold HK, Virmani R. Vascular Responses to Drug Eluting Stents - Importance of Delayed Healing. Arteriosclerosis Thrombosis and Vascular Biology 2007;27(7):1500-1510.

48. Stone GW, Midei M, Newman W, Sanz M, Hermiller JB, Williams J, Farhat N, Mahaffey KW, Cutlip DE, Fitzgerald PJ and others. Comparison of an Everolimus-Eluting Stent and a Paclitaxel-Eluting Stent in Patients with Coronary Artery Disease - a Randomized Trial. Jama-Journal of the American Medical Association 2008;299(16):1903-1913.

49. Kandzari DE, Leon MB, Popma JJ, Fitzgerald PJ, O'Shaughnessy C, Ball MW, Turco M, Applegate RJ, Gurbel PA, Midei MG and others. Comparison of Zotarolimus-Eluting and Sirolimus-Eluting Stents in Patients with Native Coronary Artery Disease - a Randomized Controlled Trial. Journal of the American College of Cardiology 2006;48(12):2440-2447.

50. Meredith IT, Ormiston J, Whitbourn R, Kay IP, Muller D, Popma JJ, Cutlip DE, Fitzgerald PJ, Investigators EI. Four-Year Clinical Follow-up after Implantation of the Endeavor Zotarolimus-Eluting Stent: Endeavor I, the First-in-Human Study. American Journal of Cardiology 2007;100(8B):56M-61M.

51. Middleton JC, Tipton AJ. Synthetic Biodegradable Polymers as Orthopedic Devices. Biomaterials 2000;21(23):2335-2346.

52. Dake MD, Scheinert D, Tepe G, Tessarek J, Fanelli F, Bosiers M, Ruhlmann C, Kavteladze Z, Lottes AE, Ragheb AO and others. Nitinol Stents with Polymer-Free Paclitaxel Coating for Lesions in the Superficial Femoral and Popliteal Arteries above the Knee: Twelve-Month Safety and Effectiveness Results from the Zilver Ptx Single-Arm Clinical Study. Journal of Endovascular Therapy 2011;18(5):613-623.

53. Minami Y, Kaneda H, Inoue M, Ikutomi M, Morita T, Nakajima T. Endothelial Dysfunction Following Drug-Eluting Stent Implantation: A Systematic Review of the Literature. International Journal of Cardiology 2013;165(2):222-228.

54. Erbel R, Di Mario C, Bartunek J, Bonnier J, de Bruyne B, Eberli FR, Erne P, Haude M, Heublein B, Horrigan M and others. Temporary Scaffolding of Coronary Arteries with Bioabsorbable Magnesium Stents: A Prospective, Non-Randomised Multicentre Trial. The Lancet;369(9576):1869-1875.

55. Ormiston JA, Serruys PW, Regar E, Dudek D, Thuesen L, Webster MWI, Onuma Y, Garcia-Garcia HM, McGreevy R, Veldhof S. A Bioabsorbable Everolimus-Eluting Coronary Stent System for Patients with Single De-Novo Coronary Artery Lesions (Absorb): A Prospective Open-Label Trial. The Lancet;371(9616):899-907.

56. Serruys PW, Onuma Y, Dudek D, Smits PC, Koolen J, Chevalier B, de Bruyne B, Thuesen L, McClean D, van Geuns R-J and others. Evaluation of the Second Generation of a Bioresorbable Everolimus-Eluting Vascular Scaffold for the Treatment of De Novo Coronary Artery Stenosis 12-Month Clinical and Imaging Outcomes. Journal of the American College of Cardiology 2011;58(15):1578-1588.

57. Bezerra H, Chamie D, Kanaya T, Fujino Y, Kuang Y, Naimark W, Palasis M, Tanaka K, Attizzani G, Costa M. Serial Optical Coherence Tomography Morphometric Assessment of the Novel Stanza™ Bioresorbable Vascular Scaffold Implanted in Superficial Femoral Arteries in a Pre–Clinical Sheep Model. Journal of the American College of Cardiology 2013;61(10_S).

58. Karanasos A, van Geuns R-J, Zijlstra F, Regar E. Very Late Bioresorbable Scaffold Thrombosis after Discontinuation of Dual Antiplatelet Therapy. European Heart Journal 2014.

59. Sigwart U, Puel J, Mirkovitch V, Joffre F, Kappenberger L. Intravascular Stents to Prevent Occlusion and Restenosis after Trans-Luminal Angioplasty. New England Journal of Medicine 1987;316(12):701-706.

60. Baxter TJ, Bennett RC, Obrien BM, Henderso.Pn. Histopathology of Small Vessels Following Microvascular Repair. British Journal of Surgery 1972;59(8):617-&.

61. Zhu S, Malhotra A, Zhang L, Deng S, Zhang T, Freedman NJ, Storms R, Peppel K, Goldschmidt-Clermont PJ, Dong C. Human Umbilical Cord Blood Endothelial Progenitor Cells Decrease Vein Graft Neointimal Hyperplasia in Scid Mice. Atherosclerosis 2010;212(1):63-69.

62. Giessen WVd, Serruys P, Visser W, Verdouw P, Schalkwijk Wv, Jongkind J. Endothelialization of Intravascular Stents. Journal of Interventional Cardiology 1988;1:109-120.

63. Kutryk MJ, van Dortmont LM, de Crom RP, van der Kamp AW, Verdouw PD, van der Giessen WJ. Seeding of Intravascular Stents by the Xenotransplantation of Genetically Modified Endothelial Cells. Seminars in interventional cardiology : SIIC 1998;3(3-4):217-20.

64. Scott NA, Candal FJ, Robinson KA, Ades EW. Seeding of Intracoronary Stents with Immortalized Human Microvascular Endothelial-Cells. American Heart Journal 1995;129(5):860-866.

65. Zhu W, Tian Y, Zhou L-F, Wang Y, Song D, Mao Y, Yang G-Y. Development of a Novel Endothelial Cell-Seeded Endovascular Stent for Intracranial Aneurysm Therapy. Journal of Biomedical Materials Research Part A 2008;85A(3):715-721.

66. Shirota T, Yasui H, Shimokawa H, Matsuda T. Fabrication of Endothelial Progenitor Cell (Epc)-Seeded Intravascular Stent Devices and in Vitro Endothelialization on Hybrid Vascular Tissue. Biomaterials 2003;24(13):2295-2302.

67. Shi HJ, Cao AH, Teng GJ. Seeding Endothelial Progenitor Cells on a Self-Expanding Metal Stent: An in Vitro Study. Journal of Vascular and Interventional Radiology 2010;21(7):1061-1065.

68. Dichek DA, Neville RF, Zwiebel JA, Freeman SM, Leon MB, Anderson WF. Seeding of Intravascular Stents with Genetically Engineered Endothelial-Cells. Circulation 1989;80(5):1347-1353.

69. Fine E, Zhang L, Fenniri H, Webster TJ. Enhanced Endothelial Cell Functions on Rosette Nanotube-Coated Titanium Vascular Stents. International Journal of Nanomedicine 2009;4(1):91-97.

70. Wang GX, Deng XY, Tang CJ, Liu LS, Xiao L, Xiang LH, Quan XJ, Legrand AP, Guidoin R. The Adhesive Properties of Endothelial Cells on Endovascular Stent Coated by Substrates of Poly-L-Lysine and Fibronectin. Artificial Cells Blood Substitutes and Biotechnology 2006;34(1):11-25.

71. Flugelman MY, Virmani R, Leon MB, Bowman RL, Dichek DA. Genetically Engineered Endothelial-Cells Remain Adherent and Viable after Stent Deployment and Exposure to Flow Invitro. Circulation Research 1992;70(2):348-354.

72. Pislaru SV, Harbuzariu A, Gulati R, Witt T, Sandhu NP, Simari RD, Sandhu GS. Magnetically Targeted Endothelial Cell Localization in Stented Vessels. Journal of the American College of Cardiology 2006;48(9):1839-1845.

73. van Beusekom HMM, Ertas G, Sorop O, Serruys PW, van der Giessen WJ. The Genous (Tm) Endothelial Progenitor Cell Capture Stent Accelerates Stent Re-Endothelialization but Does Not Affect Intimal Hyperplasia in Porcine Coronary Arteries. Catheterization and Cardiovascular Interventions 2012;79(2):231-242.

74. Garg S, Duckers HJ, Serruys PW. Endothelial Progenitor Cell Capture Stents: Will This Technology Find Its Niche in Contemporary Practice? European Heart Journal 2010;31(9):1032-1035.

75. Simper D, Stalboerger PG, Panetta CJ, Wang SH, Caplice NM. Smooth Muscle Progenitor Cells in Human Blood. Circulation 2002;106(10):1199-1204.

76. Beijk MAM, Klomp M, van Geloven N, Koch KT, Henriques JPS, Baan J, Vis MM, Tijssen JGP, Piek JJ, de Winter RJ. Two-Year Follow-up of the Genous (Tm) Endothelial Progenitor Cell Capturing Stent Versus the Taxus Liberte Stent in Patients with De Novo Coronary Artery Lesions with a High-Risk of Restenosis: A Randomized, Single-Center, Pilot Study. Catheterization and Cardiovascular Interventions 2011;78(2):189-195.

77. Haude M, Lee SWL, Worthley SG, Silber S, Verheye S, Erbs S, Rosli MA, Botelho R, Meredith I, Sim KH and others. The Remedee Triala Randomized Comparison of a Combination Sirolimus-Eluting Endothelial Progenitor Cell Capture Stent with a Paclitaxel-Eluting Stent. JACC: Cardiovascular Interventions 2013;6(4):334-343.

78. Lim W-H, Seo W-W, Choe W, Kang C-K, Park J, Cho H-J, Kyeong S, Hur J, Yang H-M, Cho H-J and others. Stent Coated with Antibody against Vascular Endothelial-Cadherin Captures Endothelial Progenitor Cells, Accelerates Re-Endothelialization, and Reduces Neointimal Formation. Arteriosclerosis Thrombosis and Vascular Biology 2011;31(12):2798-U141.

79. Yoder MC, Mead LE, Prater D, Krier TR, Mroueh KN, Li F, Krasich R, Temm CJ, Prchal JT, Ingram DA. Redefining Endothelial Progenitor Cells Via Clonal Analysis and Hematopoietic Stem/Progenitor Cell Principals. Blood 2007;109(5):1801-1809.

80. Matsuda T, Kuwana M, Aomizu T, Yamagishi M, Ohtake H, Watanabe G. Surface Design for in Situ Capture of Endothelial Progenitor Cells: Vegf-Bound Surface Architecture and Behaviors of Cultured Mononuclear Cells. Journal of Biomedical Materials Research Part B-Applied Biomaterials 2013;101B(1):50-60.

81. Blindt R, Vogt F, Astafieva I, Fach C, Hristov M, Krott N, Seitz B, Kapurniotu A, Kwok C, Dewor M and others. A Novel Drug-Eluting Stent Coated with an Integrin-Binding Cyclic Arg-Gly-Asp Peptide Inhibits Neointimal Hyperplasia by Recruiting Endothelial Progenitor Cells. Journal of the American College of Cardiology 2006;47(9):1786-1795.

82. Avci-Adali M, Ziemer G, Wendel HP. Induction of Epc Homing on Biofunctionalized Vascular Grafts for Rapid in Vivo Self-Endothelialization - a Review of Current Strategies. Biotechnology Advances 2010;28(1):119-129.

83. Wei Y, Ji Y, Xiao L-L, Lin Q-k, Xu J-p, Ren K-f, Ji J. Surface Engineering of Cardiovascular Stent with Endothelial Cell Selectivity for in Vivo Re-Endothelialisation. Biomaterials 2013;34(11):2588-2599.

84. Suuronen EJ, Zhang P, Kuraitis D, Cao X, Melhuish A, McKee D, Li F, Mesana TG, Veinot JP, Ruel M. An Acellular Matrix-Bound Ligand Enhances the Mobilization, Recruitment and Therapeutic Effects of Circulating Progenitor Cells in a Hindlimb Ischemia Model. Faseb Journal 2009;23(5):1447-1458.

85. Hoffmann J, Paul A, Harwardt M, Groll J, Reeswinkel T, Klee D, Moeller M, Fischer H, Walker T, Greiner T and others. Immobilized DNA Aptamers Used as Potent Attractors for Porcine Endothelial Precursor Cells. Journal of Biomedical Materials Research Part A 2008;84A(3):614-621.

86. Kunz GA, Liang G, Cuculi F, Gregg D, Vata KC, Shaw LK, Goldschmidt-Clermont PJ, Dong C, Taylor DA, Peterson ED. Circulating Endothelial Progenitor Cells Predict Coronary Artery Disease Severity. American Heart Journal 2006;152(1):190-195.

87. Asahara T, Murohara T, Sullivan A, Silver M, vanderZee R, Li T, Witzenbichler B, Schatteman G, Isner JM. Isolation of Putative Progenitor Endothelial Cells for Angiogenesis. Science 1997;275(5302):964-967.

88. Ingram DA, Mead LE, Tanaka H, Meade V, Fenoglio A, Mortell K, Pollok K, Ferkowicz MJ, Gilley D, Yoder MC. Identification of a Novel Hierarchy of

Endothelial Progenitor Cells Using Human Peripheral and Umbilical Cord Blood. Blood 2004;104(9):2752-2760.

89. Jantzen AE, Lane WO, Gage SM, Haseltine JM, Galinat LJ, Jamiolkowski RM, Lin F-H, Truskey GA, Achneck HE. Autologous Endothelial Progenitor Cell-Seeding Technology and Biocompatibility Testing for Cardiovascular Devices in Large Animal Model. Journal of visualized experiments : JoVE 2011(55):N/A.

90. Brown MA, Wallace CS, Angelos M, Truskey GA. Characterization of Umbilical Cord Blood-Derived Late Outgrowth Endothelial Progenitor Cells Exposed to Laminar Shear Stress. Tissue Engineering Part A 2009;15(11):3575-3587.

91. Povsic TJ, Goldschmidt-Clermont PJ. Endothelial Progenitor Cells: Markers of Vascular Reparative Capacity. Therapeutic advances in cardiovascular disease 2008;2(3):199-213.

92. Farb A, Weber DK, Kolodgie FD, Burke AP, Virmani R. Morphological Predictors of Restenosis after Coronary Stenting in Humans. Circulation 2002;105(25):2974-2980.

93. Tiwari A, Salacinski HJ, Hamilton G, Seifalian AM. Tissue Engineering of Vascular Bypass Grafts: Role of Endothelial Cell Extraction. European Journal of Vascular and Endovascular Surgery 2001;21(3):193-201.

94. Jarrell BE, Williams SK, Stokes G, Hubbard FA, Carabasi RA, Koolpe E, Greener D, Pratt K, Moritz MJ, Radomski J and others. Use of Freshly Isolated Capillary Endothelial-Cells for the Immediate Establishment of a Monolayer on a Vascular Graft at Surgery. Surgery 1986;100(2):392-399.

95. Shi Z, Neoh K, Kang E. In Vitro Endothelialization of Cobalt Chromium Alloys with Micro/Nanostructures Using Adipose-Derived Stem Cells. Journal of Materials Science: Materials in Medicine 2013;24(4):1067-1077.

96. Schreml S, Babilas P, Fruth S, Orso E, Schmitz G, Mueller MB, Nerlich M, Prantl L. Harvesting Human Adipose Tissue-Derived Adult Stem Cells: Resection Versus Liposuction. Cytotherapy 2009;11(7):947-957.

97. Stroncek JD, Grant BS, Brown MA, Povsic TJ, Truskey GA, Reichert WM. Comparison of Endothelial Cell Phenotypic Markers of Late-Outgrowth Endothelial Progenitor Cells Isolated from Patients with Coronary Artery

Disease and Healthy Volunteers. Tissue Engineering Part A 2009;15(11):3473-3486.

98. Shepherd RM, Capoccia BJ, Devine SM, DiPersio J, Trinkaus KM, Ingram D, Link DC. Angiogenic Cells Can Be Rapidly Mobilized and Efficiently Harvested from the Blood Following Treatment with Amd3100. Blood 2006;108(12):3662-3667.

99. Migliavacca F, Petrini L, Montanari V, Quagliana I, Auricchio F, Dubini G. A Predictive Study of the Mechanical Behaviour of Coronary Stents by Computer Modelling. Medical Engineering & Physics 2005;27(1):13-18.

100. Zunino P, D'Angelo C, Petrini L, Vergara C, Capelli C, Migliavacca F. Numerical Simulation of Drug Eluting Coronary Stents: Mechanics, Fluid Dynamics and Drug Release. Computer Methods in Applied Mechanics and Engineering 2009;198(45-46):3633-3644.

101. Rebelo N, Fu R, Lawrenchuk M. Study of a Nitinol Stent Deployed into Anatomically Accurate Artery Geometry and Subjected to Realistic Service Loading. Journal of Materials Engineering and Performance 2009;18(5-6):655-663.

102. Berry JL, Santamarina A, Moore JE, Jr., Roychowdhury S, Routh WD. Experimental and Computational Flow Evaluation of Coronary Stents. Annals of Biomedical Engineering 2000;28(4):386-398.

103. LaDisa JF, Guler I, Olson LE, Hettrick DA, Kersten JR, Warltier DC, Pagel PS. Three-Dimensional Computational Fluid Dynamics Modeling of Alterations in Coronary Wall Shear Stress Produced by Stent Implantation. Annals of Biomedical Engineering 2003;31(8):972-980.

104. Gundert TJ, Marsden AL, Yang W, LaDisa JJF. Optimization of Cardiovascular Stent Design Using Computational Fluid Dynamics. Journal of Biomechanical Engineering 2012;134(1):011002-8.

105. Theriault P, Terriault P, Brailovski V, Gallo R. Finite Element Modeling of a Progressively Expanding Shape Memory Stent. Journal of Biomechanics 2006;39(15):2837-2844.

106. Gong X-Y, Pelton AR, Duerig TW, Rebelo N, Perry K. Finite Element Analysis and Experimental Evaluation of Superelastic Nitinol Stent. In: Pelton A, Duerig T, editors; 2003; Pacific Grove, California, USA. p 453-462.

107. Pelton AR, Schroeder V, Mitchell MR, Gong X-Y, Barney M, Robertson SW. Fatigue and Durability of Nitinol Stents. Journal of the Mechanical Behavior of Biomedical Materials 2008;1(2):153-164.

108. Jaff MR. The Nature of Sfa Disease. Endovascular Today 2004;2004(October):3-5.

109. LaDisa JF, Olson LE, Guler I, Hettrick DA, Audi SH, Kersten JR, Warltier DC, Pagel PS. Stent Design Properties and Deployment Ratio Influence Indexes of Wall Shear Stress: A Three-Dimensional Computational Fluid Dynamics Investigation within a Normal Artery. Journal of Applied Physiology 2004;97(1):424-430.

110. LaDisa JF, Jr., Olson LE, Hettrick DA, Warltier DC, Kersten JR, Pagel PS. Axial Stent Strut Angle Influences Wall Shear Stress after Stent Implantation: Analysis Using 3d Computational Fluid Dynamics Models of Stent Foreshortening. Biomedical engineering online 2005;4:59.

111. Liu SQ, Goldman J. Role of Blood Shear Stress in the Regulation of Vascular Smooth Muscle Cell Migration. Ieee Transactions on Biomedical Engineering 2001;48(4):474-483.

112. LaDisa JF, Olson LE, Molthen RC, Hettrick DA, Pratt PF, Hardel MD, Kersten JR, Warltier DC, Pagel PS. Alterations in Wall Shear Stress Predict Sites of Neointimal Hyperplasia after Stent Implantation in Rabbit Iliac Arteries. American Journal of Physiology-Heart and Circulatory Physiology 2005;288(5):H2465-H2475.

113. Wentzel JJ, Krams R, Schuurbiers JCH, Oomen JA, Kloet J, van der Giessen WJ, Serruys PW, Slager CJ. Relationship between Neointimal Thickness and Shear Stress after Wallstent Implantation in Human Coronary Arteries. Circulation 2001;103(13):1740-1745.

114. Sprague EA, Luo J, Palmaz JC. Endothelial Cell Migration onto Metal Stent Surfaces under Static and Flow Conditions. Journal of Long-Term Effects of Medical Implants 2000;10(1-2):97-110.

115. Frank AO, Walsh PW, Moore JE. Computational Fluid Dynamics and Stent Design. Artificial Organs 2002;26(7):614-621.

116. Frangos JA, Huang TY, Clark CB. Steady Shear and Step Changes in Shear Stimulate Endothelium Via Independent Mechanisms - Superposition of Transient and Sustained Nitric Oxide Production. Biochemical and Biophysical Research Communications 1996;224(3):660-665.

117. White CR, Haidekker M, Bao X, Frangos JA. Temporal Gradients in Shear, but Not Spatial Gradients, Stimulate Endothelial Cell Proliferation. Circulation 2001;103(20):2508-2513.

118. Bao XP, Lu CY, Frangos JA. Temporal Gradient in Shear but Not Steady Shear Stress Induces Pdgf-a and Mcp-1 Expression in Endothelial Cells - Role of No, Nf Kappa B, and Egr-1. Arteriosclerosis Thrombosis and Vascular Biology 1999;19(4):996-1003.

119. Lietz K, Miller LW. Destination Therapy: Current Results and Future Promise. Seminars in thoracic and cardiovascular surgery 2008;20(3):225-33.

120. Selgrade BP, Truskey GA. Computational Fluid Dynamics Analysis to Determine Shear Stresses and Rates in a Centrifugal Left Ventricular Assist Device. Artificial Organs 2012:E89-E96.

121. Achneck HE, Sileshi B, Parikh A, Milano CA, Welsby IJ, Lawson JH. Pathophysiology of Bleeding and Clotting in the Cardiac Surgery Patient from Vascular Endothelium to Circulatory Assist Device Surface. Circulation 2010;122(20):2068-2077.

122. Schillinger M, Sabeti S, Dick P, Amighi J, Mlekusch W, Schlager O, Loewe C, Cejna M, Lammer J, Minar E. Sustained Benefit at 2 Years of Primary Femoropopliteal Stenting Compared with Balloon Angioplasty with Optional Stenting. Circulation 2007;115(21):2745-2749.

123. Maleux G, Marrannes J, Heye S, Daenens K, Verhamme P, Thijs V. Outcome of Carotid Artery Stenting at 2 Years Follow-Up: Comparison of Nitinol Open Cell Versus Stainless Steel Closed Cell Stent Design. Journal of Cardiovascular Surgery 2009;50(5):669-675.

124. Dick P, Wallner H, Sabeti S, Loewe C, Mlekusch W, Lammer J, Koppensteiner R, Minar E, Schillinger M. Balloon Angioplasty Versus Stenting with Nitinol Stents in Intermediate Length Superficial Femoral Artery Lesions. Catheterization and Cardiovascular Interventions 2009;74(7):1090-1095.

125. Slottow TLP, Waksman R. Drug-Eluting Stent Safety. American Journal of Cardiology 2007;100(8B):10M-17M.

126. Achneck HE, Jamiolkowski RM, Jantzen AE, Haseltine JM, Lane WO, Huang JK, Galinat LJ, Serpe MJ, Lin F-H, Li M and others. The Biocompatibility of Titanium Cardiovascular Devices Seeded with Autologous Blood-Derived Endothelial Progenitor Cells Epc-Seeded Antithrombotic Ti Implants. Biomaterials 2011;32(1):10-18.

127. Velik-Salchner C, Schnurer C, Fries D, Mussigang PR, Moser PL, Streif W, Kolbitsch C, Lorenz IH. Normal Values for Thrombelastography (Rotem (R)) and Selected Coagulation Parameters in Porcine Blood. Thrombosis Research 2006;117(5):597-602.

128. Kang C, Bonneau M, Brouland JP, Sollier CBD, Drouet L. In Vivo Pig Models of Venous Thrombosis Mimicking Human Disease. Thrombosis and Haemostasis 2003;89(2):256-263.

129. Dal Nogare AR, Toews GB. Characteristics of Alveolar Macrophages in an Animal Model of Resolving Pulmonary Inflammation. American Review of Respiratory Disease 1990;142(3):660-667.

130. Ueberrueck T, Tautenhahn J, Meyer L, Kaufmann O, Lippert H, Gastinger I, Wahlers T. Comparison of the Ovine and Porcine Animal Models for Biocompatibility Testing of Vascular Prostheses. Journal of Surgical Research 2005;124(2):305-311.

131. Achneck HE, Serpe MJ, Jamiolkowski RM, Eibest LM, Craig SL, Lawson JH. Regenerating Titanium Ventricular Assist Device Surfaces after Gold/Palladium Coating for Scanning Electron Microscopy. Microscopy Research and Technique 2010;73(1):71-76.

132. DeGarmo P, Black J, Kohser R. Materials and Processes in Manufacturing. 9th Ed. Wiley 2003;223.

133. Seldinger SI. Catheter Replacement of the Needle in Percutaneous Arteriography: A New Technique. Acta Radiologica [Old Series] 1953;39(5):368-376.

134. Truskey GA, Yuan F, Katz DF. Transport Phenomena in Biological Systems. Upper Saddle River, N.J.: Pearson/Prentice Hall; 2009.

135. Raymond MA, Smith ER, Liesegang J. The Physical Properties of Blood - Forensic Considerations. Science & Justice 1996;36(3):153-160.

136. Jantzen AE, Lane WO, Gage SM, Jamiolkowski RM, Haseltine JM, Galinat LJ, Lin F-H, Lawson JH, Truskey GA, Achneck HE. Use of Autologous Blood-Derived Endothelial Progenitor Cells at Point-of-Care to Protect against Implant Thrombosis in a Large Animal Model. Biomaterials 2011;32(33):8356-8363.

137. Wegener J, Janshoff A, Galla HJ. Cell Adhesion Monitoring Using a Quartz Crystal Microbalance: Comparative Analysis of Different Mammalian Cell Lines. European Biophysics Journal with Biophysics Letters 1998;28(1):26-37.

138. Rameis M-T, Cei S, Bernardi J, Watzek G, Gruber R. Development of an in Vitro Model on Cellular Adhesion on Granular Natural Bone Mineral under Dynamic Seeding Conditions - a Pilot Study. Journal of Biomedical Materials Research Part B-Applied Biomaterials 2009;91B(2):766-771.

139. Fisher RA. Statistical Methods for Research Workers. 10th Edn. Revised & Enlarged; 1946. 1-354 p.

140. Moulder J, Stickle W, Sobol P, editors. Handbook of X Ray Photoelectron Spectroscopy (P/N 624755). Perkin-Elmer, Physical Electronics Division;; 1992.

141. Samaroo HD, Lu J, Webster TJ. Enhanced Endothelial Cell Density on Niti Surfaces with Sub-Macron to Nanometer Roughness. International Journal of Nanomedicine 2008;3(1):75-82.

142. Nappo F, Esposito K, Cioffi M, Giugliano G, Molinari AM, Paolisso G, Marfella R, Giugliano D. Postprandial Endothelial Activation in Healthy Subjects and in Type 2 Diabetic Patients: Role of Fat and Carbohydrate Meals. Journal of the American College of Cardiology 2002;39(7):1145-1150.

143. Li H, Cybulsky MI, Gimbrone MA, Libby P. An Atherogenic Diet Rapidly Induces Vcam-1, a Cytokine-Regulatable Mononuclear Leukocyte Adhesion Molecule, in Rabbit Aortic Endothelium. Arteriosclerosis and Thrombosis 1993;13(2):197-204.

144. Rashid ST, Salacinski HJ, Hamilton G, Seifalian AM. The Use of Animal Models in Developing the Discipline of Cardiovascular Tissue Engineering: A Review. Biomaterials 2004;25(9):1627-1637.

145. Achneck HE, Sileshi B, Lawson JH. Review of the Biology of Bleeding and Clotting in the Surgical Patient. Vascular 2008;16:S6-S13.

146. Jaffer AK, Barsoum WK, Krebs V, Hurbanek JG, Morra N, Brotman DJ. Duration of Anesthesia and Venous Thromboembolism after Hip and Knee Arthroplasty. Mayo Clinic Proceedings 2005;80(6):732-738.

147. Ellsworth WA, Basu CB, Iverson RE. Perioperative Considerations for Patient Safety During Cosmetic Surgery - Preventing Complications. Canadian Journal of Plastic Surgery 2009;17(1):9-16.

148. Forbes TJ, Rosenthal GL, Reul GR, Ott DA, Feltes TF. Risk Factors for Life-Threatening Cavopulmonary Thrombosis in Patients Undergoing Bidirectional Superior Cavopulmonary Shunt: An Exploratory Study. American Heart Journal 1997;134(5):865-871.

149. Zhao T, Zhang Z-N, Rong Z, Xu Y. Immunogenicity of Induced Pluripotent Stem Cells. Nature 2011;474(7350):212-U251.

150. Hsiao H-M, Chiu Y-H, Lee K-H, Lin C-H. Computational Modeling of Effects of Intravascular Stent Design on Key Mechanical and Hemodynamic Behavior. Computer-Aided Design 2012;44(8):757-765.

151. Hyre M, Pulliam R, Squire J. Modeling Stent Expansion Dynamics and Blood Flow Patterns in a Stenotic Artery. Modelling in Medicine and Biology 2011:115.

152. McVeigh GE, Burns DE, Johnston GD, Finkelstein SM, Cohn JN. Reduced Arterial Vascular Compliance as a Marker for Essential-Hypertension. British Journal of Clinical Pharmacology 1990;29(5):P587-P587.

153. Gundert TJ, Shadden SC, Williams AR, Koo B-K, Feinstein JA, LaDisa JF, Jr. A Rapid and Computationally Inexpensive Method to Virtually Implant Current and Next-Generation Stents into Subject-Specific Computational Fluid Dynamics Models. Annals of Biomedical Engineering 2011;39(5):1423-1437.

154. Ku DN, Giddens DP, Zarins CK, Glagov S. Pulsatile Flow and Atherosclerosis in the Human Carotid Bifurcation Positive Correlation between Plaque Location and Low and Oscillating Shear Stress. Arteriosclerosis 1985;5(3):293-302.

155. Augst AD, Ariff B, Thom SAGM, Xu XY, Hughes AD. Analysis of Complex Flow and the Relationship between Blood Pressure, Wall Shear Stress, and Intima-Media Thickness in the Human Carotid Artery. American Journal of Physiology-Heart and Circulatory Physiology 2007;293(2):H1031-H1037.

156. Holdsworth DW, Norley CJD, Frayne R, Steinman DA, Rutt BK. Characterization of Common Carotid Artery Blood-Flow Waveforms in Normal Human Subjects. Physiological Measurement 1999;20(3):219-240.

157. Masuda M, Emoto T, Suzuki A, Akutagawa M, Kitawaki T, Kitaoka K, Tanaka H, Obara S, Yoshizaki K, Konaka S and others. Evaluation of Blood Flow Velocity Waveform in Common Carotid Artery Using Multi-Branched Arterial Segment Model of Human Arteries. Biomedical Signal Processing and Control 2013;8(6):509-519.

158. Weissler AM, Peeler RG, Roehll WH. Relationships between Left Ventricular Ejection Time, Stroke Volume, and Heart Rate in Normal Individuals and Patients with Cardiovascular Disease. American Heart Journal 1961;62(3):367-378.

159. Gelfand BD, Epstein FH, Blackman BR. Spatial and Spectral Heterogeneity of Time-Varying Shear Stress Profiles in the Carotid Bifurcation by Phase-Contrast. Journal of Magnetic Resonance Imaging 2006;24(6):1386-1392.

160. Avolio AP, Deng FQ, Li WQ, Luo YF, Huang ZD, Xing LF, Orourke MF. Effects of Aging on Arterial Distensibility in Populations with High and Low Prevalence of Hypertension - Comparison between Urban and Rural Communities in China. Circulation 1985;71(2):202-210.

161. Vaitkevicius PV, Fleg JL, Engel JH, Oconnor FC, Wright JG, Lakatta LE, Yin FCP, Lakatta EG. Effects of Age and Aerobic Capacity on Arterial Stiffness in Healthy-Adults. Circulation 1993;88(4):1456-1462.

162. Pearson AC, Guo RQ, Orsinelli DA, Binkley PF, Pasierski TJ. Transesophageal Echocardiographic Assessment of the Effects of Age, Gender, and Hypertension

on Thoracic Aortic-Wall Size, Thickness, and Stiffness. American Heart Journal 1994;128(2):344-351.

163. Feaver RE, Gelfand BD, Blackman BR. Human Haemodynamic Frequency Harmonics Regulate the Inflammatory Phenotype of Vascular Endothelial Cells. Nature Communications 2013;4.

164. Dolan JM, Sim FJ, Meng H, Kolega J. Endothelial Cells Express a Unique Transcriptional Profile under Very High Wall Shear Stress Known to Induce Expansive Arterial Remodeling. American Journal of Physiology-Cell Physiology 2012;302(8):C1109-C1118.

165. Chiu J-J, Chien S. Effects of Disturbed Flow on Vascular Endothelium: Pathophysiological Basis and Clinical Perspectives. Physiological Reviews 2011;91(1):327-387.

166. Brooks AR, Lelkes PI, Rubanyi GM. Gene Expression Profiling of Human Aortic Endothelial Cells Exposed to Disturbed Flow and Steady Laminar Flow. Physiological Genomics 2002;9(1):27-41.

167. Hsiai TK, Cho SK, Reddy S, Hama S, Navab M, Demer LL, Honda HM, Ho CM. Pulsatile Flow Regulates Monocyte Adhesion to Oxidized Lipid-Induced Endothelial Cells. Arteriosclerosis Thrombosis and Vascular Biology 2001;21(11):1770-1776.

168. Thomas JA, Deaton RA, Hastings NE, Shang Y, Moehle CW, Eriksson U, Topouzis S, Wamhoff BR, Blackman BR, Owens GK. Pdgf-Dd, a Novel Mediator of Smooth Muscle Cell Phenotypic Modulation, Is Upregulated in Endothelial Cells Exposed to Atherosclerosis-Prone Flow Patterns. American Journal of Physiology-Heart and Circulatory Physiology 2009;296(2):H442-H452.

169. Zhao SZ, Xu XY, Hughes AD, Thom SA, Stanton AV, Ariff B, Long Q. Blood Flow and Vessel Mechanics in a Physiologically Realistic Model of a Human Carotid Arterial Bifurcation. Journal of Biomechanics 2000;33(8):975-984.

170. Nagai Y, Helwegen J, Fleg JL, Beemer MK, Earley CJ, Metter EJ. Associations of Aortic Windkessel Function with Age, Gender and Cardiovascular Risk Factors. Ultrasound in medicine & biology 2001;27(9):1207-1210.

171. Wu T-Y, Chou H-H, Chang S-H, Tsai Y-J, Hsieh C-A, Cheng S-T, Yeh K-H, Chang H-J, Ko Y-L, Huang H-L. Comparison of Immediate and 2-Year Outcomes between Excimer Laser-Assisted Angioplasty with Spot Stent and Primary Stenting in Intermediate to Long Femoropopliteal Disease. Scientific World Journal 2013.

172. Finn AV, Joner M, Nakazawa G, Kolodgie F, Newell J, John MC, Gold HK, Virmani R. Pathological Correlates of Late Drug-Eluting Stent Thrombosis - Strut Coverage as a Marker of Endothelialization. Circulation 2007;115(18):2435-2441.

173. Farb A, Burke AP, Kolodgie FD, Virmani R. Pathological Mechanisms of Fatal Late Coronary Stent Thrombosis in Humans. Circulation 2003;108(14):1701-1706.

174. O'Riordan M. Medscape. First Bioabsorbable Stent Approved in Europe. http://www.medscape.com/viewarticle/735561. Accessed March 3, 2014.

175. Granada JF, Inami S, Aboodi MS, Tellez A, Milewski K, Wallace-Bradley D, Parker S, Rowland S, Nakazawa G, Vorpahl M and others. Development of a Novel Prohealing Stent Designed to Deliver Sirolimus from a Biodegradable Abluminal Matrix / Clinical Perspective. Circulation: Cardiovascular Interventions 2010;3(3):257-266.

176. Ichikawa M, Yutani C, Hayashi T, Nakata T, Iwata A, Lim Y-J, Mishima M. Angioscopic Findings of Delayed Healing at Sites of Sirolimus-Eluting Stent Overlap after 21-Month Implantation. International Journal of Cardiology 2008;129(1):E10-E11.

177. van Beusekom HMM, Saia F, Zindler JD, Lemos PA, Hoor SLS-t, Leeuwen MAHv, de Feijter PJ, Serruys PW, van der Giessen WJ. Drug-Eluting Stents Show Delayed Healing: Paclitaxel More Pronounced Than Sirolimus. European Heart Journal 2007;28(8):974-979.

178. Rodriguez AE, Rodriguez-Granillo GA, Palacios IF. Late Stent Thrombosis: The Damocle's Sword of Drug Eluting Stents? EuroIntervention : journal of EuroPCR in collaboration with the Working Group on Interventional Cardiology of the European Society of Cardiology 2007;2(4):512-7.

179. Luescher TF, Steffel J, Eberli FR, Joner M, Nakazawa G, Tanner FC, Virmani R. Drug-Eluting Stent and Coronary Thrombosis - Biological Mechanisms and Clinical Implications. Circulation 2007;115(8):1051-1058.

180. Grumann T, Diehl P, Bode C, Moser M. Is Stent Thrombosis the New Achilles Heel of Interventional Cardiology? State of the Art Clinical Trials, Causes and Approaches for Prevention. Hamostaseologie 2007;27(5):344-50.

181. Hofma SH, van der Giessen WJ, van Dalen BM, Lemos PA, McFadden EP, Sianos G, Ligthart JMR, van Essen D, de Feyter PJ, Serruys PW. Indication of Long-Term Endothelial Dysfunction after Sirolimus-Eluting Stent Implantation. European Heart Journal 2006;27(2):166-170.

182. Togni M, Raber L, Cocchia R, Wenaweser P, Cook S, Windecker S, Meier B, Hess OM. Local Vascular Dysfunction after Coronary Paclitaxel-Eluting Stent Implantation. International Journal of Cardiology 2007;120(2):212-220.

183. Joner M, Finn AV, Farb A, Mont EK, Kolodgie FD, Ladich E, Kutys R, Skorija K, Gold HK, Virmani R. Pathology of Drug-Eluting Stents in Humans - Delayed Healing and Late Thrombotic Risk. Journal of the American College of Cardiology 2006;48(1):193-202.

184. Tura O, Skinner EM, Barclay GR, Samuel K, Gallagher RCJ, Brittan M, Hadoke PWF, Newby DE, Turner ML, Mills NL. Late Outgrowth Endothelial Cells Resemble Mature Endothelial Cells and Are Not Derived from Bone Marrow. Stem Cells 2013;31(2):338-348.

185. Truskey GA, Yuan F, Katz DF. Transport Phenomena in Biological Systems. In: MJ H, editor. Upper Saddle River, N.J.: Pearson/Prentice Hall; 2009.

186. Lauer T, Preik M, Rassaf T, Strauer BE, Deussen A, Feelisch M, Kelm M. Plasma Nitrite Rather Than Nitrate Reflects Regional Endothelial Nitric Oxide Synthase Activity but Lacks Intrinsic Vasodilator Action. Proceedings of the National Academy of Sciences 2001;98(22):12814-12819.

187. Wallace CS, Strike SA, Truskey GA. Smooth Muscle Cell Rigidity and Extracellular Matrix Organization Influence Endothelial Cell Spreading and Adhesion Formation in Coculture. American Journal of Physiology-Heart and Circulatory Physiology 2007;293(3):H1978-H1986.

188. Livak KJ, Schmittgen TD. Analysis of Relative Gene Expression Data Using Real-Time Quantitative Pcr and the 2(T)(-Delta Delta C) Method. Methods 2001;25(4):402-408.

189. Jantzen AE, Achneck HE, Truskey GA. Surface Projections of Titanium Substrates Increase Antithrombotic Endothelial Function in Response to Shear Stress. Journal of Biomedical Materials Research Part A 2013;101(11):3181-3191.

190. Sheehy AM, Burson MA, Black SM. Nitric Oxide Exposure Inhibits Endothelial Nos Activity but Not Gene Expression: A Role for Superoxide. American Journal of Physiology - Lung Cellular and Molecular Physiology 1998;274(5):L833-L841.

191. Boo YC, Hwang J, Sykes M, Michell BJ, Kemp BE, Lum H, Jo H. Shear Stress Stimulates Phosphorylation of Enos at Ser635 by a Protein Kinase a-Dependent Mechanism. American Journal of Physiology - Heart and Circulatory Physiology 2002;283(5):H1819-H1828.

192. Boo YC, Sorescu G, Boyd N, Shiojima I, Walsh K, Du J, Jo H. Shear Stress Stimulates Phosphorylation of Endothelial Nitric-Oxide Synthase at Ser1179 by Akt-Independent Mechanisms. Journal of Biological Chemistry 2002;277(5):3388-3396.

193. Dimmeler S, Fleming I, Fisslthaler B, Hermann C, Busse R, Zeiher AM. Activation of Nitric Oxide Synthase in Endothelial Cells by Akt-Dependent Phosphorylation. Nature 1999;399(6736):601-605.

194. Fulton D, Gratton J-P, McCabe TJ, Fontana J, Fujio Y, Walsh K, Franke TF, Papapetropoulos A, Sessa WC. Regulation of Endothelium-Derived Nitric Oxide Production by the Protein Kinase Akt. Nature 1999;399(6736):597-601.

195. Perez de Prado A, Perez-Martinez C, Cuellas-Ramon C, Manuel Gonzalo-Orden J, Regueiro-Purrinos M, Martinez B, Garcia-Iglesias MJ, Ajenjo JM, Altonaga JR, Diego-Nieto A and others. Time Course of Reendothelialization of Stents in a Normal Coronary Swine Model: Characterization and Quantification. Veterinary Pathology 2011;48(6):1109-1117.

196. Kang S, Carlon T, Jantzen A, Lin F-H, Ley M, Allen J, Stabler T, Haley NR, Truskey G, Achneck H. Isolation of Functional Human Endothelial Cells from Small Volumes of Umbilical Cord Blood. Annals of Biomedical Engineering 2013;41(10):2181-2192.